Synthesis and Characterization of Biodegradable Gelatin Based Carbon Nanotube

Composites for Energy Storage Applications

by

Rabeya Binta Alam
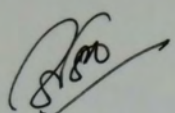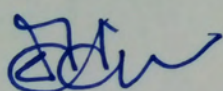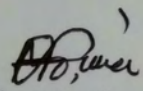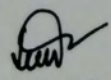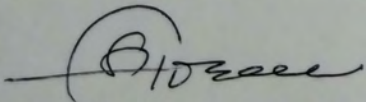
MASTER OF SCIENCE IN PHYSICS

Department of Physics

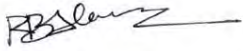BANGLADESH UNIVERSITY OF ENGINEERING AND TECHNOLOGY

May 2021

The thesis titled "Synthesis and Characterization of Biodegradable Gelatin Based Carbon Nanotube Composites for Energy Storage Applications" Submitted by Rabeya Binta Alam, Roll No.: 1018142509F, Session: October-2018 has been accepted as satisfactory in partial fulfillment of the requirement for the degree MASTER OF SCIENCE IN PHYSICS on 29 May, 2021.

BOARD OF EXAMINERS

1.   (Signature)
Dr. Muhammad Rakibul Islam (Supervisor)   Chairman
Associate Professor
Department of physics, BUET, Dhaka

2.   (Signature)   Member
Dr. Md. Rafi Uddin   (Ex- officio)
Professor & Head
Department of physics, BUET, Dhaka

3.   (Signature)
Dr. Md. Forhad Mina   Member
Professor
Department of physics, BUET, Dhaka

4.   (Signature)
Dr. Mohammad Jellur Rahman   Member
Associate Professor
Department of physics, BUET, Dhaka

5.   (Signature)
Dr. Khandker Saadat Hossain   Member
Professor   (External)
Department of Physics, University of Dhaka

CANDIDATE'S DECLARATION

It is hereby declared that this thesis or any part of it has not been submitted elsewhere for the award of any degree or diploma.

……………………
Rabeya Binta Alam

Dedication

To all my respected teachers from childhood till now. Without their help and support, I could never have done this.

To my beloved parents.

Acknowledgments

First of all, I express all my admiration and devotion to the almighty Allah, the gracious, benevolent and merciful who has given me the strength and opportunity and has shown me the right path for completing the research work.

With much pleasure, I would like to express my profound gratitude and sincere thanks to my honorable supervisor, Dr. Muhammad Rakibul Islam, Associate Professor, Department of Physics, Bangladesh University of Engineering and Technology (BUET), for his scholastic guidance, supervision and continuous encouragement with care throughout the research. His boundless enthusiasm, ambition and innovative thoughts for solving scientific problems inspired me in pursuing the whole investigation. For any problem of his students, he is always there with his valuable suggestions, worthy comments and constructive criticisms. Words will always be insufficient for expressing in how many ways he has inspired me in life. I consider myself lucky to be a member of his team.

I am deeply grateful to Professor Dr. Md. Rafi Uddin, Head, Department of Physics, BUET, for his kind permission for providing me the necessary facilities and administrative support to carry out this research work. I am very much grateful to Professor Dr. Jiban Podder, Professor Dr. Md. Forhad Mina, Dr. Mohammad Jellur Rahman, of the Department of Physics, BUET for their generous support to this work. I would like to convey my deep gratitude to all other respected teachers and would like to thank all the staff and employees of the Department of Physics, BUET for their co-operation.

I also like to thank all of my fellow lab mates. Working with them during all these years has truly been a wonderful experience. I would like to especially thank Muhammad Hasive Ahmad, my friend and lab mate, for his constant help and support.

Finally, I would like to extend my sincere thanks to all my family members specially to my parents for their unlimited love and blessing. This dissertation would never have been possible without their moral support and affection.

Abstract

In this study, gelatin/Multi-Walled Carbon Nanotube (Gel/MWCNT), and gelatin/Single-Walled Carbon Nanotube (Gel/SWCNT) nanocomposites with different concentrations of CNTs were prepared by a facile solution casting process. Field Emission Scanning Electron Microscope (FESEM) images and Fourier Transform Infrared (FTIR) spectroscopy analysis showed an increased interaction between the CNTs and the polymer. The contact angle measurement showed the transition from the hydrophilic to the hydrophobic due to the addition of CNTs. Specific capacitance as high as 12.7 F/g at a current density of 0.3 $\mu A/cm^2$ together with capacitance retention of 95% of the initial capacitance after completing 5000 charging-discharging cycles was obtained for the Gel/0.05% MWCNT sample. The Nyquist plot showed a decrease in charge-transfer resistance from 127 Ω to 75 Ω, and an increase in double-layer capacitance from 4 nF to 9 nF due to the incorporation of CNTs resulting in improved capacitive performance. Dielectric constant as high as ~10^4 and a loss tangent of 0.91 were obtained for the Gel/SWCNT nanocomposite. The mechanism behind the improvement of the electrochemical performance was also elucidated. The biodegradability study showed that the nanocomposites fully degraded in few hours while emerging into the water. The Gel/CNT nanocomposites with improved electrochemical performance synthesized by a simple, low-cost process will pave the way to the production of sustainable, bio-friendly flexible energy storage devices.

Contents

List of Figures

List of Tables

List of Abbreviation

Gel	Gelatin
CNT	Carbon Nanotube
MWCNT	Multi walled Carbon Nanotube
SWCNT	Single walled Carbon Nanotube
FTIR	Fourier Transformed Infrared spectroscopy
FESEM	Field Emission Scanning Electron Microscopy
UV-Vis	Ultra-violate Visible
WCA	Water Contact Angle
DSC	Differential Scanning Calorimetry
CV	Cyclic Voltammetry
GCD	Galvanostatic Charging-Discharging
EIS	Electrochemical Impedance Spectroscopy
CPE	Constant Phase Element

CHAPTER 1
INTRODUCTION

1.1 Introduction

With the ongoing technological development, the colossal demand for electronics leads to a massive amount of waste produced from electrical and electronic equipment. The junk or solid wastes produced from electrical appliances after their lifetime are called electronic waste or 'E-wastes' [1, 2] which is a matter of great concern for both the environment and mankind. With the recent boom in the electrical and electronics industries, the amount of whole yearly production of E-wastes also increased. Subsequently filling up the landfills, E-wastes are now endangering nature by taking place into the rivers, seas, and oceans [3, 4]. Most of the components of these wastes are produced from toxic and non-biodegradable materials, making them a constant threat to nature [5]. The scraps derived from the E-wastes are mainly plastics, glass, and metals [3]. Synthetic plastics are called the greatest threat to nature in modern civilization for their non-biodegradable nature. Heavy metals like lead, mercury, cadmium, thallium, nickel, etc. are extremely harmful to any living being [6]. Some of the heavy metallic residues of E-wastes are radioactive (wastes produced from the battery of a device) and are tremendously hazardous for living bodies and the natural environment not only in the present time but also for future generations [6]. As per an estimation by the UN, only in the year 2020, the overall discarded E-wastes from the whole world were approximately 53.6 million metric tons [3, 7]. So, to ensure a sustainable energy future it is a call of time to invent efficient novel materials for device applications (such as sensor, actuator, battery, supercapacitor, etc.) that can meet the quality expectation with less or no harmful footprints on nature. To meet these demands, materials from nature-derived or renewable resources have recently attracted researcher's attention widely. Fig. 1.1 shows the harmful impact of E-waste on the environment and the health of the human.

Varieties of devices such as sensors, actuators, drug delivery devices, etc. used in the biomedical and environmental sector need to perform efficiently for a certain period of time and then disappear from the system without causing any hamper [8-10]. They do not need a

Fig. 1.1 E-waste dumped in (a) landfills and (b) rivers.

constant source of energy as well as a long-lasting structural body. These devices should have made with fully bio-derived materials that can perform swiftly for the desired period and then disappear from the system without leaving any harmful footprints. These kinds of devices are called transient devices [11, 12]. It is an emerging and promising field where the invention of bio-derived novel materials appropriates for use in the devices is the main focus. More recently, electronic devices fabricated from transient materials, named transient electronics have gained significant research attention [11-13].

Polymer materials obtained from bio-derived sources are the most suitable candidates for transient device applications [8, 12-14]. Polymers present in different biological bodies are abundant, cost-efficient, and nature-friendly materials that possess all the advantages of polymers like flexibility, heat and electron resistivity, mechanical strength, lightweight, etc. [15-17]. So far, several biopolymers, such as cellulose, starch, chitosan, gelatin, etc. have shown applications in different fields such as food thickening, binding, and packaging material, etc. [18-20]. However, the poor dielectric constant of polymers is one of the major bottlenecks that hinder the fabrication of efficient capacitive devices with polymer because materials with high dielectric constant and low dielectric loss are suitable for applications in high-efficiency capacitive devices [21, 22].

The different physical properties of the polymer can be tuned, improved and its area of applicability can be widened by adding fillers into the polymer matrix [23, 24]. Recently,

nanostructured materials have gained significant research attention as filler materials because of possessing unique and promising physical, chemical, structural, and mechanical characteristics [3-5]. Among the available alternatives, carbon nanotube (CNT), rolled up a cylinder of a layer of the graphene sheet, has been considered as a popular nanofiller for polymer-based nanocomposites because of their unique electronic properties, high thermal conductivity together with extraordinary mechanical strength and flexibility [6-8]. The excellent electronic conductivity and a large body to surface area ratio allow accumulation of electric charges within the capacitor electrolyte on the electrode surface and ions of opposite charges in the electrolyte side, resulting in an electric double-layer capacitance [9-11]. Thus, these interesting properties make CNT an attractive material for electrical energy storage purposes [12, 13]. So far, several attempts have been made to achieve a significantly higher dielectric constant together with a smaller dielectric loss tangent by introducing CNT nanofillers into the polymer matrix. For instance, Xiao et al. reported a higher dielectric constant of 5200 and a tangent loss of 1.2 [16]. In another work, synthesis of polyethylene-MWCNT with Cyanate ester nanocomposite was reported by Wang et al. where a lesser dielectric loss tangent of 0.008 was obtained but the dielectric constant was not impressing, only 168 [17].

Among the available bio-polymer, gelatin has gained significant research attention because of its renewability, abundance, low cost, and easy biodegradability [18-20]. Gelatin biopolymer is obtained from hydrolysis of the fibrous insoluble collagen present in bones and skin is regarded as one of the most promising candidates for biodegradable and transient device applications. Gelatin is widely used in drug delivery, biomedical implants, body monitoring sensors, food packaging, environmental sensors, secure memory devices, etc. [21-23]. Study shows that the area of applications of gelatin can be broadened by modifying its structural, thermal, electrical, and mechanical properties by incorporating nanofiller into the polymer matrix [24, 25]. However, a report on the effect of nanofiller on the dielectric performance and electrochemical properties is very rare. To the best of our knowledge, gelatin-based carbon nanotube nanocomposites as electrode material in an electrostatic capacitor have never been investigated and the dielectric performance of this type of material has not been reported. Considering its importance in the fabrication of eco-friendly, flexible,

and efficient energy storage devices it is imperative to study the effect of CNT nanofiller on the physical properties of the gelatin nanocomposite and the corresponding change on their electrochemical and dielectric performance.

The properties and performance of a nanocomposite can differ depending on its synthesis process. Several techniques, such as hydrothermal, surface activation, modification, in situ polymerization, etc. techniques are used for the synthesis of nanocomposites [26, 27]. Among them, solution processing is considered one of the most promising composite preparation techniques because of its easy processing, low cost, and high yield fabrication [28].

In this research, bio-nanocomposite have been fabricated using gelatin as biopolymer matrix and Carbon Nanotube (MWCNTs or SWCNTs) as a conductive filler. Furthermore, the different physical properties together with the capacitive performance and biodegradability of the nanocomposites have been studied.

1.2 Objectives

The main objectives of this research work are as follows:

➢ Synthesis of Gel/MWCNT and Gel/SWCNT nanocomposites using solution cast technique.

➢ Investigation of the structural and electrical properties of the nanocomposites.

➢ Study the mechanical and optical properties of the Gel/MWCNT and Gel/SWCNT nanocomposites.

➢ Evaluate the dielectric performance of the as-prepared nanocomposites.

➢ Study the electrochemical properties of the Gel/MWCNT and Gel/SWCNT nanocomposites.

1.3 Outline of the Thesis

In **Chapter 1**, a brief introduction on the background and motivation of this research and the present state of the problem is given. Some reported articles on relevant works are discussed.

In **chapter 2**, a literature review of some previously reported studies regarding the present work is provided. An overview of the materials used in this research is stated. Their synthesis procedure, classification, important physical properties are discussed. A brief discussion on the dielectric and electrochemical properties is also provided for a better understanding of this research work.

In **chapter 3**, the methodology of the nanocomposite synthesis is presented. Comprehensible flow charts of the procedure are exemplified. Additionally, the electrode preparation method required for electrochemical property analysis is also provided.

In **chapter 4**, different properties of the prepared nanocomposites are investigated with different characterization techniques and the outcomes are analyzed and discussed. Software simulation and some relevant models are applied for getting a better analysis of the results. A self-designed technique is discussed to test the biodegradability of the nanocomposites.

In **chapter 5**, the summary and conclusions of this research work are discussed with possible fields of their application. Several possible experiments related to this work are also suggested.

CHAPTER 2
LITERATURE REVIEW AND THEORETICAL ASPECTS

2.1 Literature Review

Many works have been reported with both the SWCNT and MWCNT for different purposes including electrical energy storage performance. Zhao et al. synthesized a chitosan-based MWCNT nanocomposite and the gel actuator formed showed a specific capacitance of 13.6 mF/g at a voltage scan rate of 100 mV/s for 10 wt% doping of MWCNT in chitosan [29].

Li et al. synthesized MWCNT/epoxy nanocomposite where they used gelatin as a bio-surfactant for defect controlling [30]. Their study showed a significant improvement in
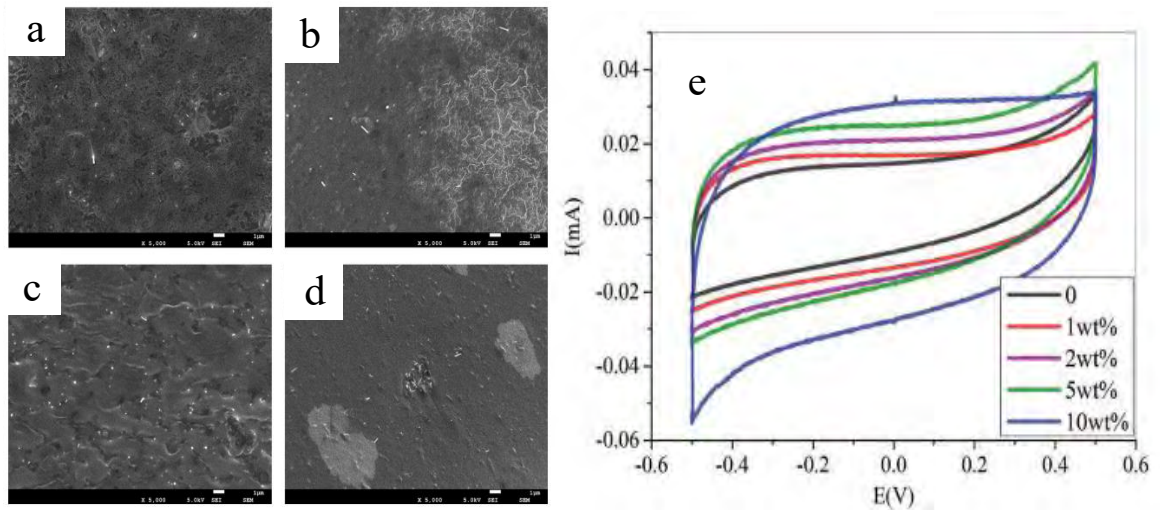
Fig. 2.1 SEM images (a-d) and cyclic voltammetry (e) of chitosan-based nanocomposite Gel actuator fabricated by doping multi-walled carbon nanotubes [29].

the electrical and mechanical properties of the nanocomposite. The percolation threshold that changes the composites from insulators to conductors is approximately 0.05 wt% CNTs in the epoxy resin. Pristine CNTs/epoxy demonstrates the electrical conductivity from 10^{-12}
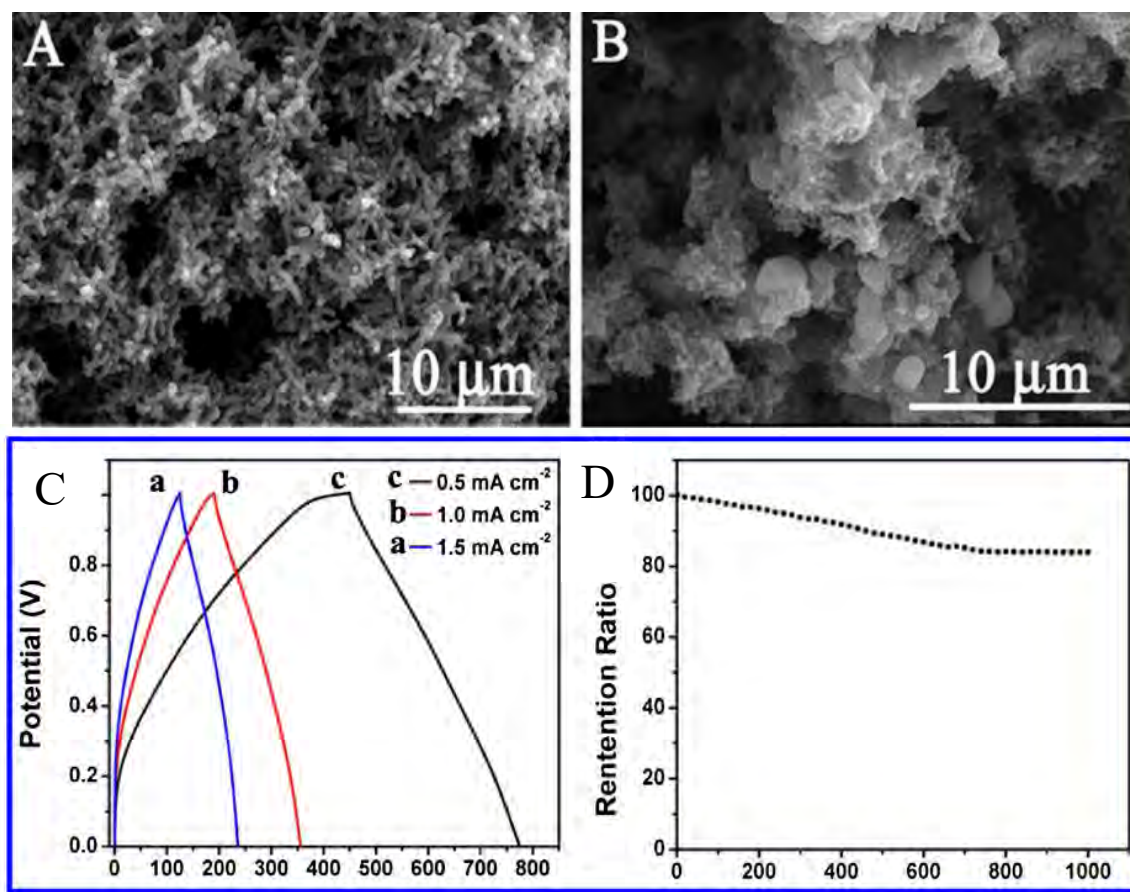
Fig. 2.2 SEM images (A, B), Galvanostatic charging-dischanging (C), and capacitance retention (D) of Polyaniline-Carbon Nanotubes@Zeolite Imidazolate Framework 67-Carbon Cloth [32].

S/m to 10^{-3} S/m. the amino-functionalized CNTs/epoxy also presents better mechanical properties than the pristine one [30].

Sui et al. synthesized SWCNT/epoxy nanocomposites and the mechanical properties including tensile ultimate strength, Young's modulus, and toughness were found 40.97 MPa, 1.13 GPa, and 3.11 MJ/m^3, which increased by 93.53%, 59.15%, and 146.83%, respectively, compared to those of pure epoxy [31]. The tensile stress reached the maximum value of 23 MPa before necking when the tensile strain was 2.3%. It was observed that resistance increased with the increase of tensile strain from the initial value of 50 Ω to the maximum value of 100 Ω [31].

Polyaniline-based MWCNT carbon cloth was made and studied for supercapacitor electrode purposes by Wang et al. [32]. The specific capacitance was found to be 3511 mF/cm^2 at a current density of 0.5 mA/cm^2. And capacitance retention up to 83% after 1000 charging-discharging cycles.

Fan et al. reported a sandwich-structured composite polydimethylsiloxane/carbon nanotube (PDMS/CNT) film fabricated by spin-coating method [14]. The composites showed a dielectric constant of 40 and dielectric loss of 0.01 at 100 Hz.

Liao et al. worked with Polyimide, MWCNT, and Graphene oxide (GO) [15]. The composites with homogeneous dispersion of CNTs and graphene oxide (hdC-G)/PI show dielectric permittivity and dielectric loss of 124.9 and 1.97 at 100 Hz, respectively.

Xiao et al. reported a higher dielectric constant of 5200 and a tangent loss of 1.2 for carbon nanotube added composite of poly(vinylidene fluoride) (PVDF)/boron nitride (BN) [16]. They also found the simultaneous addition of 30 vol% BN and 1 vol% CNTs resulted in a massive 743% increase in thermal conductivity (1.913 $Wm^{-1}K^{-1}$, compared to 0.227 $Wm^{-1}K^{-1}$ that of neat epoxy).
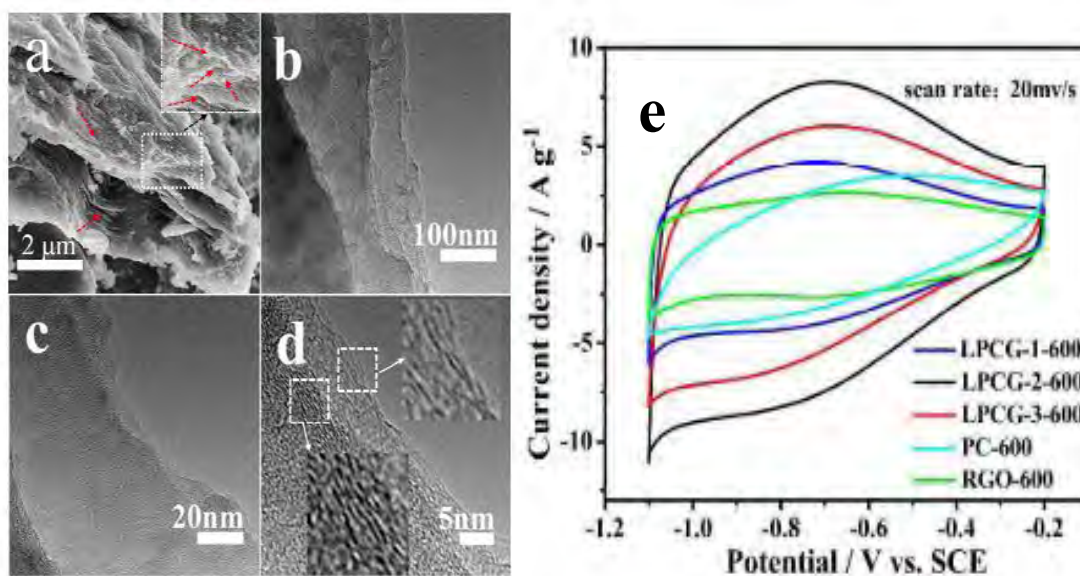
Fig. 2.3 SEM images (a-d) and cyclic voltammetry (e) of Graphene Oxide induced assembly of Gelatin [35].

In another work, polyethylene-MWCNT with cyanate ester nanocomposite was synthesized by Wang et al. where a lesser dielectric loss tangent of 0.008 was obtained but the dielectric constant was not impressive, only 168 [17].
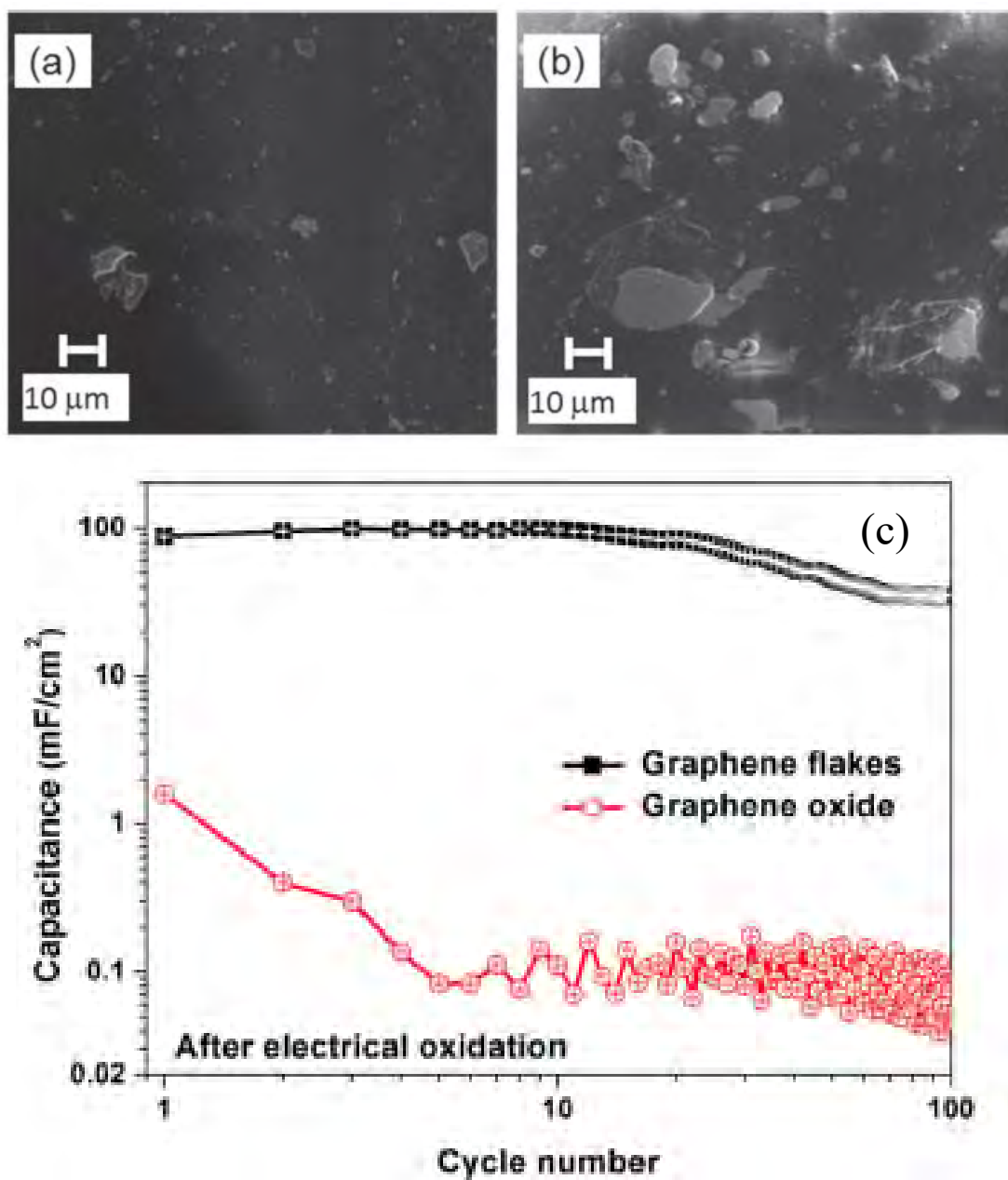
Fig. 2.4 SEM images (a, b) and cyclic stability (c) of Gelatin/Graphene flakes and Gelatin/Graphene Oxide composites [24].

Gelatin has also been reported in several articles with different filler concentrations used for a variety of purposes. Torkaman et al. reported a gelatin-forsterite (Mg_2SiO_4) nanocomposite coating on AISI 316L stainless steel for the potential use of orthopedic implants [33]. Nyquist diagram of gelatin and gelatin-forsterite nanocomposite coated substrates showed a higher polarization resistance due to their lower corrosion current density than uncoated AISI 316L.

Yan et al. reported gelatin/polyacrylamide/graphene oxide (GO) hydrogels with elastic modulus, tensile stress, and strain of 187.3 kPa, 0.324 MPa, 45.5 mm/mm, and toughness of 10.18 MJ/m^3, respectively [34]. It was also found that the gel composite showed a much larger hysteresis loop and a certain self-recovery property than that of polyacrylamide gel.

Rajkumar et al. reported a sensor for dopamine detection by using gelatin/graphite composites and the modified electrode demonstrates good storage stability, reproducibility, and repeatability [23]. The average recovery of the sensor in serum and urine samples was found as 95–98.3%.

Du et al. have made a gelatin/Co_3O_4 nanocomposite as anode material for high-performance Lithium-ion batteries [27]. The material delivers a high charge capacity of 751.3 mAh/g after 150th cycles.

A GO-induced assembly of gelatin was prepared by Zhang et al. for advanced supercapacitor application [35]. The specific capacitance was found to be 455F/g at a current density of 0.5 A/g and capacitance retention of 96% over 5000 cycles.

Landi et al. have made gelatin/graphene nanocomposites and investigated their cyclic stability and dielectric properties [36]. Specific capacity of 380 F/g and surface capacity of 100 mF/cm^2 for the nanocomposite was reported.

In another study, Landi et al. compared the energy storage properties of gelatin/graphene flakes with gelatin/graphene oxide nanocomposites [24]. They found the specific capacitance for the wet blend with 0.2 wt% of graphene oxide and graphene flakes were 1.6 mF/cm^2 and 8 mF/cm^2 respectively at a voltage scan rate of 8 mV/sec.

Although gelatin and Carbon Nanotubes have been reported in many articles separately, however, their combined effect has not been studied or reported so far. To the

best of our knowledge, no study has been reported yet with gelatin/MWCNT and gelatin/SWCNT nanocomposites for energy storage investigations.

2.2 Polymer Nanocomposite

Polymer nanocomposites consist of a polymer or copolymer having nanoparticles or nanofillers dispersed in the polymer matrix. These may be of different shapes (e.g., platelets, fibers, spheroids), but at least one dimension must be in the range of 1–50 nm [37]. These systems require controlled mixing/compounding, stabilization of the achieved dispersion, the orientation of the dispersed phase, and the compounding strategies. Alternatively, the polymer can be infiltrated into 1D, 2D, 3D preforms creating high content polymer nanocomposites.

2.3 Biopolymer

Polymer is a large molecule composing, hundreds of thousands of atoms formed by successive linking of one or two, occasionally more types of small molecules into the chain or network structures. Biopolymers are a class of polymers produced by living organisms [25, 38, 39]. Cellulose and starch, proteins and peptides, and DNA and RNA are all examples of biopolymers, in which the monomeric units, respectively, are sugars, amino acids, and nucleotides [40]. Biopolymers are polymers formed in nature during the growth cycles of all organisms; hence, they are also referred to as natural polymers [25]. Their synthesis generally involves enzyme-catalyzed, chain-growth polymerization reactions of activated monomers, which are typically formed within cells by complex metabolic processes.

2.4 Gelatin

Gelatin is also a protein obtained by partial hydrolysis of collagen, the main component present in the bone and skin of animals [41]. Gelatin is derived from collagenous materials via thermal denaturation [42]. Practically, gelatin is extracted with hot water at a temperature higher than its mother collagen's thermal transition temperature. It has been widely applied in the food, pharmaceutical, biomedical, cosmetic, and photographic industries. Gelatin is produced from collagenous materials, mainly from porcine and bovine

skin and bone [41]. Most of the raw materials for gelation production are from animal slaughtering or animal source food processing.

2.4.1 Classification of gelatin

The major raw materials of gelatin production are generally from bovine and porcine bone or skin, which are approximately 46% and 52% of the global demand, respectively [42]. Raw materials from other mammals such as goatskin and camel bone have been proved to be promising sources for gelatin production. Fish skin, bone, and scale, etc., generated as the leftover from fish processing, are widely used for the production of gelatin and its derivatives [20]. Those raw materials are abundant and cheap. Moreover, gelatin can be also extracted from the other parts of fish, such as the fish head and swim bladder. Apart from porcine, bovine, and fish collagenous materials, avian and amphibian processing leftovers are also used for gelatin production. Chicken and duck feet and chicken and turkey heads obtained from slaughtering or dressing could be used as the alternative raw material for gelatin production.

2.4.2 Synthesis of gelatin

Gelatin production can be divided into 3 major steps, including pretreatments (non-collagenous material removal and swelling processes), extraction with water at high temperature, and clarification/drying (hot air drying or spray drying or freeze-drying) [20]. Evaporation, clarification, deodorization (only for fish gelatin), and sterilization can be implemented prior to drying as optional steps. This is dependent on the type of material and specification of final products [41]. Non-collagenous proteins are generally removed by an alkaline solution such as sodium hydroxide, while fat and minerals are eliminated by non-polar solvent and HCl, respectively. The swelling process is carried out by acidic or alkaline processes, based on the complexity of raw material. The acid and alkaline processes are used for materials with a low and high degree of crosslinking, respectively [41]. The gelatin obtained by the acidic process is called type A gelatin, whereas the gelatin manufactured from the alkaline-treated raw material is named type B gelatin. Acid introduced for acid pretreatment is generally organic acid, especially acetic acid, while the alkali used are sodium hydroxide or calcium hydroxide [42].

2.4.3 Properties of gelatin

Characteristics of gelatin are influenced by both intrinsic and extrinsic factors. These include isoelectric point, amino acid compositions, and molecular weight distribution, etc., and are considered as the factors determining the functional properties and applications of gelatin. The amount of aspartic acid and glutamic acid in type B gelatin is higher than that of type A gelatin. Gelatin contains glycine (33%), proline (12%), alanine (11%), and hydroxyproline (10%) as the major amino acids but has the low contents of histidine, methionine, and tyrosine [41, 42]. The functional property of gelatin can be divided into two groups. The first group is the functionality associated with surface or interfacial behavior, such as the formation of emulsion, foam, and film. The latter group is functionality related to gelling properties. Gelatin can be used as a gelling agent or provide elasticity, consistency, and stability to food products. Gelatin can be also served as coating or edible/biodegradable packaging due to its film-forming ability, where transmission of light and oxygen into agricultural produces or foods during storage can be prevented [20].

2.5 Carbon Nanotube

Carbon Nanotubes (CNTs) are one of the most interesting carbon allotropes in the form of cylinders arranged by rolling graphite sheets, which results in the deformation of their sp^2 hybrid orbitals with the formation of a σ-p rehybridization structure [43, 44]. These were discovered soon after the laboratory synthesis of fullerene by Sumio Iijima in 1991 of the NEC Corporation in the soot of an arc discharge apparatus. Two years later, in 1993, two groups: NEC and IBM reported CNT consisting of a single layer of graphene. Since their discovery, CNT showed a huge contribution in the field of physics, chemistry, mathematical modeling, material sciences, etc. [45, 46]. Fig. 2.5 shows a schematic illustration of different types of CNTs.
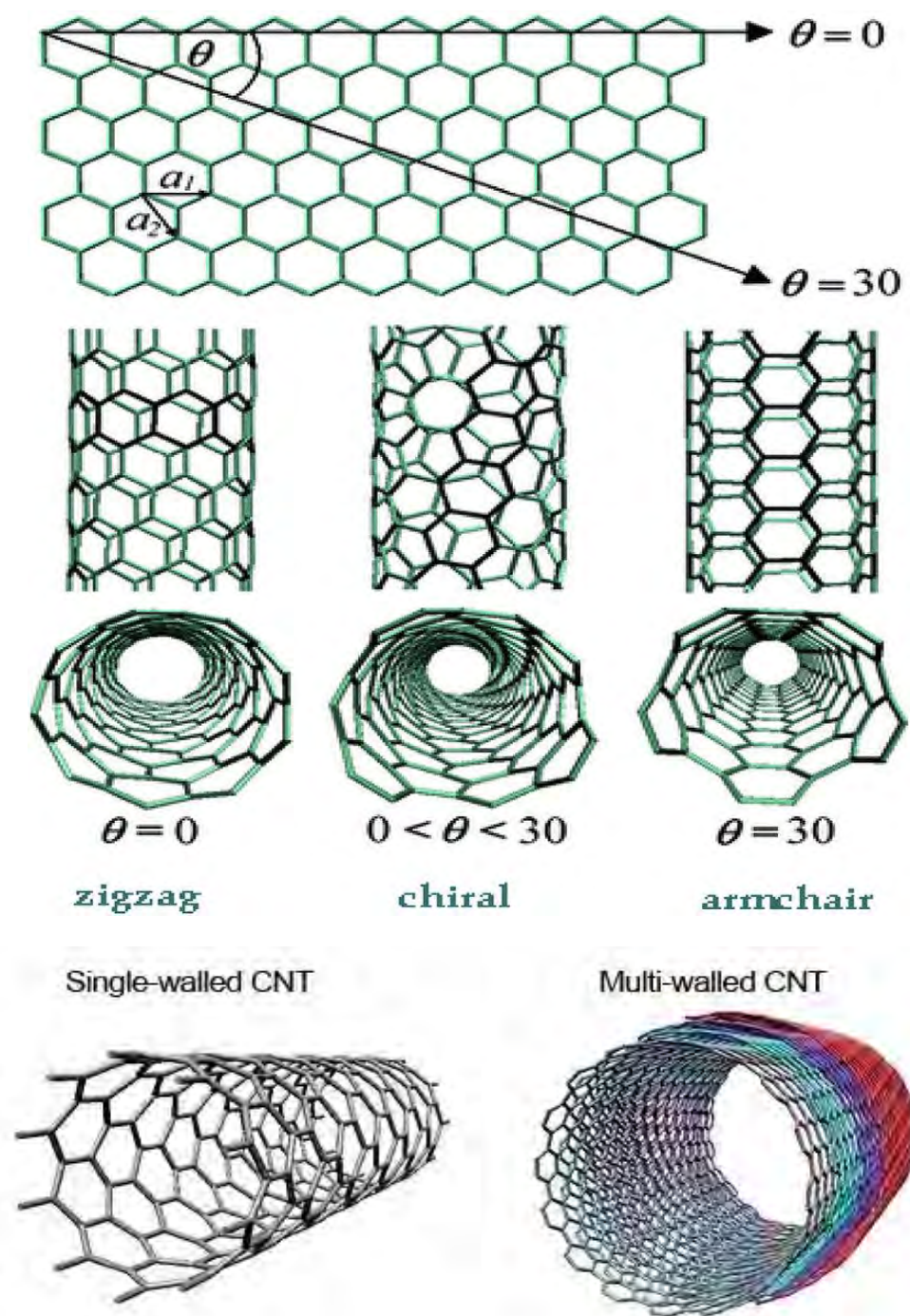
Fig. 2.5 Schematic illustration of different types of CNTs [42].

2.5.1 Classification of CNT

There are mainly two types of CNTs: single-walled carbon nanotube (SWCNT), and multi-walled carbon nanotube (MWCNT).

2.5.1.1 SWCNT

SWCNTs generally contain single sheets of graphite wrapped seamlessly to form a cylinder structure with hexagonal and pentagonal faces. The properties and geometry of SWCNTs are denoted by the rolling direction (or chiral angle, h) and diameter resulting from a pair of integers (n, m). SWCNTs form a metal-like material with an arm chiral geometry, while they are most likely to behave as semiconductors in a zigzag geometry [43, 44].

2.5.1.2 MWCNT

In the case of MWCNTs, they consist of an array of concentric cylinders similar to rings in a tree trunk. Synthesis methods for CNTs include carbon arc discharge, laser ablation, and chemical vapor deposition (CVD) [43, 44]. The first two methods can produce amounts of SWCNTs at the gram level and involve the evaporation of solid carbon to generate hot gaseous condensation. However, special equipment is required and the high energy consumption rate makes these methods generally undesirable.

2.5.2 Synthesis of CNT

2.5.2.1 Laser method

This method involves shooting a laser at a graphite target in the presence of a metal catalyst. When the target is hit with the laser, the carbon ablates and jets out. The ablated carbon phase includes the metal catalysts, which then cool and crystallize into nanoparticles from which the SWCNTs grow. A continuous flow of a gas, such as Ar, is used to move the product to the collector. The type of catalyst used, whether a pure metal or a mixture of atom types, can influence whether the CNTs are straight and graphitized or tangled with potentially more defects. The catalytic particles play a crucial role in the synthesis of nanotubes through the laser method [43].

2.5.2.2 Arc method

In this method, a high current electric arc goes through graphite electrodes in the presence of catalytic particles to form CNTs and soot. The MWCNTs produced this way were first made as a byproduct of the production of fullerenes. As such, much of the optimization of arc production for MWCNTs has been developed as a secondary process. However, currently, the largest commercial suppliers of MCWNT materials utilize the core material from arc production [44]. The presence of specific metal catalytic particles determines whether the method produces MWCNTs or SWCNTs.

2.5.2.3 Chemical vapor deposition method

The chemical vapor deposition (CVD) process is catalytically driven, wherein a metal catalyst is used in conjunction with the thermal decomposition of a hydrocarbon vapor to produce nanotubes. In most cases, the resultant growth of nanotubes occurs on a fixed substrate within the process. A wide range of transition metals and rare earth promoters have been investigated for the synthesis of both SWCNTs and MWCNTs by CVD [7, 9, 10]. The most common metals found to be successful in the growth of SWCNTs and MWCNTs are Fe, Co, and Ni. On the whole, Fe and Ni constituents the most commonly used catalysts.

2.5.3 Properties of CNT

Carbon nanotube has the simplest chemical composition and atomic bonding configuration but exhibits an extreme variety and richness in structures and structure-property relations. CNT derive most of their properties from graphene. In graphene, the arrangement of carbon atoms is a regular sp^2-bonded atomic-scale honeycomb (hexagonal) pattern. CNT structure may be considered as a graphene sheet rolled into a tube. Among all the allotropes of carbon, CNT is the most widely studied because it possesses a unique hollow structure which gives it extraordinary mechanical, thermal, and electrical properties like low density, high tensile strength/stiffness better than any metal (high Young's modulus at 1200 GPa and tensile strength at 150 GPa), enhanced thermal conductivity exceeding diamond, high electrical conductivity, high ductility, high thermal and chemical stability, etc., which makes them suitable for various applications. They are

1D ballistic conductors, i.e., they can transmit electrons over a long distance. The low-temperature specific heat and thermal conductivity indicate direct evidence of 1D quantization of the phonon band structure [43, 44].

2.6 Dielectric Properties

Dielectrics are non-conductors of electricity, but because they consist of positively and negatively charged particles bound together, their interaction with the applied electrical field is significant. The fundamental action of the field is to separate positive and negative charges of the entire volume of the dielectric, causing what is known as the polarization of the dielectric. Fig. 2.6 shows the effect of the polarization. The charges create their electric field E_p which is directed to the left and thus oppose the external field E_0. When we add this polarization field E_p to the external field E_0, to obtain resultant field E, we find that $E < E_0$. Thus, the polarization of the medium reduces the electric field in its interior. Now, if each of the particles of a solid possesses a dipole moment, the total dipole moment of the sample would be, $p = \sum_i q_{i r_i}$. The polarization P in a solid is defined as the dipole moment per unit volume, $P = \frac{p}{V}$ [36].
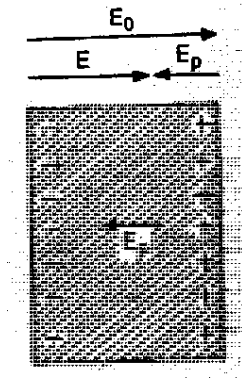
Fig. 2.6 Effect of polarization in dielectric materials

The electric field E is defined as the force F per unit charge acting on a test charge q, $E = \frac{F}{q}$. Measurement of E in space is easy because all we have to do is to place a small test charge there and observe the force on it [36].

2.6.1 Dielectric constant:

Consider a parallel-plate capacitor consisting of two plane-parallel plates of area A and separation d, charge with a surface charge density σ. If the space between the plates is a vacuum and if d small compared with the dimensions of the plates, there will result in an electric field between the plates, its strength is given by, $E_{Vac} = \frac{\sigma}{\varepsilon_0}$ [37]. The potential difference between the plates is equal to, $V_{Vac} = E_{Vac}d$, and the capacitance of the capacitor is defined by, $C_{Vac} = \frac{A\sigma}{V_{Vac}}$. Suppose now that the space between the plates is filled with an insulating substance, the charge on the plates being kept constant. It is then observed that the new V is lower than V_{vac} and the capacitance C of the capacitor is increased. The dielectric constant ε is then defined by, $\varepsilon = \frac{V_{Vac}}{V} = \frac{C}{C_{Vac}}$ [37].

2.6.2 Frequency dependence of dipolar polarizability

When the field is switched on, the dipoles tend to line up with the field. But it takes time i.e., there is a lag in the attainment of equilibrium polarization. The time required to reach equilibrium polarization is expressed in terms of the relaxation time, τ which is defined as the time that makes the polarization attain nearly two-third of its equilibrium value. On account of this finite time, it is clear that if the applied field changes (say, it is switched off and on frequently) in a time short compared to τ the dipole system cannot respond to the changes. Consequently, the polarizability dies off at high frequencies of the applied field. In particular, if, $E(t) = E_0 e^{i\omega t}$, then polarizability approaches to zero value when, $\omega \gg \frac{1}{\tau}$ and its dc value if $\omega \ll \frac{1}{\tau}$ i.e. if the oscillations are slow compared to τ [38]. Now, from the definition of the complex dielectric constant, $\varepsilon(\omega) = \varepsilon'(\omega) - i\varepsilon''(\omega)$; the expressions result, $\varepsilon'(\omega) = n^2 + \frac{\varepsilon(0) - n^2}{1 + i\omega^2\tau^2}$ and, $\varepsilon''(\omega) = n^2 + \frac{\varepsilon(0) - n^2}{1 + i\omega^2\tau^2}\omega\tau$ [38, 39]. These equations are frequently referred to as the Debye equations. Fig. 2.7 shows these equations graphically. We note that the real part $\varepsilon'(\omega)$ is a constant, equal to $\varepsilon(0)$ for all frequencies in the range, $\omega \ll \frac{1}{\tau}$; this frequency range usually covers all frequencies up to the microwave region. In the frequency range, $\omega \geq \frac{1}{\tau}$, it decreases, eventually reaching the

value n^2. This result is quite expected. The imaginary part $\varepsilon''(\omega)$ has its maximum at $\omega = \frac{1}{\tau}$ and decreases as the frequency departs from this value in either direction. It may be added here that a part of the electrical energy is dissipated in the dielectric in the form of heat. This is a consequence of the fact that the polarization in alternating fields lags in phase relative to the applied field. It can be proved that the rate of this loss is proportional to, $\varepsilon''(\omega)$, and is thus maximum at, $\omega = \frac{1}{\tau}$ [39].
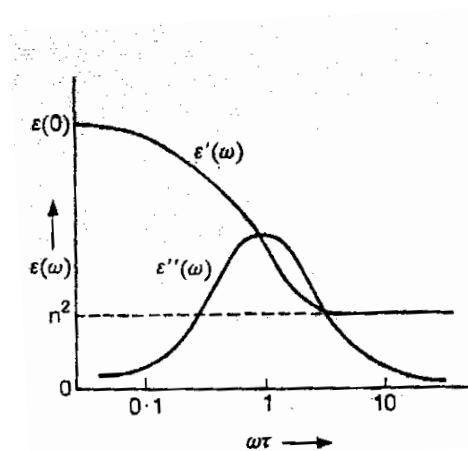
Fig. 2.7 Debye curves for ε' and ε'' for a dipolar substance.

2.7 Electrochemical Properties

Electrochemistry is a powerful tool to probe reactions involving electron transfers. Electrochemistry relates the flow of electrons to chemical changes. In inorganic chemistry, the resulting chemical change is often the oxidation or reduction of a metal complex. An electrode is an electrical conductor, typically platinum, gold, mercury, or glassy carbon [44]. Through the use of an external power source, the voltage can be applied to the electrode to modulate the energy of the electrons in the electrode. The driving force for this electrochemical reaction is again the energy difference between that the electrodes. Changing the driving force of a chemical reduction requires changing the identity of the molecule used as the reductant. Fig. 2.8 shows the electrochemical workstation equipment established in the nanocomposite laboratory.

Fig. 2.8 Electrochemical workstation in the nanocomposite laboratory.

2.7.2 Introduction to the electrochemical cell

In the experimental section of papers describing electrochemical measurements, a brief description is generally given for the experimental setup used to collect the data. The vessel used for a cyclic voltammetry experiment is called an electrochemical cell. Fig. 2.9 shows a schematic representation of an electrochemical cell for CV experiments. All the components of this cell are described briefly in the later sections.
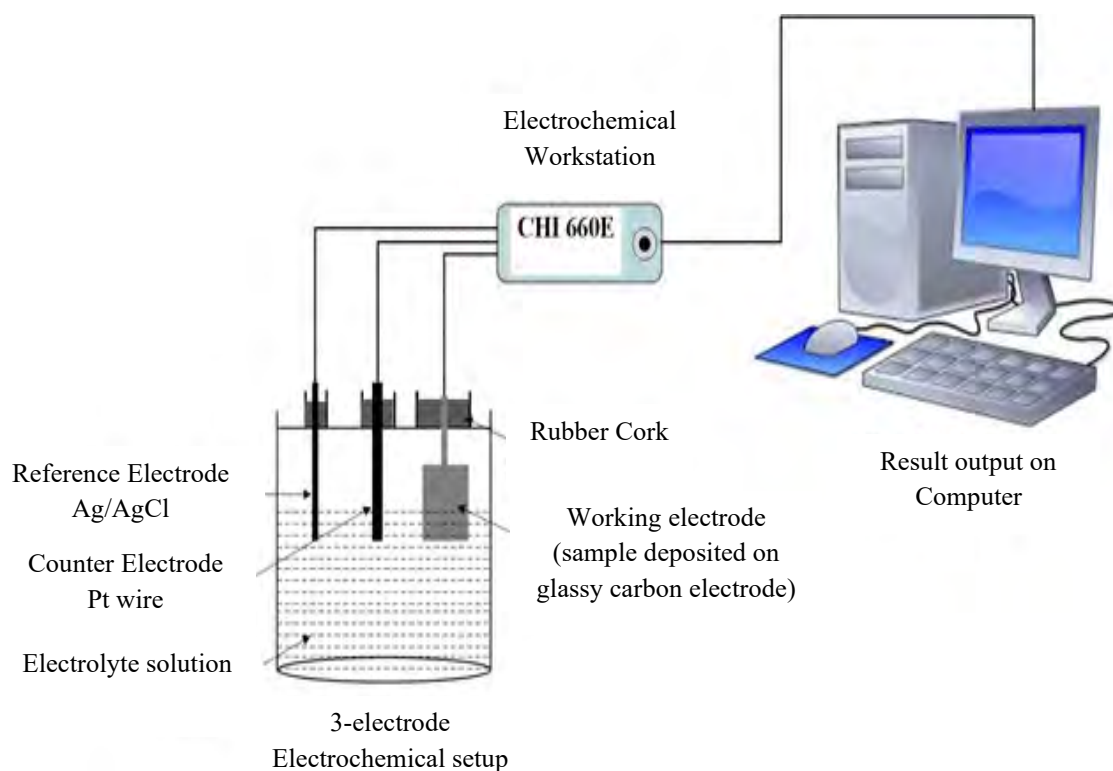
Fig. 2.9 Schematic representation of an electrochemical cell for experiments.

2.7.3 Preparation of electrolyte solution

As electron transfer occurs during a CV experiment, electric neutrality is maintained via the migration of ions in the solution. As electrons transfer from the electrode to the analyte, ions move in solution to compensate for the charge and close the electrical circuit. A salt, called a supporting electrolyte, is dissolved in the solvent to help decrease the solution resistance. The mixture of the solvent and supporting electrolyte is commonly termed the "electrolyte solution." Solvent. The conductivity of the solution is dependent on the concentrations of the dissolved salt [45]. Without the electrolyte available to achieve charge balance, the solution will be resistive to charge transfer.

2.7.4 Working electrode

The working electrode carries out the electrochemical event of interest. A potentiostat is used to control the applied potential of the working electrode as a function of the reference electrode potential. The most important aspect of the working electrode is that it is composed of redox inert material in the potential range of interest [46]. The type of working electrode can be varied from experiment to experiment to provide different potential windows or to reduce/promote surface adsorption of the species of interest. Because the electrochemical event of interest occurs at the working electrode surface, the electrode surface must be extremely clean and it's surface area well-defined. When using electrodes such as glassy carbon or platinum, clean electrode surfaces can be prepared via mechanical polishing. To remove particles, the electrode is then sonicated in ultrapure water. It is often also necessary to perform several CV scans in simple electrolytes across a wide potential window to remove any adsorbed species left over from the polishing procedure. This procedure is sometimes referred to as "pretreating" the electrode [47].

2.7.5 Reference electrode

A reference electrode has a well-defined and stable equilibrium potential. It is used as a reference point against which the potential of other electrodes can be measured in an electrochemical cell. The applied potential is thus typically reported as "vs" a specific reference [48]. There are a few commonly used (and usually commercially available) electrode assemblies that have an electrode potential independent of the electrolyte used in the cell. Some common reference electrodes used in aqueous media include the saturated calomel electrode (SCE), standard hydrogen electrode (SHE), and the AgCl/Ag electrode. These reference electrodes are generally separated from the solution by a porous frit. In nonaqueous solvents, reference electrodes based on the Ag^+/Ag couple are commonly employed [49]. These consist of a silver wire in a solution containing an Ag^+ salt, typically $AgNO_3$.

2.7.6 Counter electrode

When a potential is applied to the working electrode such that reduction (or oxidation) of the analyte can occur, the current begins to flow. The purpose of the counter electrode is to complete the electrical circuit [52]. Current is recorded as electrons flow between the WE and CE. To ensure that the kinetics of the reaction occurring at the counter electrode does not inhibit those occurring at the working electrode, the surface area of the counter electrode is greater than the surface area of the working electrode [55]. A platinum wire or disk is typically used as a counter electrode, though carbon-based counter electrodes are also available. When studying a reduction at the WE, oxidation occurs at the CE. As such, the CE should be chosen to be as inert as possible [55, 56].

CHAPTER 3

MATERIALS AND METHOD

3.1 Materials

Gelatin powder (type B from bovine skin, ~200 Bloom) and glycerol (98% pure) were obtained from Sigma-Aldrich. Materials were used as bought freshly without any further modification.
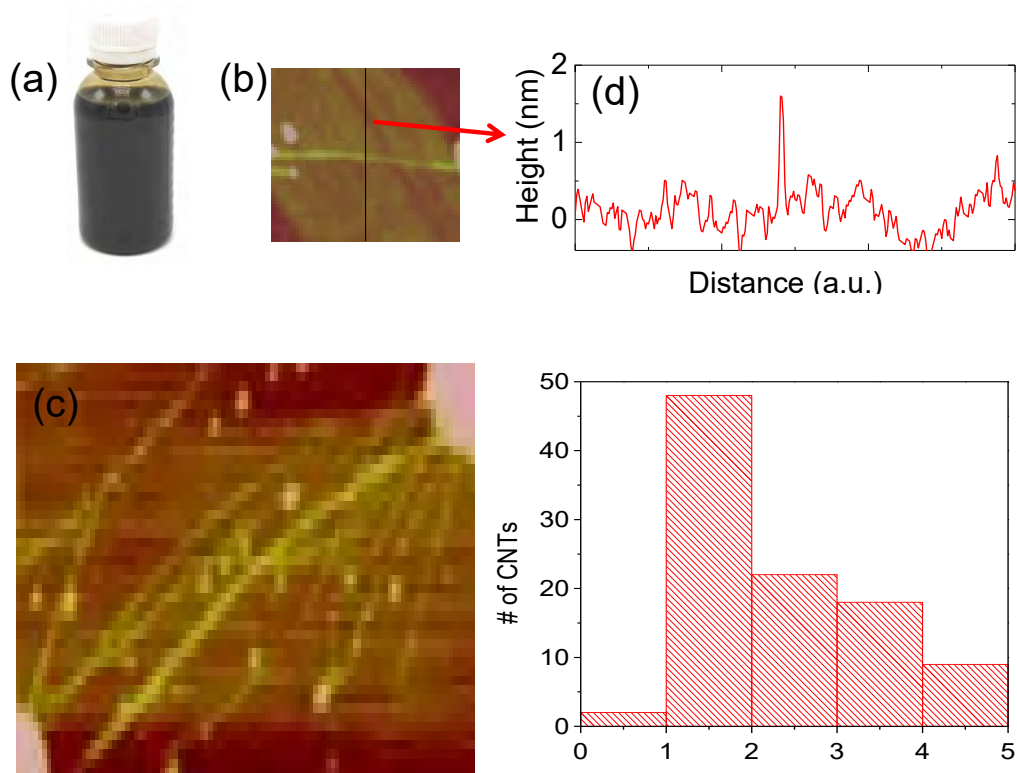
Fig. 3.1 Solution-processed CNT (a), their AFM images (b-c), average height distribution (d) and diameter (e) obtained from AFM.

The single-wall carbon nanotube (well-dispersed aqueous suspension) with a concentration of SWNTs ~50 μg/ml was obtained from Brewer Science. The solution contains mostly individual SWNTs with an average length of ~1–2 μm [8, 10]. Fig. 3.1

displays the tapping-mode AFM image and the diameter distributions of a couple of CNTs respectively. The bar diagram shows that the diameter of the SWCNTs varies between 0.5 – 5.0 nm [47]. The average height and diameter measured through AFM images of the MWCNT and the SWCNTs are as follows:

- ❖ The average diameter of the MWCNT: 30 nm

- ❖ The average length of the MWCNT: 10 μm

- ❖ The average diameter of the SWCNT: 1.4 nm

- ❖ The average length of the SWCNT: 1.5 μm

3.2 Preparation of Gel/MWCNT Nanocomposite Film

All the aqueous solutions were prepared with DI water. An appropriate amount of gelatin was mixed with DI water and was heated up to 50 °C with continuous magnetic stirring until they dissolved properly. For the synthesis of nano-composite, high quality, MWCNTs were dispersed in DI water with a little amount of gelatin solution using a probe sonicator. They were sonicated for some time until a homogenously dispersed solution was attained. MWCNT of different proportions (0 wt% to 0.05 wt%) were mixed in the previously obtained gelatin solution. At that point, glycerol was added with this solution as a plasticizer. Furthermore, the solution was stirred at 70 °C for about half an hour approximately. The obtained solution was then cast on a glass petri dish and was kept open

at room temperature for several hours. Later the films were peeled out carefully from the petri dish and they were ready for studying different characteristics.
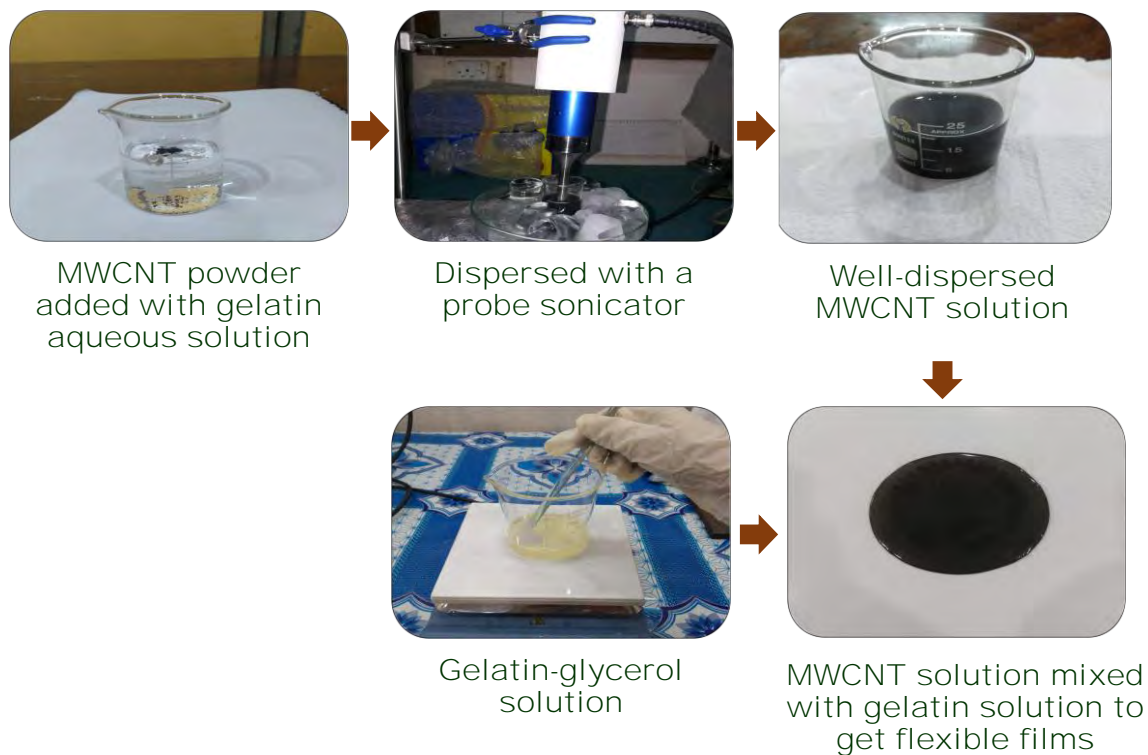
Fig. 3.2 The synthesis procedure of Gel/MWCNT nanocomposites by solution casting method.

Fig. 3.3 Color transformation of the Gel/MWCNT nanocomposites from pale yellow to dark ash with the gradual increase of the filler content.

3.3 Preparation of Gel/SWCNT Nanocomposite Film

To prepare the composite at first, 5.25 grams of gelatin was mixed with 30 ml of DI water (17.5 w/v%) and heated up to 50 °C with continuous mechanical stirring until it dissolved properly. After making a proper solution of gelatin, 1.75 ml glycerol was used as the plasticizer here maintaining a ratio of 3:1 for gelatin to glycerol. This ratio was found to the optimal among the different gelatin to glycerol proportional samples that were made
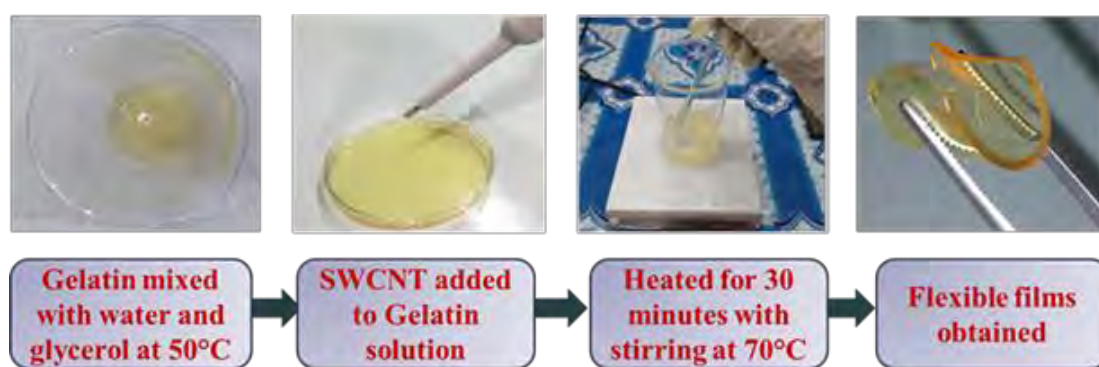
Fig. 3.4 The synthesis procedure of Gel/SWCNT nanocomposites by solution casting method.

before. For the synthesis of nano-composite, high quality, well-dispersed SWCNT aqueous solution was used. SWCNT of different proportions (0 vol%, 0.125 vol%, 0.25 vol% and 0.5 vol%) were mixed in the previously obtained gelatin solution. Furthermore, the solution will be stirred at 70 °C for another 30 minutes approximately. The obtained solution was then cast on a glass petri dish and then kept open at room temperature for 72 hours. Afterward, these samples were conditioned in 30% relative humidity for about 24 hours. Then the films were peeled out carefully from the petri dish and were ready for studying different characteristics. Later the films were stored covering aluminum foil paper.

3.4 Preparation of the Electrodes

The glassy carbon electrode was used as the current collector in this preparation. The electrode was cleaned by rubbing on a smooth paper in an 8-fashioned way and the mass of the electrode was measured in a digital weight machine which has an accuracy of up to

± 0.0001 gm. Then a tiny drop of the prepared material was deposited directly on the top contact surface of the electrode. Then the electrode was dried at room temperature for 2 hours. Finally, vacuum dried for 1 hour, and then again, the mass of the electrode was measured. Mass of the deposited material was found from the difference of masses measured from before and after the deposition.

3.5 Characterization Techniques

The presence of different groups in the cross-linked nanocomposites was studied by Fourier transform infrared spectroscopy (FTIR) analysis. The chemical analysis by FTIR in attenuated total reflection (ATR) mode was carried out using a (Shimadzu IRSpirit) spectrophotometer at a spectrum range of 500-4000 cm^{-1}.

Raman analysis was carried out at room temperature using a 785 nm diode laser (Power ≤ 5mW) as an excitation source (HORIVA MacroRam) to study the vibrational structure of the synthesized NPs.

The surface morphology of the cross-section of the Gel/ SWCNT nanocomposite was observed by a field emission scanning electron microscope (FESEM) using JEOL JSM-7600F at an accelerating voltage of 5 kV. Before imaging, the composites were coated with a thin gold/palladium layer.

The water contact angle was measured with a contact angle meter (Apex, India) using the sessile drop method, at room temperature and controlled humidity. The measurements were performed using a 10 µL drop of water on the film surface. The contact angles were measured by the tangential method. For each film, the contact angle was measured three times on different sites of the surface, and the average value was considered.

A UV–VIS spectrophotometer (Dynamica HALO DB-20S) was used to analyze the optical properties of the nanocomposites. The optical data were taken at room temperature within the wavelength range from 400–1000 nm.

The DC electrical properties of the nanocomposite were studied by a homemade four-point collinear probe setup featuring gold-coated spring-loaded pins. Van der Pauw

four-point collinear probe methods were applied for the investigation of the electrical properties of the nanocomposite. The resistivity, ρ of the thin films were calculated using the formula, $\rho = 2\pi s(V/I)$ [48]. Where V is the potential difference between the inner probes in volt, I is the current through the outer pair of probes in ampere, s is the spacing between the probes in meter.

The Young modulus, tensile strength, elongation break, ductility, and toughness of the samples were measured on a universal testing machine (Wance ETM 501, maximum capacity 50 KN) at room temperature with gauge length 5 mm, width 2 mm, and thickness less than 0.2 mm and a crosshead speed of 10 mm/min. A standard test method for tensile properties of thin plastic sheeting (specification D882-02) was followed. An average value of five replicates for each sample was taken for the tensile tests.

Thermal properties of Gel/CNT nanocomposites were studied by differential scanning calorimetric (DSC) analysis. For DSC, the samples were heated from 25 ^{0}C to 250 ^{0}C. Each time the samples were heated at a rate of 10 ^{0}C/min and were kept in a nitrogen atmosphere at a flow of 40 ml/minutes to avoid thermo-oxidative degradation.

The dielectric properties of the samples were measured with a portable network analyzer (FieldFox N9923A, Agilent Technologies Inc.). Dielectric permittivity ε' was evaluated by measuring the capacitance (C) of the film, $\varepsilon' = \frac{Cd}{A\varepsilon_0}$; where d = thickness of the film, A = effective area of the film, ε_0 = permittivity of free space. Dielectric loss tangent, $tan\delta$ was obtained directly from the analyzer. The formula used to calculate the imaginary part of the dielectric permittivity is, $\varepsilon'' = \varepsilon' tan\delta$. The formula has been used to determine AC conductivity is, $\sigma_{AC} = \omega\varepsilon_0\varepsilon' tan\delta$ [15, 59].

Electrochemical properties of the nanocomposites were analyzed in a three-electrode system consisting of the glassy carbon electrode as a working electrode, a platinum foil plate (1×1 cm^2) as the counter electrode, and silver/silver chloride electrode (Ag/AgCl) as reference electrode, and 0.1 M KCl was used as an ionic aqueous electrolyte solution. The cyclic voltammetry (CV), Galvanostatic charge/discharge (GCD), and electrochemical impedance spectroscopy (EIS) were measured by using CS310 Electrochemical Working

Station (Corrtest, China). The CV and GCD were observed over a voltage range from -0.2 V to 0.7 V, and the EIS was recorded in the frequency range of 0.01– 100,000 Hz by applying an AC voltage perturbation of 10 mV. 2000 GCD cycles were performed at a current density of 100 mA/gm from -0.2 V to 0.7 V voltage window. All the electrochemical tests were carried out at room temperature. The specific capacitance C_S (Fg^{-1}) of the biocomposites was calculated integrating the area under the cyclic voltammogram (CV) curves according to the following equation, $Cs = \frac{1}{v.m.(V2-V1)} \int_{V1}^{V2} i(V)dV$ [50, 51]. Here, v is the voltage scan rate, m is the weight of the active material, and $(V_2–V_1)$ is the applied potential window. The specific capacitance can also be calculated from the Galvanostatic charging-discharging curve, using the equation, $Cs = \frac{Idisch}{m} \frac{dt}{dV}$ [36, 50]. Here, I_{disch} is the discharge current and dV/dt is the slope of the discharging curve. The energy density, E and the power density, P is calculated with the following formula, $E = \frac{Cs \times \Delta V^2}{7.2}$ and $P = \frac{E \times 3600}{\Delta t}$; where, C_S = specific capacitance calculated from GCD graph, ΔV = operating voltage window and Δt = discharge time [50, 52].

CHAPTER 4
RESULTS AND DISCUSSION

4.1 Characterization of Gel/MWCNT Nanocomposite

4.1.1 Structural properties analysis using FTIR spectroscopy

Fourier Transform Infrared (FTIR) spectroscopy was performed to analyze the structural properties of the as-prepared Gel and Gel/MWCNT nanocomposites. Fig. 4.1.1

Fig. 4.1.1 FTIR Spectra of Gel/MWCNT nanocomposites for various amounts of MWCNT filler content.

illustrates the FTIR spectra of all the nanocomposite samples from 500 cm^{-1} to 4000 cm^{-1} wavenumber range. From Fig. 4.1.1 a broad and deep absorption peak is observed between 3100 cm^{-1} to 3600 cm^{-1} which corresponds to the strong stretching vibration of the -OH

group of the trapped moister from the solution that remained in the sample [53]. Other characteristic peaks for the peptide groups of gelatins such as amide-A, B, I, II, III are also noticed here. The peak at 2935 cm^{-1} for amide-A represents the NH- stretching coupled with hydrogen bonding. The peak of Amide B situated at 2883 cm^{-1} originates from the stretching of CH- and NH_4^+ [54]. Absorption peaks located at 1638 cm^{-1}, 1542 cm^{-1}, 1254 cm^{-1} are corresponding to amide-I, II, III, respectively. Amide- I arise from the C=O stretching vibrations whereas amide -II represents the bending of N-H groups associated with the stretching of C-N groups. Amide -III arises due to vibration of CH_2 group [55]. The addition of MWCNT does not add any additional peak may be due to low concentration. However, the increase of intensity and slight shift of the peak's position with accordance to MWCNT concentration indicates a possible interaction has occurred among the MWCNTs and the -OH group of water and glycerol of the solution along with NH_2- groups of gelatins. Thus, MWCNTs allocate themselves to these intermediate locations. A reduction in the intensity, as well as a peak shift towards the higher wavenumber side of the absorbance peaks, are observed with the addition of more filler content. These happen maybe for additional interaction between the glycerol-modified gelatin and MWCNT fillers [42, 55]. The MWCNTs might have attached themselves to the suitable functional sites (different amide groups and hydroxyl groups) of the polymer skeleton [56].

4.1.2 Structural properties analysis using Raman spectroscopy

Raman spectroscopy technique has been used to probe the interaction between the polymers and the nanotubes. Generally, in the Raman spectrum, the interaction between nanotubes and polymer is reflected by a peak shift or a peak width change [58].

Fig. 4.1.2 shows Raman spectra of the film taken in the frequency region between 1150-1550 cm^{-1}. There exist the G-band that consists of the broadband at 1450 cm^{-1} and a structured group of the bands at about 1270 cm^{-1} assigned to G^+ and G^- modes, respectively. The G^+ and G^- modes are originated from E_{2g} graphite mode due to the circumferential confinement in CNT [57]. No visible change in the polymer peak locations as a result of the insertion of nanotubes could be detected but only some of the peaks shifted slightly towards

Fig. 4.1.2 Raman Spectra for Gel/MWCNT nanocomposites with different concentrations of MWCNT nanofiller.

the higher wavenumber side. This occurs for the shortening of the bond length between the molecular components. These results from the breathing mode of MWCNTs are largely affected by the surroundings of the individual tube. For instance, the outer diameter of the nanotubes is reduced as a consequence of the physical constraint introduced by the surrounding polymer chains, and this radial deformation is believed to contribute to a local mechanical interlocking mechanism for nanotubes [58]. The polymer exerts pressure on the individual tubes, thereby increasing the breathing mode frequencies. Hence the bond length shortens between the polymer Gel and MWCNT molecules and therefore the good dispersion of MWCNTs into the Gel matrix is verified evidentially. Intensity is significantly changed as the more MWCNTs embed into the Gel matrix the stronger the interaction between them occurs.

4.1.3 Surface morphology

The surface morphology of the Gel/MWCNT nanocomposites was observed by the Field Emission Scanning Electron Microscope (FESEM). The FESEM images of the nanocomposites at × 5000 magnification are shown in Fig. 4.1.3 The fracture surface of the pure Gel sample looked smooth, and no residual structure of MWCNT was observed. The good dispersion of MWCNT was confirmed by the SEM images up to 0.02 wt% MWCNT nanocomposites. An increment in the density and a slight overlapping of the MWCNT fillers
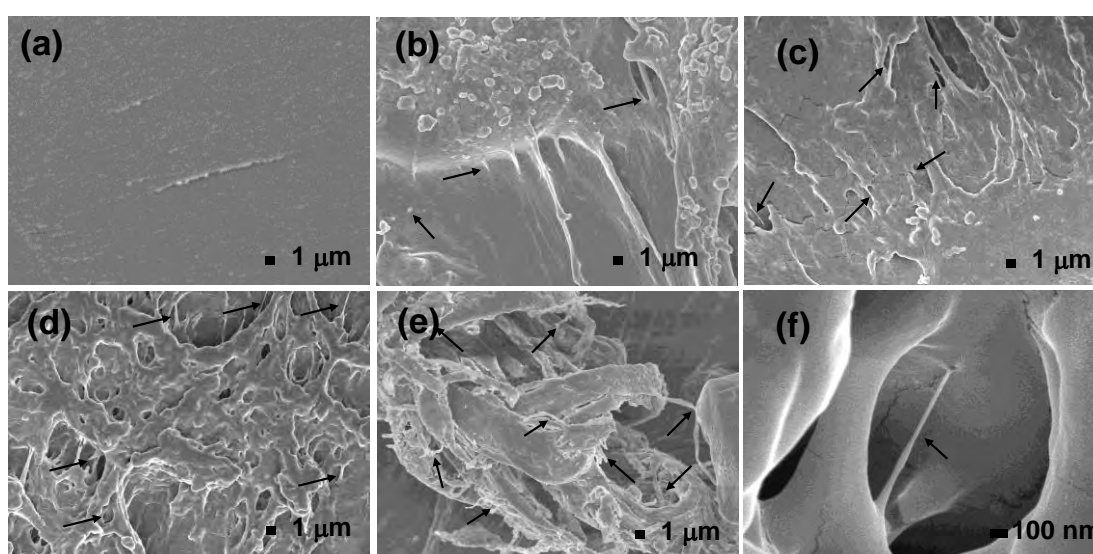
Fig. 4.1.3 FESEM images of the Gel/MWCNT nanocomposites with (a) 0 wt%, (b) 0.005 wt%, (c) 0.01 wt%, (d) 0.02 wt% and (e) 0.05 wt% of MWCNT concentrations at ×5000 magnification (a-e). Fig (f) shows the FESEM images for the Gel/0.02 wt% MWCNT nanocomposite at × 50000 magnification.

in the Gel matrix was found in the highest MWCNT concentration sample. From Fig. 4.1.3(e) it was observed that the CNTs form a cluster in the Gel/0.05% MWCNT nanocomposite. At higher concentrations, the CNTs tend to agglomerate due to the van der Walls force [64]. Similar morphological behavior was also observed for Gel-based carbon nanotube composite films where CNTs form a bundle at higher concentrations [47]. Additionally, the roughness of the nanocomposite increases with the concentration of MWCNT. The increase in roughness means a larger surface area is created.

4.1.4 Surface wettability

The surface wettability property of the as-prepared nanocomposites was observed by contact angle meter and is displayed in Fig. 4.1.4. The water contact angle (WCA) for the
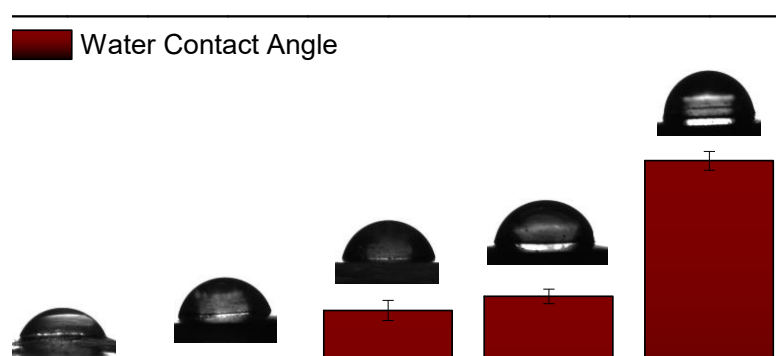
Fig. 4.1.4 The change in water contact angle of Gel/MWCNT nanocomposites for different concentration of MWCNTs.

materials showed a transition from hydrophilic to a moderately hydrophobic character for incorporation of MWCNT into the Gel sample. This might be because of the uneven surface and surface roughness of the sample with MWCNT [39, 59]. The contact angle for Gelatin was found to be 67° which confirmed its hydrophilic nature, but with the incorporation of MWCNTs WCA rose. After incorporating 0.02 wt% of MWCNT, the WCA increased to 120.25° and the nanocomposite became hydrophobic. This happens as the MWCNTs are generally highly hydrophobic due to their non-polar structure [10, 48], so only a trifling amount of filler can make the Gel material moderately hydrophobic. The carboxyl groups of

MWCNTs along with the hydroxyl groups of gelatins are responsible for the lesser water uptake [30].

4.1.5 Optical properties

Fig. 4.1.5 (a) shows the absorption spectrum of the pure Gel and Gel/MWCNT nanocomposites. This graph shows that the absorbance of the composite samples increased with the increase of the CNT content. The addition of MWCNTs showed a visible change of the sample's color and displayed good absorbance in this spectrum of light. With the incorporation of CNTs, more light has been absorbed. The energy band gaps of the nanocomposites were calculated from the intercept of the plots of $(\alpha h v)^{1/2}$ versus photon energy (hv) which is shown in Fig. 4.1.5 (b). A direct and simple method for probing the band structure of the nanocomposites is the measurement of the absorption spectrum. The absorption coefficient, $\alpha (v)$ was calculated from the absorbance, $A (v)$ and the value of $\alpha (v)$ was calculated using the Beer-Lambert law, $I = I_0 \, exp \, (-\alpha X)$ [60] where I_0 and I are the incident and the transmitted intensity, and X is the thickness of the cuvette (here, is the sample's thickness). The relationship between the fundamental absorption and the optical energy gap is given from the optical band gap energy, $E_g = hc/\lambda$. Here, c is the velocity of light and at high absorption coefficient levels for non-crystalline materials. The absorption coefficient is calculated using the Tauc and Devis-Mott relation as follows: $(\alpha h v)^n = \beta(hv - E_g)$ [61, 62] where β is a constant and the exponent, n can assume the values of 1, 2, and 3 for allowed direct transition, and for allowed indirect transition, it takes the values of $\frac{1}{2}$ and $\frac{3}{2}$. The best fit to the absorption spectra was obtained using n equal to $\frac{1}{2}$ that suggests the electron transition allows indirect transition for the nanocomposites [63]. It can be seen that the plots are linear in the region of strong absorption near the fundamental

absorption edge and indicate absorption takes place through an indirect transition. Adding the CNT to the gelatin matrix causes easy transmission of a photon through the composite's materials. This may be giving evidence of decreasing the energy gap by the addition of the

Fig. 4.1.5 (a) Optical absorbance of the Gel/MWCNT nanocomposites, (b) Tauc plot for calculating the optical bandgap of the materials.

Table. 4.1 Optical bandgap of different Gel/MWCNT nanocomposite samples.

MWCNT concentration (wt%)	Optical Band Gap Energy (eV)
0	1.25
0.005	1.20
0.01	1.18
0.02	1.17
0.05	1.10

MWCNT in the polymer matrix. Adding MWCNTs to the gelatin matrix causes localized states of different color centers to overlap and extend in the mobility gap [63, 64]. This

overlap may give evidence for decreasing the energy gap by the addition of the MWCNTs in the polymer matrix. The values of energy band gaps (E_g) for the pure gelatin and gelatin/MWCNT nanocomposites obtained from Fig. are summarized in Table 4.1.

4.1.6 Electrical properties

The variation of the DC resistivity of the Gel and Gel/MWCNT composites is shown in Fig. 4.1.6. The DC resistivity of the nanocomposites was found to be significantly decreased by about 4 orders of magnitude due to the incorporation of MWCNTs in the Gel matrix. For the pure gelatin sample, DC resistivity was measured around 57 MΩ-cm. This value decreased down to only 12 kΩ-cm for incorporation of only 0.005 wt% MWCNT in the polymer matrix. Gel/0.05 wt% MWCNT sample showed DC resistivity of around 2.5

Fig. 4.1.6 Variation of the DC resistivity of Gel/MWCNT nanocomposites as a function of MWCNT content.

kΩ-cm. Gelatin is a biopolymer and electrically behaves like an insulator [30]. But the incorporation of MWCNTs nanofillers gradually builds a pathway of electrons to pass through the insulating polymer complex. The main reason for this outcome is the atomic

structure of MWCNTs. MWCNTs are the folded form of sp^2 hybridized graphene sheets [43, 44]. In their atomic arrangement, there remains one free electron which shows electronic properties. When a voltage is applied to the nanocomposites the unhybridized electron take part in conducting electricity from one tube to another throughout the polymer matrix through different processes like as tunneling, hopping, or jumping where hopping or jumping is the mechanism for ionic conduction and tunneling is for electron conduction of electricity [65, 66].

4.1.7 Dielectric properties

4.1.7.1 Dielectric constant

The alteration of the real part of permittivity or the dielectric constant (ε') of the material as a function of frequency for various weight percentages of MWCNTs in Gel at room temperature is shown in Fig. 4.1.7. At lower frequency region, up to 100 Hz, all nanocomposites show near frequency-independent behavior as they undergo a sharp decrease from infinitely higher to comparatively lower value of the permittivity. The high value of dielectric permittivity at low frequency is because of the Maxwell-Wagner-Sillars (MWS) effect which is also called the interfacial polarization [67, 68]. This effect is observed in heterogeneous systems consist of two or more elements having different electrical properties. Space-charge accumulates in the microscopic interfaces of the elements of the compound mainly for the difference in the conductivities and permittivity of the constituents. The higher dielectric constant of the MWCNTs than the base polymer marks the greater dielectric constant of the nanocomposites. The sp^2 hybridized structures of MWCNT exhibit electronic properties. Due to the delocalization of the unsaturated pi bond, the electrons move freely through them under an applied electric field [43, 44]. But the insulating nature of the Gel matrix forms a boundary around the MWCNTs. As a result, MWCNT fillers in the polymer matrix act as nanocapacitors [69]. Additionally, the better dispersion of MWCNTs (confirmed by the SEM images) allows for the formation of more nanocapacitors and improves the dielectric constant of the composites. Here gelatin itself works as a surfactant, thus interacts with MWCNTs and reduces the chances of agglomeration [70]. The dielectric constant increase of Gel/0.05 wt% MWCNT sample is

fifth order in magnitude ($\varepsilon' = 10000$) the value for that of pure Gel sample ($\varepsilon' = 0.5$) at 100 Hz. Other types of polarization (atomic, electronic, dipolar) are produced by the displacement or orientation of bound charge carriers [71, 72]. All these types of polarizations may be active at low frequencies but when the frequency is increased, the dipoles find themselves unable to keep pace with the fast-changing field, so the value of ε' decreases [69, 73]. It is observed that the charge carriers undergo a decrease of dipole polarization i.e., the electrical relaxation processes at a particular frequency region, from 100 Hz to 4000 Hz for all the composites [71, 72].

Fig. 4.1.7 Frequency dependance of the dielectric constant of the Gel/MWCNT nanocomposites.

4.1.7.2 Dielectric loss factor

Fig. 4.1.8 shows the variation of the imaginary part of permittivity or the dielectric loss factor (ε'') with frequency for a different amount of MWCNT content in gelatin at room temperature. The dielectric loss factor indicates the amount of energy required to align the dipoles in the direction of the field. It is observed that the ε'' decreases as a function of
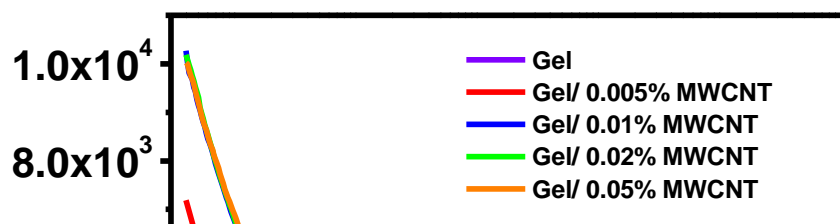
Fig. 4.1.8 Frequency dependance of the dielectric loss factor of the Gel/MWCNT nanocomposites.

increasing applied frequencies. ε'' has a low value at a higher frequency maybe because of the motion of free charges through the nanocomposites. The dielectric property depends on the conductivity of nanocomposites which may cause a decrease in both permittivity of the real part and the imaginary part as a function of the increasing frequency and a time of relaxation that exhibit low ε'' by at particular point of swiped higher frequency range. The measured imaginary part of permittivity (ε'') is a contribution of two phenomena i.e., the dipolar orientation as well as interfacial polarization of surface charges between the

electrode and Gel/MWCNT nanocomposite surface [71, 72]. And as we know that the MWCNTs provide a higher surface area to volume aspect ratio and porous structure which gives a high surface area for interfacial polarization [71, 72]. from the trap, states result in an accumulation of charge carriers and leading to an increase of the value of the dielectric constant. This interfacial polarization, also known as the Maxwell-Wagner effect, is responsible for the enhancement of the dielectric constant observed at low frequency. When an electric field is applied to the composite film, charge carriers originating from the external electrode migrate and accumulate at the interface due to the difference in relaxation time between the two components. The accumulated charge carriers can induce a polarization, ultimately resulting in an increased dielectric constant. Besides these factors, defects also play an important role; there are numerous lattices and/or topological defects and interfaces, which can bring changes in positive and negative space charge distributions, creating conditions for the formation of numerous dipole moments which enhance dielectric loss. Dielectric losses are caused by Maxwell-Wagner polarization, ionic conduction, dipole, electronic, and atomic mechanisms [71, 72]. The dielectric loss consists of two parts: One is due to Debye-type relaxation, and the other originates from the leakage current that happens near percolation. The leakage current usually leads to a large loss factor given their small percolation threshold [17, 74].

4.1.7.3 Fitting with Cole-Cole formula

Many theoretical models can be used to explain the dielectric properties of materials with the dielectric permittivity curve, depending on the number of reorientation processes or dispersions of relaxation time taking place in the material when an oscillating electric field is applied. For materials with a single reorientation or monodispersed process, the Debye relaxation model can be utilized to fully obtain the dielectric parameters of a material [75, 76]. The mathematical relation of the Debye model which relates the complex dielectric constant, $\varepsilon^*(\omega) = \varepsilon' - i\varepsilon''$, with the frequency of electric field, can be rewritten as, $\varepsilon^*(\omega) = \varepsilon_\infty + \frac{\varepsilon_s - \varepsilon_\infty}{1 + i\omega\tau}$; where ε_∞ is called the dynamic permittivity measured at the high-frequency limit of a polarizable entity when it is unable to respond to the electric field, ε_s is called the static permittivity, which is the limiting low-frequency permittivity, ω is the

angular frequency, i is $\sqrt{-1}$ and τ is the time characteristic of the response or relaxation time. Plotting ε'' with ε' in the complex plane yields a semicircle that its center is on the horizontal axis at $(\frac{\varepsilon_s+\varepsilon_\infty}{2}, 0)$ with a radius of $\frac{\varepsilon_s+\varepsilon_\infty}{2}$ [77].

Later on, Cole and Cole modified the Debye formula for the materials with polydisperse relaxation system as the Cole-Cole formula [77], $\varepsilon^*(\omega) = \varepsilon_\infty + \frac{\varepsilon_s-\varepsilon_\infty}{1+(i\omega\tau)^{1-\alpha}}$; where, α is the dispersion of the relaxation time and τ is the average relaxation time. With the help this

Fig. 4.1.9 Dielectric constant of the Gel /MWCNT nanocomposites simulated with Cole-Cole formula.

equation, the values of ε_s, ε_∞, and α have been extracted by fitting the experimental dielectric permittivity data. The average relaxation time τ has been obtained by finding the angular frequency ω at which the dielectric loss reaches its maximum value [78] (see more on the dielectric loss tangent section), so that $\tau = \frac{1}{\omega}$; The angular frequency is equal to *2πf*, where *f* is the frequency in units of Hz [77]. The best-fitted curves are shown in Fig. 4.1.9 and obtained parameters are listed in Table 4.2.

Table 4.2 Parameters obtained from the simulated dielectric constant curves of the
Gel/MWCNT nanocomposites with the Modified Cole-Cole Formula.

MWCNT concentration (wt%)	Static permittivity, ε_s	Dynamic permittivity, ε_∞	Dielectric strength, $\Delta\varepsilon=(\varepsilon_s-\varepsilon_\infty)$	Relaxation time, τ_o (µs)	α
0	0.78	-415.15	415.93	----	1.11
0.005	2.10	-2482.86	2484.96	7.3	1.37
0.01	2.71	-2741.71	2744.42	2.5	1.38
0.02	1.93	-5522.45	5524.38	0.93	1.36
0.05	2.21	-5323.28	5325.49	31.8	1.34

From the obtained fitting parameters, it can be concluded that the dielectric strength ($\Delta\varepsilon = \varepsilon_s - \varepsilon_\infty$) [77] which represents the effective moment of the orienting unit, increases with the addition of MWCNT in the Gel matrix. From pure Gel where no relaxation peak was observed, the calculated relaxation time of for sample Gel/0.005 wt% MWCNT, Gel/0.01 wt% MWCNT, Gel/0.02 wt% MWCNT, and Gel/0.05 wt% MWCNT are 7.5 µs, 6.54 µs, 2.5 µs, and 31.82 µs respectively. The relaxation time decreases with increasing more amount of MWCNT means that the direction of polarization tends to align with the AC field with a shorter delay [17]. A shorter relaxation time means that the dielectric loss reaches the maximum at a higher frequency, so measuring the relaxation time is important to develop a material with stable dielectric properties. As the AC conductivity is inversely proportional to the relaxation time. So decreased value of relaxation times may result in the high value of AC conductivity.

It was observed that the dielectric strength decreased in the Gel/ 0.05% MWCNT nanocomposite. The possible reason is occurring agglomeration of nanotubes which limits the interface regions by decrement of the interfacial area between polymer chains and nanoparticles.

4.1.7.4 Dielectric loss tangent

Fig. 4.1.10 shows the dielectric loss tangent (*tanδ*), with frequency for different concentrations of MWCNT in Gel matrix at room temperature. The tangent loss for all the samples shows a single nearly Debye type relaxation peak [77]. Initially, the increase in the loss with an increase in the frequency is observed and the maxima at the particular frequency (where $\omega\tau = 1$) followed by a decrease in the high-frequency range [77]. This plot can be divided into three regions for a better understanding of the variation of tangent loss with frequency, the first is a low-frequency region, the second is a moderate frequency region, and the third one is a high-frequency region. In the low-frequency region increase of the loss may be related to the dominance of the Ohmic resistive component i.e. friction of dipoles while they tend to align with the field. While the presence of the maxima is observed only at a single frequency when the perfect matching between the frequency of electric field and frequency of molecule rotation of gelatin occurs. This resonance leads to the maximum power transfer to the dipoles in the system and hence the maximum dissipation of field energy through different processes mainly as heat [69]. Now, in the high-frequency window, the tangent loss that goes downwards may be because of the complete idleness of the dipoles to the field. Here, the part becomes frequency independent, while the capacitive part grows with the frequency. It is noticeable from Fig. that the relaxation peak shifts towards the high-frequency side which indicates the faster electron transport dynamics from one coordinating site to another due to a decrease of relaxation time [75-77].

To achieve excellent dielectric properties, a very well dispersion of CNTs throughout the polymer matrix is a must. If CNTs get agglomerated, the nanocomposite will be conductive rather than dielectric. We observed that the dielectric loss of the composite increases with increased MWCNT loading, which is because when the MWCNT loading increased, agglomeration of MWCNTs occurred and highly conductive MWCNT particles easily formed a conductive path in the composites. When the composites become more conductive, a leakage current occurred, causing part of the electrical energy to be transformed into other energy (mainly thermal) [79, 80]. As a result, the dielectric loss

Fig. 4.1.10 Variation of dielectric loss tangent of the Gel/MWCNT nanocomposites as a function of applied frequency.

(*tan δ*) of the composite increased due to the dissipation of energy when the MWCNT loading increased and a conductive route created in the whole sample, the high leakage current originated from direct contact between the MWCNTs.

4.1.7.5 AC conductivity (σ_{AC})

Fig. 4.1.11 Variation of AC conductivity of the Gel /MWCNT nanocomposites as a function of applied frequency.

The variation of the AC conductivity as a function frequency for all nanocomposites at room temperature is presented in Fig. 4.1.11. The plot consists of three distinct regions depending upon the frequency. First is the low-frequency region with a sharp rise in the conductivity due to electrode polarization, followed by a frequency-independent plateau region at an intermediate frequency (corresponds to maximum relaxation time) and, high-frequency dispersive region owing to the fast reversal of the field. All Fig. indicates that at low frequency there was a decrease in the conductivity value and may be due to the dominance of the electrode polarization effect [71, 72]. The nearly pleatue region in the intermediate frequency window may be attributed to the long-range conduction of the

charged carriers and the maximum relaxation peak slows down the increase of AC conductivity. The high-frequency dispersion region is due to the short-range ion transport (hopping) associated with AC conductivity [17].

At a lower frequency range, the interfacial polarization takes place in between the electrode and sample surface as well as between the grains and other heterogeneous areas of the sample can be observed. The bulk resistance decreases with an increase in the filler content. The conduction process is controlled by inter-filler tunneling. MWCNT is fairly well dispersed randomly in the gelatin matrix composite. Moreover, the MWCNT may connect in part, and form a partly continuous random cluster. Therefore, charges transfer easily from one domain to another results increase in conductivity. Among all nanocomposites, the Gel/0.05 wt% MWCNT sample shows high conductivity of 8×10^{-4} S/m at 10 kHz when compared to others. Whereas the pure sample (A) exhibits low conductivity of about 0.5×10^{-5} S/m at the same frequency. The low AC conductivity at a lower frequency may be due to different types of polarization (i.e., interfacial, dipolar, atomic, ionic, electronic contribution) in the material [71, 72]. The doping of MWCNT results in a decrease in both permittivity because of the contribution of the presence of dielectric relaxation characteristics in the nanocomposites. MWCNT helps in the formation of the dipole in nanocomposites i.e. dipole polarization phenomena. The overall results enhance the conductivity of the nanocomposites. Another cause for increasing the frequency-dependent conductivity may be caused by the hopping of the charge carriers in the localized states and also due to the excitation of the charge carriers to the states in the conduction band [80].

At higher frequencies, CNTs agglomerate due to van der Waals forces. The agglomeration hinders the creation of conducting paths throughout the polymer matrix that results in the decrement of the AC conductivity of the Gel/0.05% MWCNT nanocomposite.

4.1.7.6 Cole-Cole plot

The Cole-Cole plot is constructed by plotting the imaginary impedance, *Z″* as a function of the real impedance, *Z′* and is shown in Fig. 4.1.12. The modulus of the complex impedance of the composites is, $|Z| = Z′+iZ″$ [81].

Fig. 4.1.12 clearly shows that there is a semicircular arc at the higher frequency region
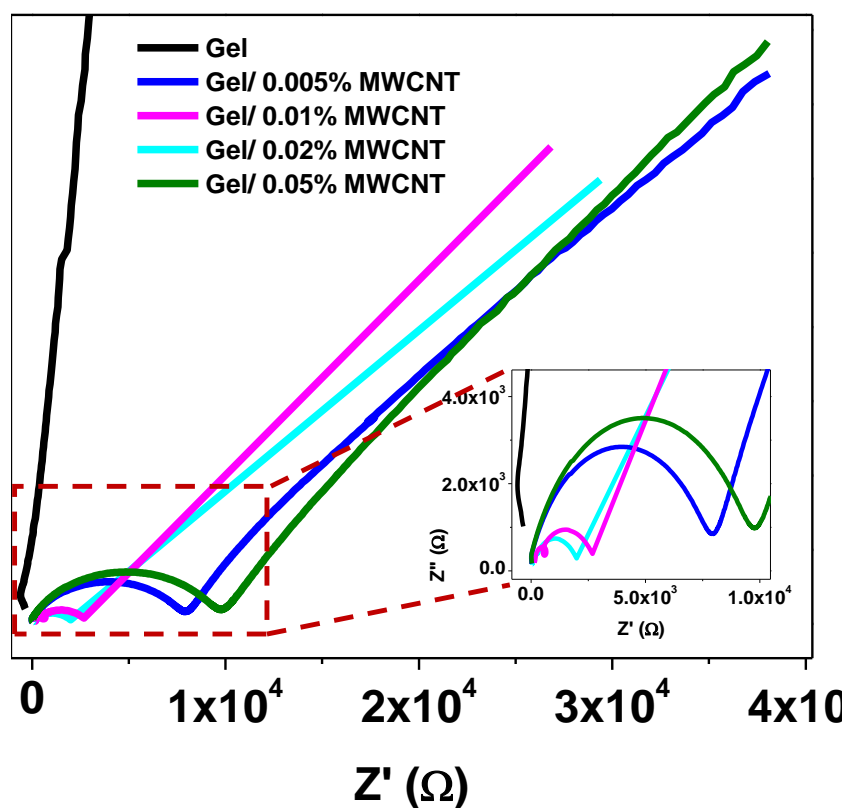
Fig. 4.1.12 Cole-Cole plots of Gel/MWCNT nanocomposites at room temperature for different amounts of filler incorporation (the high frequency region is shown in the image inset).

followed by an inclined straight line at the lower frequency region which is due to a non-Debye type relaxation in the nanocomposites [82]. In general, the values of resistance (*R*) and capacitance (*C*) of a perfect crystal can be analyzed by an equivalent circuit of one parallel resistance-capacitance (*RC)* element. This *RC* element gives rise to one semicircular arc on the complex plane, which intercepts the X-axis. For a bulk crystal containing interfacial layers, the equivalent circuit may be considered as several parallel RC elements

connected in serial. It is observed that, as the filler content increases, the intercept of the semicircular arcs on the real axis approaches the origin of the complex plane, indicating a decrease in the sample's resistivity properties.

For a quantitative analysis of the Cole-Cole plots of the Gel/MWCNT nanocomposites, different circuits were chosen to match the equivalent circuit of the complex impedance spectra of materials using EC-Lab software. The simulated impedance spectra best fitted with the equivalent circuit shown in Fig. 4.1.13 The equivalent circuit for the nanocomposites consists of two parallel circuits in series, each of them contains a resistance, R and a Constant Phase Element (CPE), Q, which is a capacitive element.

Table 4.3 Different parameters of the equivalent circuit components of the fitting Cole-Cole curves of the Gel/MWCNT nanocomposites.

MWCNT concentration (wt%)	Electrode Res., R_1 (kΩ)	Electrode Cap., Q_1 (nF)	Grain Boundary Res., R_2 (kΩ)	Grain Boundary Cap., Q_2 (nF)	Grain Res., R_3 (kΩ)	Grain Cap., Q_3 (µF)
0	65	0.002	5935	0.012	---	---
0.005	9.45	0.18	972	8.42	12.43	0.23
0.01	7.43	46.13	316	232	9.52	0.70
0.02	5.14	231.5	261	540	0.032	23.25
0.05	6.03	1.08	294	0.142	7.38	0.21
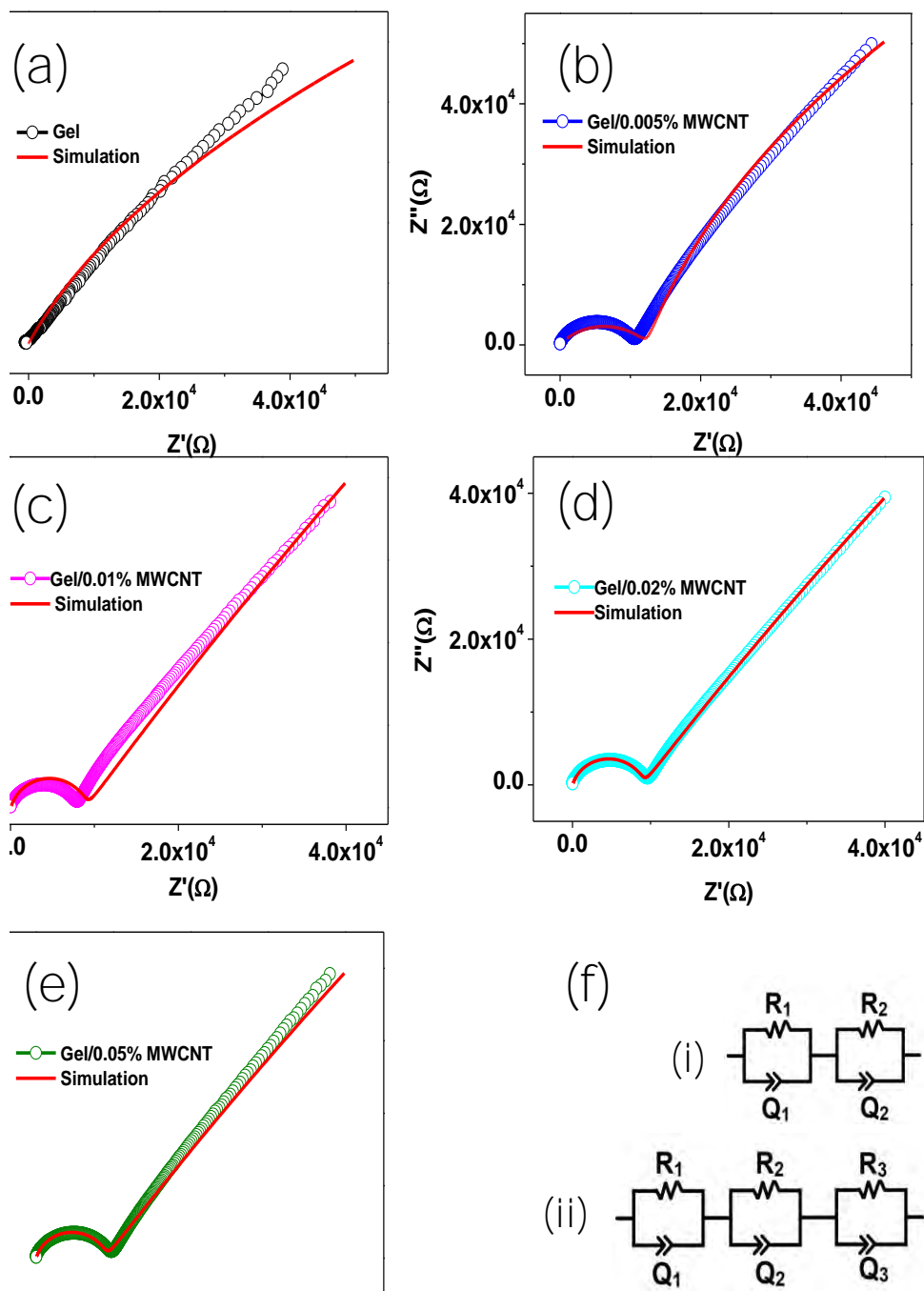
Fig. 4.1.13 The simulated complex impedance spectra of the pure Gel (a) and the different Gel/MWCNT nanocomposites (b-e). The equivalent circuits for the best fitted curves are shown in (f); where the pure Gel sample best fits for the circuit (i) and all the nanocomposite samples fit for the circuit (ii).

For getting the best fitting results, *CPE* is defined as: $Z_{CPE} = Z_0 \frac{1}{(j\omega)^n}$; where Z_{CPE} is the impedance of the constant phase angle component; Z_0 is a constant; ω is the angular frequency; j is the imaginary unit, and n is the exponential factor. When n = 1, -1, or 0, CPE is equivalent to an ideal capacitor, an inductance, or a pure resistance, respectively [17, 83, 84]. Table 4.3 gives the corresponding parameters of equivalent circuits for the Gel/MWCNT nanocomposite.

Fig. 4.1.13(f) shows the two circuits used for the simulation. The Gel sample followed the circuit (i) and Gel/MWCNT samples followed the circuit (ii). The first RC parallel circuit originates for the electrode's contribution, mainly depends on the element of the electrode. R_1 is the electrode resistance and Q_1 is the electrode capacitive element. The second parallel part of the circuit contains the grain boundary resistance R_2 and the grain boundary capacitive element Q_2. They refer to the region separating two conductive regions. The grain boundary resistance displays a huge reduction of about three orders of magnitude from 6 MΩ for Gel sample to 261 kΩ for Gel/0.02 wt% MWCNT sample. The last parallel circuit of the equivalent circuit of the nanocomposites refers to the grain i.e., the conductive regions created between the incorporated MWCNTs in the Gel matrix. From Fig. (a) it is observed that there is no such region or grain formed in the pure Gel sample. Later with the addition of MWCNT into the Gel matrix grains were formed. The grain resistance R_3 decreases from 12.43 kΩ to 0.032 kΩ and the value of the capacitive element of the grain Q_3 increases with the increasing of MWCNT. Grain and grain boundary elements show changes of a similar trend which confirm less reactive and more capacitive behavior of the nanocomposites. However, the Gel/0.05% MWCNT nanocomposite does not follow this trend. That is may be due to the agglomeration of CNTs in the higher concentrations. FESEM images also confirm the formation of the CNT cluster in Gel/0.05% MWCNT nanocomposite.

4.1.7.7 The charge transport mechanism

Based on the results obtained from the equivalent circuit analysis of the complex impedance measurements, a suitable mechanism is proposed to understand the charge transport process. Fig. 4.1.14 depicts a model to explain the complex impedance spectra of the Gel/CNT nanocomposites.
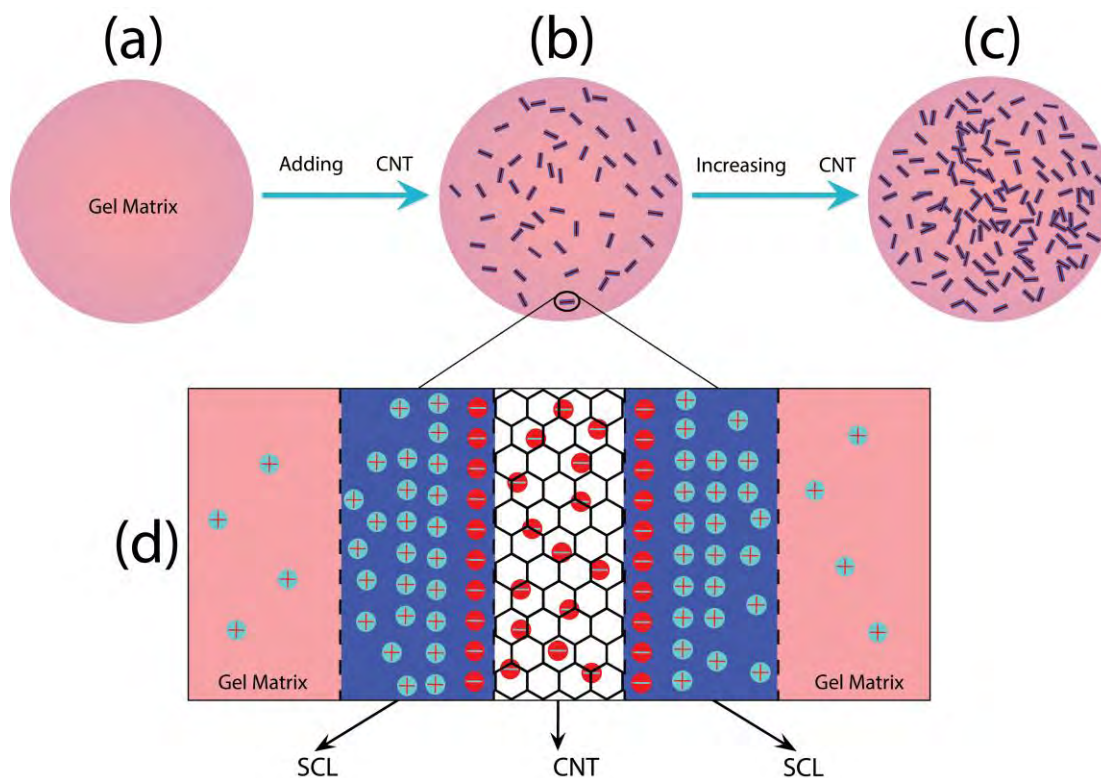
Fig. 4.1.14 Schematic representations of the mechanism of CNTs creating a capacitive layer in the nanocomposites. (a) Gel matrix, (b) incorporation of CNTs in Gel matrix at low content, (c) more CNTs creating conductive paths in Gel matrix, (d) the formation of nanocapacitive layer between the contact area of CNT and Gel matrix.

Fig. 4.1.14(a) shows the basic polymer, Gel matrix. As in Fig. 4.1.14(b) when CNTs are incorporated into the Gel matrix, the CNT provides more surface area for charge accumulation, the capacitance of the material increases (the space charge effect). The well dispersion of CNTs in the nanocomposite also facilitates to achieve larger surface area i.e., higher value of capacitance by incorporating only a trifling amount of CNT. The increased amount of CNTs as shown in the Fig. 4.1.14 (c) contributes to further enhancement of the

surface area and consequently results in a higher value of capacitance. This also assists to understand the gigantic dielectric constant of the nanocomposite material. The greater capacitive area rises the dielectric constant to the enormous value. The electrical conductivity can also be described with this model. The incorporation of CNTs in the Gel matrix enhances electron transportation throughout the matrix. Electron gets transported from one CNT to the nearby CNT through different processes like tunneling, hopping, jumping, etc. When the number of CNTs gets further increased, some of them might come close to each other and subsequently creates a conductive network throughout the matrix. This cluster of CNTs which is shown in Fig. 4.1.14(c) is also the reason for dielectric loss of the material as the probability of some leakage current arises here.

The charge accumulation between the CNT and Gel contact surface is illustrated in Fig. 4.1.14(d). When a voltage is applied to the nanocomposite material the non-hybridized electrons of each carbon atom want to take part in electron conduction, but the insulating Gel matrix hinders the flow of electrons. Therefore, electrons get accumulated near the contact surface. On the other hand, the Gel matrix is less conductive and the positive charge carriers of gelatin, glycerol, and protons of trapped water molecules get accumulated adjacent to the negatively charged CNT wall. Thus, a nanoscale capacitive layer is created in this region. More CNTs provide more capacitive regions thus capacitance increases. But the increasing concentration of CNT connects or nearly connects these regions and electrons can get transported from CNT to CNT; the conductive region i.e., grains, avoiding the Gel matrix; high resistive regions i.e., grain boundaries. This nanocapacitor formation model elucidates all the dielectric behavior of Gel/CNT nanocomposite material.

4.1.8 Electrochemical properties

4.1.8.1 Cyclic voltammetry
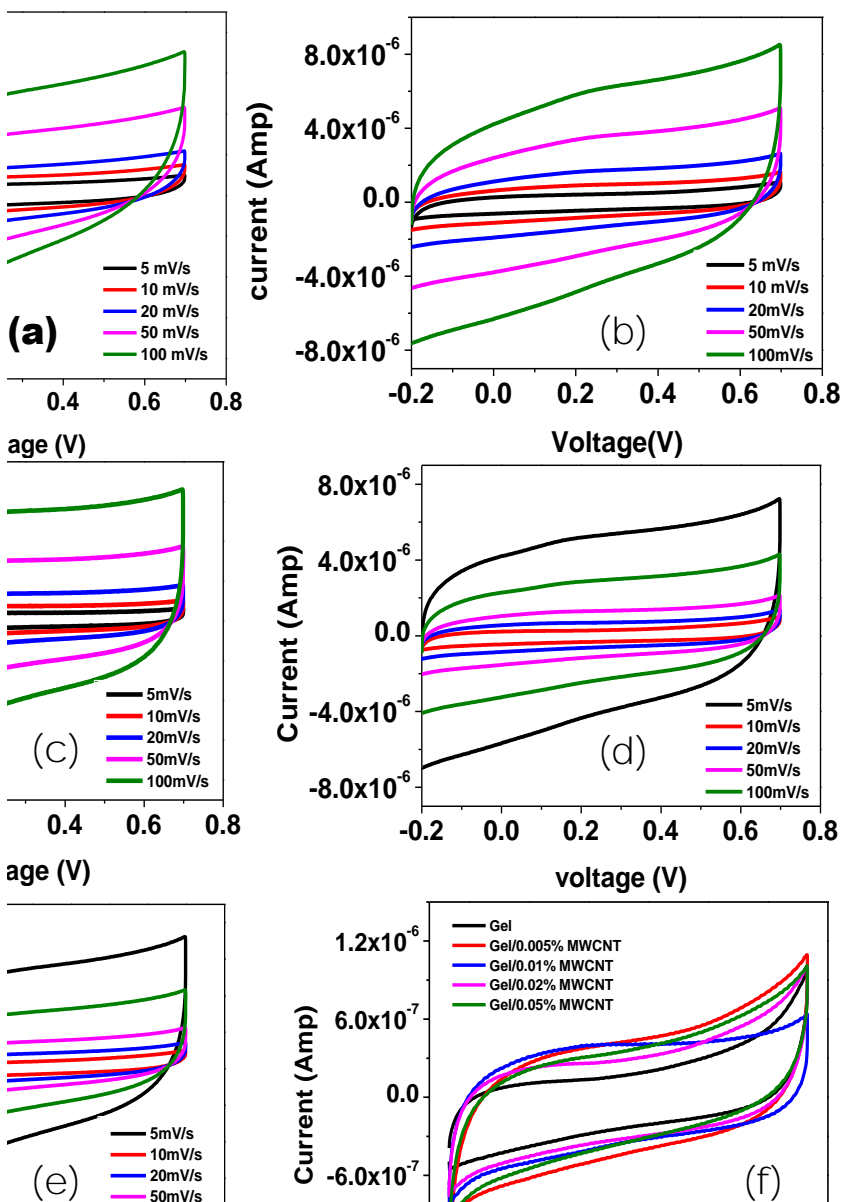
Fig. 4.1.15 Cyclic voltammetry of (a) Gel, (b) Gel/0.005 wt% MWCNT, (c) Gel/0.01 wt% MWCNT, (d) Gel/0.02 wt% MWCNT, (e) Gel/0.05 wt% MWCNT at different voltage scan rates. (f) Comparison of cyclic voltammetry of all the samples at 5 mV/s scan rate.

Cyclic voltammetry was conducted to investigate the electrochemical properties of the prepared materials. Fig. 4.1.15(a-e) shows the CV curves of the samples- at different scan rates: 5 mV/s, 10 mV/s, 20 mV/s, 50 mV/s and 100 mV/s in the voltage range from -0.2 V to 0.7 V. Observed CV curves found to be near rectangular and approximately symmetric in shape. Fig. 4.1.15 (f) gives a comparative illustration of all the nanocomposite materials at a 5 mV/s voltage sweep rate. The area of the enclosed CV curves increased with the increase of MWCNTs into the nanocomposites. This is due to the ions of the electrolyte have enough time for getting diffused into the MWCNT intermolecular regions at low scan rates [24, 85]. Thus, ions can utilize more surface area of MWCNTs rather than they can in higher scan rates [86]. At higher scan rates the charging and discharging happens too rapidly to diffuse the ions properly thus, the C_s value decreases. Although the shape of the CV curve is nearly rectangular, a slight bump of redox peak is observed at around 2.5V. This peak and the cumulative quasi-rectangular shape of the CV curves with the incorporation of the higher amount of MWCNT in the Gel matrix confirms the existence of pseudo-capacitance [11, 87]. Pseudo-capacitance could be raised from the interaction of MWCNT with the open bonds of the gelatin skeleton in the ionic electrolyte [87]. The collective effect of forming a capacitive layer and pseudo-capacitance is the reason for the increase of the C_s value with the incorporation of MWCNT [88].

4.1.8.2 Galvanostatic charging-discharging

To have more substantial information about the electrochemical properties of the Gel/MWCNT materials, Galvanostatic charging and discharging (GCD) was performed. The GCD operated at -0.2 V to 0.7 V voltage window at different current densities (0.3 µA/cm^2, 0.5 µA/cm^2, 0.8 µA/cm^2, 1 µA/cm^2, and 2 µA/cm^2). Fig. 4.1.16 (f) gives a comparative
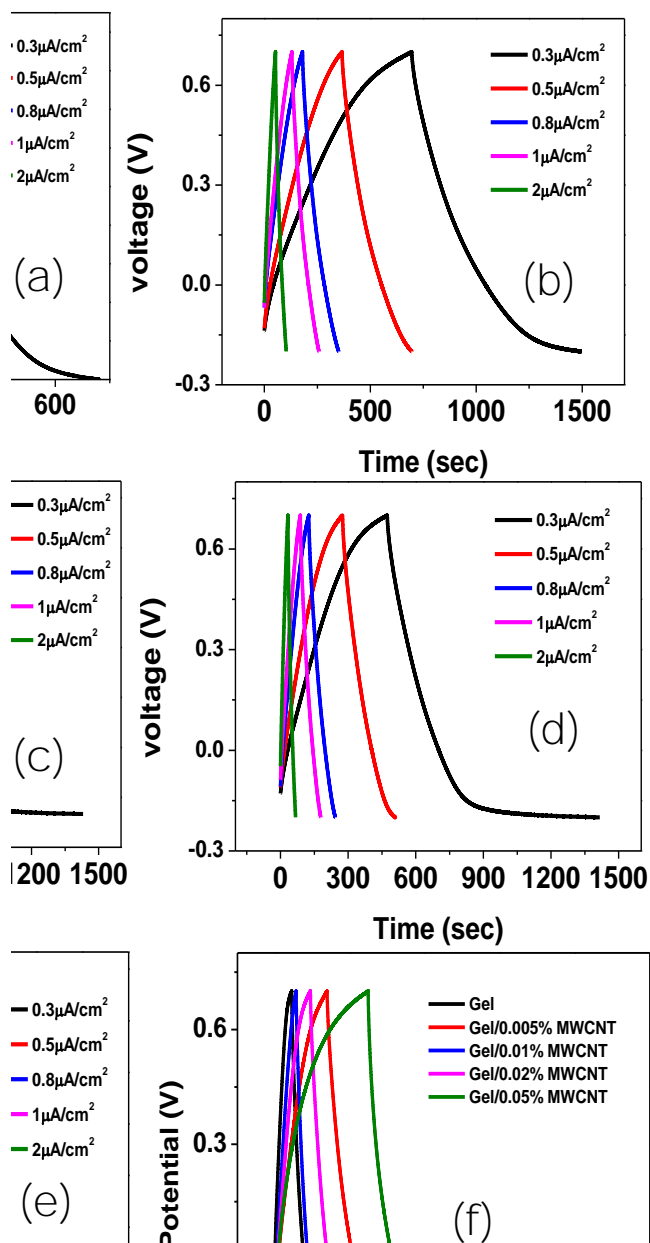
Fig. 4.1.16 Galvanostatic charging-discharging of (a) Gel, (b) Gel/0.005 wt% MWCNT, (c) Gel/0.01 wt% MWCNT, (d) Gel/0.02 wt% MWCNT, (e) Gel/0.05 wt% MWCNT at different current densities. (f) Comparison of GCD of all the samples at 0.3 μA/cm^2 current density.
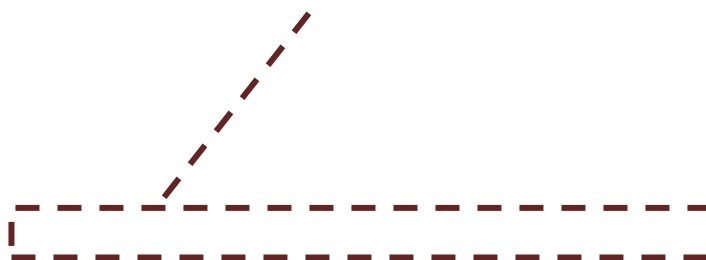
Fig. 4.1.17 Calculated specific capacitance from Galvanostatic charging-discharging of all the samples at different current densities.

all the corresponding specific capacitance, C_s values are shown in Fig. 4.1.17 exhibits an increase of C_s with MWCNT increment in the Gel matrix. Here also observed the specific capacitance is higher at lower current densities. C_s of about 12 F/g and 10 F/g were found for the Gel/0.05 wt% MWCNT respectively at 0.3 μA/cm^2 and 0.5 μA/cm^2 current densities. The reason is that at lower current density lesser amount ions come close to a certain portion of the surface area of the MWCNT wall and can diffuse themselves properly [52, 89]. Whereas at the higher surface area more ions traffic at the same certain portion of the MWCNT wall and cannot diffuse themselves enough into the MWCNT surface [89-91]. As a result, the value of C_s lowers down. Also, the charging-discharging rate accelerates at the higher current densities results in a lower value of C_s. The specific capacitance of the highest MWCNT contained sample increases about 4 times that of the pure Gel sample as the

MWCNTs form a conductive channel throughout the electrode material and increase the ion transportation [91]. The distorted triangular shape of the GCD curve also confirms the pseudocapacitance of the nanocomposites discussed in the CV part [11, 87, 88].

4.1.8.3 Electrochemical impedance spectroscopy

Nyquist plots were equipped to analyze the electrochemical impedance of the
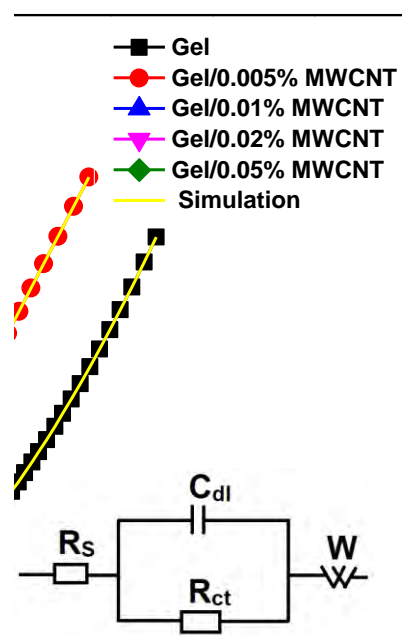
Fig. 4.1.18 The complex impedance spectra of the nanocomposites with the fitting curves. The inset image shows the higher frequency region, and the equivalent circuit for the best-fitted curves.

nanocomposite samples. To evaluate the contribution of different electrical parts in the Nyquist plot a simulation was run and the best-fitted curves along with the equivalent circuit are shown in Fig. 4.1.18. Corresponding values of the components of the equivalent circuit are recorded in Table 4.4. Different portions of the Nyquist plot carry different information about the sample's electrochemical status according to the applied frequency. In the

high-frequency region, the point where the Nyquist plot intercepts the real axis represents the value of combined series resistance, R_s; this value is the combination of the actual resistance of the electrode material, the resistance of the electrolyte, and contact resistance of the electrode and current collector [87, 92]. The value of R_s tends to decrease with the incorporation of MWCNTs in the polymer matrix from 8.4 Ω for Gel sample to 3.55 Ω for Gel/0.05 wt% MWCNT nanocomposite. MWCNTs might have created an easy route for current collectors to decrease the value of R_s [93].

The semi-circle in the high-frequency region is indicative of the electrode conductivity and

Table 4.4 Corresponding values of the different circuit components of the equivalent circuit used in simulation of the Gel/MWCNT nanocomposites.

MWCNT concentration (wt%)	Series resistance, R_s (Ohm)	Double layer capacitance, C_{dl} (nF)	CPE exponent, n	Charge-transfer resistance, R_{ct} (Ohm)
0	8.404	4	0.99	126.90
0.005	5.877	5	0.97	97.83
0.01	5.047	6	0.95	91.50
0.02	4.534	7	0.99	81.89
0.05	3.55	9	0.98	75.75

the charge transfer resistance of the electrode material [89, 93]. The radius of the semi-circle represents the value of charge transfer resistance, R_{ct} [92]. The value of R_{ct} obtained from the simulation are 126.9, 97.83, 91.50, 81.89 and 75.75 Ω for 0 wt%, 0.005 wt%, 0.01 wt%, 0.02 wt% and 0.05 wt% MWCNT sample respectively. The extraordinary electric conductivity of MWCNTs helps to decrease the charge transfer resistance of the electrode [92]. The semicircular shape arises for a parallel relation of C_{dl} with R_{ct}. C_{dl} is the capacitance of the double layer formed near the electrode-electrolyte interaction area [27, 92]. The fitted values obtained for C_{dl} are increased from 4.57 nF for the gel to 8.47 nF for Gel/0.05 wt% MWCNT nanocomposite. The internal spaces where MWCNTs are located might have

created a charge capacitive region and thus the value of C_{dl} increased [27, 92]. In the intermediate frequency region, the nearly 45° slope of the curves is described as the Warburg resistance region, which represents the ion diffusion/transport on the electrolyte and electrode contact surface [94, 95]. Overall, as electrode material, the prepared nanocomposites display well capacitive behavior.

4.1.8.4 Cyclic stability

Fig 4.1.19 The capacitive retention for 5000 cycles of GCD for the Gel/0.05% MWCNT nanocomposite. The inset shows the GCD curves for the 1st and the 5000th cycles.

Fig. 4.1.19 shows the capacitance retention of the Gel/0.05 wt% MWCNT nanocomposite and the sample retains 95% of its maximum capacitance after completing 5000 charging/discharging cycles at 2 μA/cm^2 current density. The inset image reveals the almost unchanged shape of the 1st and 5000th charging/ discharging cycle, before and after 5000 GCD cycles. The minor alteration of the resistance happens as some faradaic reaction

or corrosion occurs on the electrolyte-electrode material surface [89, 90]. This impressive cyclic stability with long cycle life enhances their compatibility as an electrode material of supercapacitor uses

4.1.9 Biodegradability analysis

Fig. 4.1.20 (a) to (h) show the degradation of the Gel/MWCNT nanocomposite film with respect to time in DI water medium at room temperature. It took only 30 hours to fully and safely disappear from the system for a $30 \times 10 \times 1$ mm^3 film. Biopolymers like gelatin are
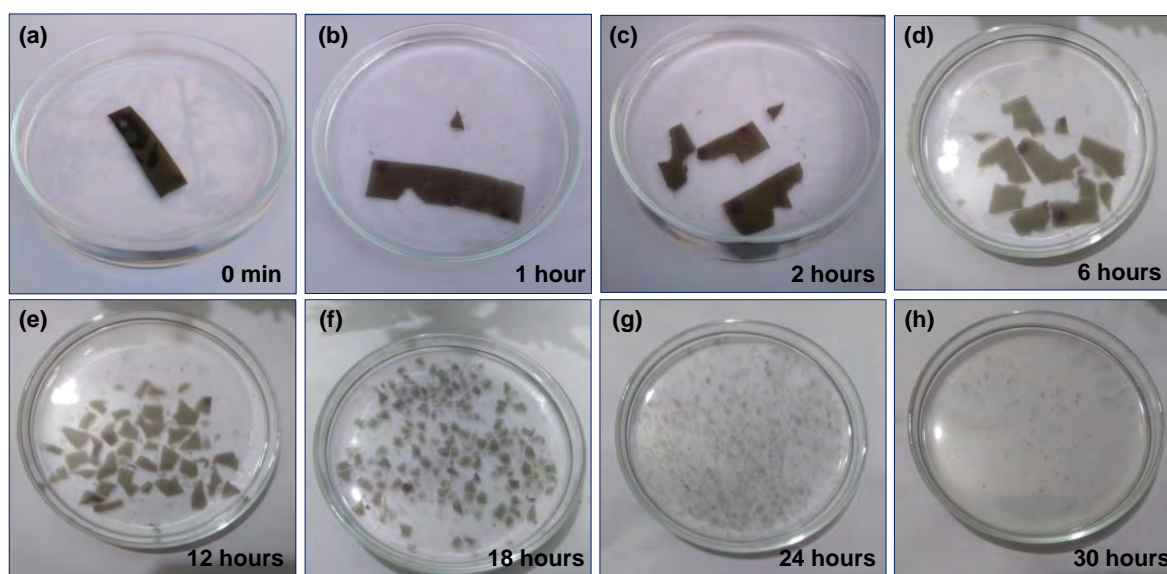
Fig. 4.1.20 Biodegradability analysis of Gel/MWCNT nanocomposites in water with respect to time.

substituted or incorporated with some hydrophilic groups such as amino acid group, alcoholic group, etc. into their backbone that can dissolve, disperse, or swell in water [36, 96]. The swelling of the gelatin sample is understandable by comparing the images. They get inflated by absorbing the water. Then the film starts to breaks into pieces only by applying a little stirring. Maintaining a fixed time interval, stirring continued as well as images were collected. Lastly, the film fully dissolves into the water without remaining any tress after 30 hours from the beginning.

4.2. Characterization of Gel/SWCNT Nanocomposite

4.2.1. Structural properties analysis using FTIR spectroscopy

Molecular components and the presence of different chemical bonds in the Gel/SWCNT nanocomposites were studied by FTIR Spectroscopy and are presented in Fig. 4.2.1. The FTIR spectra of Gel exhibits a strong, and wide absorption peak in the 3000–3600 cm^{-1} region, which corresponds to the O-H stretching vibration of hydroxyl groups of the polymer and moisture presents in the sample [23]. The peak at 1036 cm^{-1} corresponds to the alcoholic C-O bond of glycerol [42]. The peaks at 2939 cm^{-1} and

Fig 4.2.1 FTIR Spectra of Gel/SWCNT nanocomposites for various amounts of SWCNT filler content.

2865 cm^{-1} correspond to the stretching mode of the C-H group of gelatin. The peaks at 1645 cm^{-1}, 1547 cm^{-1}, and 1238 cm^{-1} correspond to the presence of amide groups [42]. No new functional bond was observed in the Gel/SWCNT nanocomposites. A reduction in the intensity, as well as a peak shift towards the higher wavenumber side of the absorbance

peaks, are observed due to the interaction between the gelatin and SWCNT fillers [54]. The SWCNTs might have attached themselves to the suitable functional sites (different amide groups, and hydroxyl groups) of the polymer skeleton.

4.2.2 Structural properties analysis using Raman spectroscopy

Raman spectroscopy technic has been used to probe the interaction between polymers and nanotubes in nanotube-based composites. Generally, the interaction between nanotubes and polymer is reflected by a peak shift or a peak width change [58].

Fig. 4.2.2 shows Raman spectra of the film taken in the frequency region of 1150-1550 cm^{-1}. There is situated the so-called G-band that consists of the broadband at 1450 cm^{-1} and a structured group of the bands at about 1270 cm^{-1} assigned to G^{+} and G^{-}

Fig. 4.2.2 Raman Spectra for Gel/SWCNT nanocomposites with different concentrations of SWCNT nanofiller.

modes, respectively. The G^+ and G^- modes are originated from E_{2g} graphite mode due to the circumferential confinement in SWCNT.

No visible change in the polymer peak locations as a result of the insertion of nanotubes could be detected but only some of the peaks shifted slightly towards the higher wavenumber side. These occur for the shortening of the bond length between the molecular components [30, 99]. These results from the breathing mode of SWCNTs are largely affected by the surroundings of the individual tube. For instance, the outer diameter of the nanotubes is reduced as a consequence of the physical constraint introduced by the surrounding polymer chains, and this radial deformation is believed to contribute to a local mechanical interlocking mechanism for nanotubes. The polymer exerts pressure on the individual tubes, thereby increasing the breathing mode frequencies. Hence the bond length shortens between the polymer Gel and SWCNT molecules and therefore the good dispersion of SWCNTs into the Gel matrix is verified evidentially.

4.2.3 Surface morphology
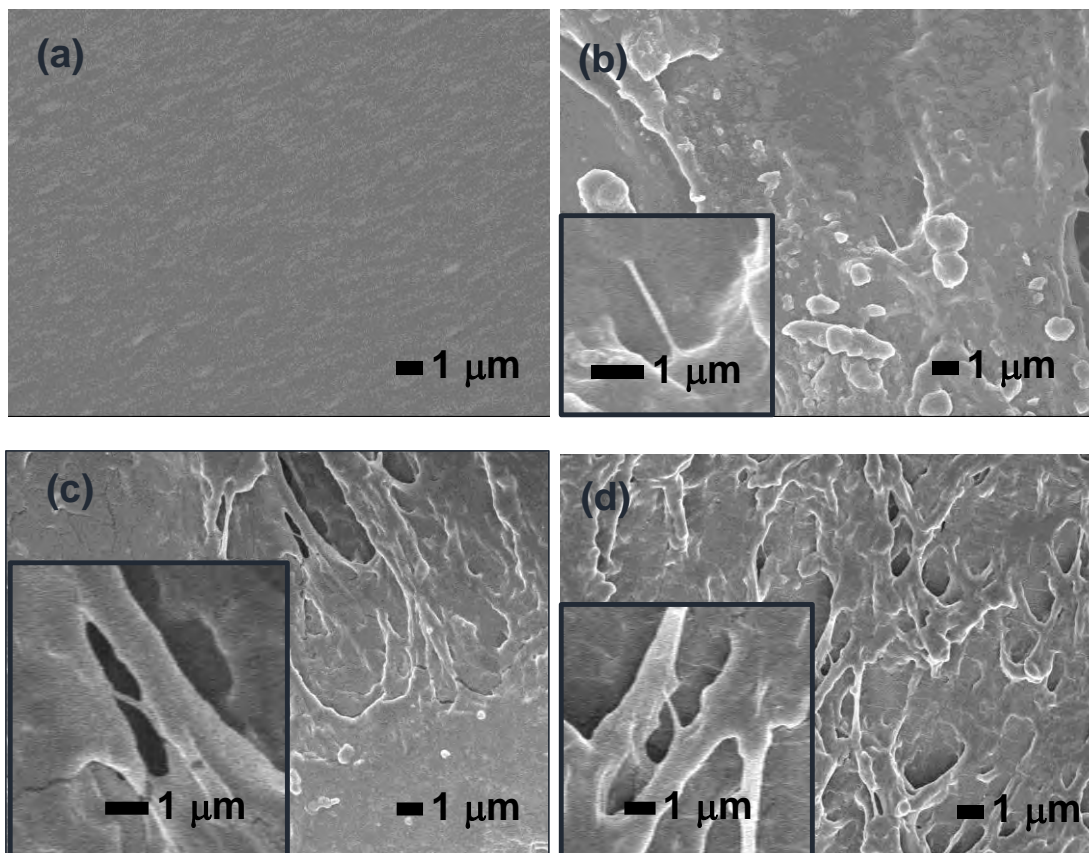
Fig. 4.2.2 SEM images of the Gel/SWCNT nanocomposites with (a) 0 vol %, (b) 0.125 vol %, (c) 0.25 vol % and (d) 0.5 vol % of SWCNT concentrations at ×3000 magnification.

The morphology of the cross-sectional surfaces of Gel/SWCNT nanocomposites was observed by the Field Emission Scanning Electron Microscope (FESEM) and is presented in Fig. 4.2.3. The surface of the nanocomposites looked smooth, and no SWCNT was observed, which may be due to the use of a very low concentration of SWCNT. However, with the increase of SWCNT filler concentration the roughness of the film got increased. Similar morphological behavior was also observed for Gel-based carbon nanotube composite films and can be attributed to the strong interfacial interactions between SWNT and the Gel matrix [97, 98]. Additionally, the roughness, as well as surface area of the nanocomposite, increased with the concentration of SWCNT creating some voids.

4.2.4 Surface wettability

The surface wettability property of the prepared material was observed and the result is displayed in Fig. 4.2.4 The water contact angle (WCA) for the materials showed a transition from hydrophilic to a moderately hydrophobic character for incorporation of SWCNT into the Gel sample. This might be because of the uneven surface and surface roughness of the sample with SWCNT [11, 59]. The contact angle for gelatin was found to
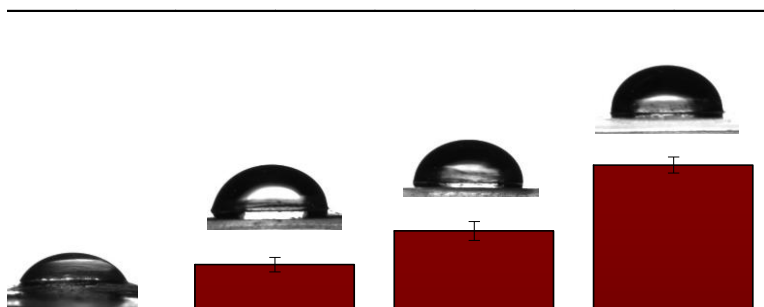
Fig. 4.2.4 The change in water contact angle of Gel/SWCNT nanocomposites with different concentration of SWCNTs.

be 66.81° which confirmed its hydrophilic nature, but with the incorporation of SWCNTs, WCA rose. After incorporating 0.5 vol% of SWCNT, the WCA rose to 106.48° and the nanocomposite became hydrophobic. This happens as the SWCNTs are generally highly hydrophobic in nature due to their non-polar structure [59, 100], so only a trifling amount of filler can make the Gel material moderately hydrophobic [117]. The carboxyl groups of

SWCNTs along with the hydroxyl groups of gelatins are responsible for the lesser water uptake [30, 59, 93].

4.2.5 Optical properties

Fig. 4.2.5 (a) presents the absorption spectrum of the pure gelatin and gelatin/SWCNT nanocomposites. This graph is showing that increasing the amount of the SWCNT content in the film improves the absorbance of the composite samples. The absorption spectra of the pure gelatin and gelatin added with 0.125 vol%, 0.25 vol%, 0.5 vol% SWCNT exhibit absorbance of 1.8%, 1.6%, 1.56%, and 1.5% respectively at the wavelength of 230 nm. As we know, the single-walled carbon nanotube is only two layers of carbon atoms and the thickness is about two atomic diameters thick. Thus, a small amount of the SWCNT acting as an antireflective coating compared to the pure gelatin sample so the absorbance decreases with increasing the filler content.

The inset image is the optical transmittance as a function of the wt% of the carbon nanotube content in the range 200 nm to 1100 nm. The optical transmittance is calculated from the absorption values using the following formula: Transmittance,
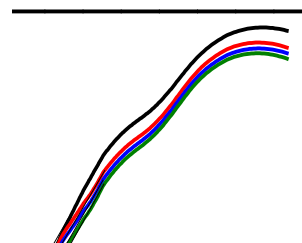
Fig. 4.2.5 (a) Optical absorbance of the Gel/SWCNT nanocomposites, optical transmittance in the inset image. (b) Tauc plot for calculating the optical bandgap of the materials.

$T = 10^{-Abs} \times 100 \%$ [30]. The addition of the SWCNT in the gelatin film shows a variation in the transmittance data. The increase of the transmittance is observed as compared to the pure gelatin thin film. The transmittance enhances from 60 % to 80 % for the increasing amount of carbon nanotube content in the visible range of the spectra which is from 500 nm to 1100 nm in the wavelength. This effect can be explained by taking into account that a

Table 4.5 Optical bandgap energy of the Gel/SWCNT nanocomposites.

Sample name	SWCNT concentration (vol%)	Optical bandgap energy (eV)
A	0	1.9
B	0.125	2.0
C	0.25	2.1
D	0.5	2.2

small amount of the SWCNT acting as an antireflective coating compared to the pure gelatin sample.

The energy band gaps of the nanocomposites were calculated based on the intercept t of the plots of $(\alpha h v)^{1/2}$ versus photon energy (hv) which is shown in Fig. 4.2.5 (b). A direct and simple method for probing the band structure of the nanocomposites is the measurement of the absorption spectrum. The absorption coefficient, $\alpha(v)$ was calculated from the absorbance, $A(v)$ and the value of $\alpha(v)$ was calculated using the Beer-Lambert law [79, 80]. It can be seen that the plots are linear in the region of strong absorption near the fundamental absorption edge and indicate absorption takes place through indirect transition [80-83]. The bandgap obtained by extrapolating the linear part to zero of the ordinates is indicated in Fig. Adding the SWCNT to the gelatin matrix causes easy transmission of a photon through the composite's materials. This may be giving evidence of decreasing the energy gap by the addition of the SWCNT in the polymer matrix. Adding the SWCNT to the gelatin matrix causes localized states of different color centers to overlap and extend in the mobility gap. This overlap may give a shred of evidence for decreasing the energy gap by the addition of

the SWCNTs in the polymer matrix [114]. The values of energy band gaps (E_g) for the pure gelatin and gelatin/SWCNT nanocomposites obtained from Fig. are summarized in Table 4.5.

4.2.6 Electrical properties

Fig. 4.2.6 Variation of the DC resistivity of the Gel/SWCNT nanocomposites as a function of SWCNT content.

The variation of the DC resistivity of the Gel and Gel/SWCNT composites is shown in Fig. 4.2.6. The DC resistivity of the nanocomposites significantly decreased for the incorporation of SWCNTs in the Gel matrix. Sample B with only 0.125 vol% of SWCNT content, exhibited a less insulating behavior in the nanocomposites. The nanocomposites displayed a dramatic decrease of around 4 orders of magnitude in their DC resistivity. For the pure gelatin sample, A, DC resistivity was measured around 57 MΩ-cm. This value decreased down to 7 kΩ-cm for incorporation of only 0.125 vol% SWCNT in the polymer matrix. Sample D with 0.5 vol% of SWCNT content showed DC resistivity of around 5.4

kΩ-cm. Gelatin is a biopolymer and electrically behaves like an insulator [50]. But the incorporation of SWCNT fillers gradually builds a pathway of electrons to pass through the insulator polymer complex. The main reason for this outcome is the atomic structure of SWCNTs. SWCNTs are the folded form of sp^2 hybridized graphene sheets. In their atomic arrangement, there remains one free electron which shows electronic properties [115, 118]. When a voltage is applied to the nanocomposites the unhybridized electron take part in conducting electricity from one tube to another throughout the polymer matrix through different processes like as tunneling, hopping, or jumping where hopping or jumping is the mechanism for ionic conduction and tunneling is for electron conduction of electricity [118].

4.2.7 Mechanical properties

Fig. 4.2.7 Stress-strain curves for the Gel/SWCNT nanocomposites.

Table. 4.6 Tensile parameters obtained from the stress-strain curves of Gel/SWCNT nanocomposites.

Sample name	SWCNT content (vol%)	Elastic Modulus, E (MPa)	Tensile Strength, s (MPa)	Elongation to break, δ (%)
A	0	0.29±0.003	1.4±0.08	37±1.2
B	0.125	0.23±0.011	1.5±0.13	47±1.1
C	0.25	0.25±0.005	1.5±0.07	46±0.8
D	0.5	0.15±0.008	1.3±0.12	59±1.5

Fig. 4.2.7 shows the stress (σ) vs. strain (ε) graph of the Gel/SWCNT nanocomposites. Different parameters obtained from this graph are displayed in Table 4.6. The elastic modulus, E was calculated using the formula, $E = \frac{\sigma}{\varepsilon}$. The elastic modulus decreased in the nanocomposites with the incorporation of CNTs in the gelatin matrix. the samples became more elastic as CNT increases. The formula used to measure the tensile strength, s is $s = \frac{p}{a}$, where, p = the force required to break and a = the cross-sectional area. The tensile strength of pure Gel was 14 MPa. The tensile strength increased at first and then decreased and gave a value of 13 MPa for Gel/0.5 vol% SWCNT. Besides, the elongation at break of the Gel/SWCNT composites was increased from 37% for the pure Gel sample to 60% for the sample with the maximum filler incorporation. The change is almost 40% of the value for pure gelatin. The formula used for the elongation at break is, δ (%) $= \frac{\Delta L}{L_0} \times 100\%$, L_0 = initial length of the material to be tested, ΔL = elongation at the breaking point [43]. These results of the mechanical properties are related to good interfacial interaction between the polymer and filler [60]. In consequence, when the nanocomposites were under tensile stress, the fillers were difficult to disconnect from the matrix and could resist and transfer

the imposed force, leading to weakening the loading stresses of the polymer matrix [116]. The abundant oxygen-containing groups created hydrogen-bonding interactions with the hydroxyl groups of gelatins resulting in improved tensile properties [43, 60].

4.2.8 Thermal properties
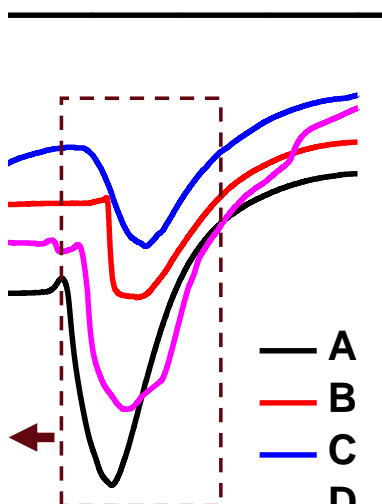
Fig. 4.2.8 DSC curves for the Gel/SWCNT nanocomposites in the temperature ranges from30 ˚C to 200 ˚C.

The thermal transition properties of the nanocomposites were studied using Differential Scanning Calorimetry (DSC) technique. Thermal information about the glass transition temperature (T_g), melting temperature (T_m), melting enthalpy (ΔH), and the degree of crystallinity (χ %) of the nanocomposites were achieved from the DSC graph is shown in Fig. 4.2.8. The degree of crystallinity was calculated using the formula, $\chi(\%) = \frac{\Delta H_f}{\Delta H_f^o} \times 100\%$ [119, 120]. Here, ΔH_f = the enthalpy of fusion of Gel/MWCNT nanocomposite and ΔH_f^o = the enthalpy of fusion of pure Gel. T_g was found to be 78 ˚C for

Gel sample and increased up to 85 ˚C with the incorporation of 0.5 vol% of SWCNT. The value of T_m also showed a similar trend. T_m increased from 248 ˚C to 256 ˚C for the highest amount of SWCNT loading. Melting enthalpy was determined by integrating the area under the melting peak, then using the above-mentioned formula degree of crystallinity was achieved [118, 119]. Their corresponding values are shown in Table 4.7. Both the melting

Table 4.7 Different parameters obtained from DSC of the Gel/SWCNT samples.

Sample	SWCNT content (vol%)	Glass Transition Temperature, T_g (°C)	Melting Peak Temperature, T_m (°C)	Enthalpy of Fusion (ΔH_f)	Degree of Crystallinity, $\varkappa$ (%)
A	0	78	248	673 (ΔH_f^0)	-----
B	0.125	80	253	380	56.46
C	0.25	81	255	405	60.18
D	0.5	85	256	636	94.50

enthalpy and the degree of crystallinity increased with the incorporation of SWCNT into the Gel matrix. The highest concentration of SWCNT contained sample D exhibited a gigantic value of the degree of crystallinity of about 94.5%. SWCNTs are highly crystalline and possess a good thermal conductivity together with heat-absorbing ability. Therefore, the addition of nanotubes accelerates the nucleation rate in gelatin. SWCNTs work as an active nucleation agent for crystallization [120, 121]. Also, all the thermal parameters tend to shift towards the higher temperature side with increasing SWCNT filler.

4.2.9 Dielectric properties

4.2.9.1 Dielectric constant

The alteration of the real part of permittivity or the dielectric constant (ε') of the material as a function of frequency for various weight percentages of SWCNTs in the Gel matrix at room temperature is as shown in Fig. 4.2.9 At lower frequency region, up to 100 Hz, all nanocomposites show near frequency-independent behavior as they undergo a sharp decrease from an infinitely higher value to a comparatively lower value of the permittivity.

Fig. 4.2.9 Frequency dependance of the dielectric constant of the Gel/SWCNT nanocomposites.

The high value of dielectric permittivity at low frequency can be explained with the Maxwell-Wagner-Sillars (MWS) effect which is also called the interfacial polarization [63, 64]. This effect is observed in heterogeneous systems consist of two or more elements having different electrical properties. Space-charge accumulates in the microscopic interfaces of the elements of the compound mainly for the difference in the conductivities and permittivity of the constituents. The higher dielectric constant of the SWCNTs than the base polymer marks

the greater dielectric constant of the nanocomposites. The sp^2 hybridized structures of SWCNT exhibit electronic properties. Due to the delocalization of the unsaturated pi bond, the electrons move freely through them under an applied electric field [22, 88]. But the insulating nature of the Gel matrix forms a boundary around the SWCNTs. As a result, SWCNT fillers in the polymer matrix act as nanocapacitors. Additionally, the better dispersion of SWCNTs (confirmed by the SEM images) allows for the formation of more nanocapacitors and improves the dielectric constant of the composites. Here gelatin itself works as a surfactant, thus interacts with SWCNTs and reduces the chances of agglomeration [63, 64]. The dielectric constant increase of Gel/ 0.5 vol% SWCNT is nearly twice (ε'=10000) the value for that of the pure Gel sample A (ε'=5000) at 100 Hz. Other types of polarization (atomic, electronic, dipolar) are produced by the displacement or orientation of bound charge carriers [89, 90]. All these types of polarizations may be active at low frequencies but when the frequency is increased, the dipoles find themselves unable to keep pace with the fast-changing field, so the value of ε' decreases. It is observed that the charge carriers undergo a decrease of dipole polarization i.e., the electrical relaxation processes at a particular frequency region, from 100 Hz to 4000Hz for all the composites [89, 90].

The comparatively higher dielectric permittivity of Gel sample A than other biopolymers [10] maybe because of the effect of the glycerol content in the polymer matrix. Glycerol can control the pH of the composite and thus may be helping in ion transportation in the nanocomposite samples [25-29]. Further investigation should be done to find the influence of glycerol on the electrical properties of gelatin composites.

4.2.9.2 Dielectric loss factor

Fig. 4.2.10 shows the variation of the imaginary part of permittivity or the dielectric loss factor (ε'') with frequency for a different amount of SWCNT content in gelatin at room temperature. The dielectric loss factor indicates the amount of energy required to align the dipoles in the direction of the field. It is observed that the ε'' decreases as a function of increasing applied frequencies. ε'' has a low value at a higher frequency maybe because of

Fig. 4.2.10 Frequency dependance of the dielectric loss factor of the Gel/SWCNT nanocomposites.

the motion of free charges through the nanocomposites. The dielectric property depends on the conductivity of nanocomposites which may cause a decrease in both permittivity of the real part and the imaginary part as a function of the increasing frequency and a time of relaxation that exhibit low ε'' by at particular point of swiped higher frequency range [89, 90]. For the low-frequency range (500 Hz to 6 kHz), the value of the imaginary part of permittivity (ε'') increases from 4500 for sample A up to 8500 for sample D. The measured imaginary part of permittivity (ε'') is the contribution of two phenomena i.e., the dipolar orientation as well as interfacial polarization of surface charges between the electrode and

gelatin/SWCNT nanocomposite surface [41, 42]. And as we know that the SWCNTs provide a higher surface area to volume aspect ratio and porous structure which gives a high surface area for interfacial polarization [89]. from the trap, states result from an accumulation of charge carriers and leading to an increase of the value of the dielectric constant. This interfacial polarization, also known as the Maxwell-Wagner effect, is responsible for the enhancement of the dielectric constant observed at low frequency [89]. In the higher frequency region, a gradual decrease in the dielectric constant was noticed. The overall decrease in the value of the dielectric constant of the composite with the increase of frequency could be due to the induced polarization process, which essentially does not follow the changes in ac frequency rapidly and causes to decrease its value gradually with the increase of frequency. The occurrence of the polarization process in the composite may be due to the existence of a large number of trap states at the grain boundaries of the synthesized samples. These trap states are generated due to the presence of defects/vacancies such as oxygen vacancies, dangling bonds, micro porosities, etc. These trap states can induce charges with different time constants. At higher frequencies, the induced charges can no longer be able to rotate with a sufficient speed and, therefore, their frequency lags behind the applied ac signal, resulting decrease in the value of the dielectric loss.

Dielectric losses are caused by Maxwell-Wagner polarization, ionic conduction, dipole, electronic, and atomic mechanisms [89, 90]. The dielectric loss consists of two parts: One is due to Debye-type relaxation, and the other originates from the leakage current that happens near percolation. The leakage current usually leads to a large loss factor given their small percolation threshold.

4.2.9.3 Fitting with modified Cole-Cole formula

As discussed in section 4.1.7.3 the Cole-Cole formula is, $\varepsilon^*(\omega) = \varepsilon_\infty + \frac{\varepsilon_s - \varepsilon_\infty}{1+(i\omega\tau)^{1-\alpha}}$ [44, 95], where, α is the dispersion exponent of the relaxation time and τ is the average relaxation time. With the help of the equation, the values of ε_s, ε_∞, and α have been extracted by fitting the experimental dielectric permittivity data. The average relaxation time τ has been obtained by finding the angular frequency ω at which the dielectric loss reaches its maximum value (see more on the dielectric loss tangent section), so that $\tau = \frac{1}{\omega}$; The angular

Fig. 4.2.11 Dielectric constant of the Gel /SWCNT nanocomposites simulated with Cole-Cole formula.

frequency is equal to $2\pi f$, where f is the frequency in units of Hz [95]. The best-fitted curves are shown in Fig. 4.2.11. All the obtained parameters are listed in Table 4.8.

Table 4.8 All the obtained parameters from the simulated dielectric constant curve of the Gel/SWCNT nanocomposites with the Modified Cole-Cole Formula.

Simulated curve	Static permittivity, ε_s	Dynamic permittivity, ε_∞	Dielectric strength, $\Delta\varepsilon = (\varepsilon_s - \varepsilon_\infty)$	Relaxation time, τ_o (µs)	α
A	6816.43	-13.82	6830.25	3.03	0.17
B	37733.24	-113.07	37846.31	1.34	0.39
C	35084.46	-89.41	35173.87	1.12	0.33
D	48109.22	-101.31	48210.53	1.01	0.34

From the obtained fitting parameters, it can be concluded that the dielectric strength ($\Delta\varepsilon = \varepsilon_s - \varepsilon_\infty$) [95] which represents the effective moment of the orienting unit, increases with the addition of SWCNT in the Gel matrix. The calculated relaxation time for samples A, B, C, and D are 3.03 µs, 1.34 µs, 1.12 µs, and 1.01 µs respectively. The relaxation time decreases with increasing more amount of SWCNT means that the direction of polarization tends to align with the AC field with a shorter delay [39]. A shorter relaxation time means that the dielectric loss reaches the maximum at a higher frequency, so measuring the relaxation time is important to develop a material with stable dielectric properties. As the AC conductivity is inversely proportional to the relaxation time. So decreased value of relaxation times may result in the high value of AC conductivity.

4.2.9.4 Dielectric loss tangent

Fig. 4.2.12 shows the dielectric loss tangent (*tanδ*), with frequency for a different

Fig. 4.2.12 Variation of the dielectric loss tangent of the Gel /SWCNT
nanocomposites as a function of applied frequency.

amount of SWCNT content in Gel at room temperature. From Fig. the dielectric loss tangent
as low as 0.91 and 4 was obtained for sample D at the frequency of 100 Hz and 10^6 Hz
respectively. The tangent loss for all the samples shows a single nearly Debye type relaxation
peak [93-95]. Initially, the increase in the loss with an increase in the frequency is observed
and the maxima at the particular frequency (where *ωτ =1*) is followed by the decrease in
high frequency [95].

This plot can be divided into three regions for a better understanding of the variation
of tangent loss with frequency, the first is a low-frequency region, the second is a moderate
frequency region, and the third one is a high-frequency region. In the low-frequency region
increase of the loss may be related to the dominance of the Ohmic resistive component i.e.
friction of dipoles while they tend to align with the field. While the presence of the maxima

is observed only at a single frequency when the perfect matching between the frequency of electric field and frequency of molecule rotation of gelatin occurs. This resonance leads to the maximum power transfer to the dipoles in the system and hence the maximum dissipation of field energy through different processes mainly as heat [22, 93]. Now, in the high-frequency window, the tangent loss that goes downwards may be because of the complete idleness of the dipoles to the field. Here, the part becomes frequency independent, while the capacitive part grows with the frequency. It is noticeable from Fig. that the relaxation peak shifts towards the high-frequency side which indicates the faster electron transport dynamics from one coordinating site to another due to a decrease of relaxation time [93-95]. The calculated values for maximum relaxation time that found nearly 5×10^5 Hz with the condition, $\omega\tau = 1$ (where $\omega = 2\pi f$) [95] are 3.03 µs, 1.34 µs, 1.12 µs, and 1.01 µs respectively for the samples A, B, C, and D.

To achieve excellent dielectric properties, a very well dispersion of CNTs throughout the polymer matrix is a must [39]. If CNTs get agglomerated, the nanocomposite will be conductive rather than dielectric. We observed that the dielectric loss of the composite increases with increased SWCNT loading, which is because when the SWCNT loading increased, agglomeration of SWCNTs occurred and highly conductive SWCNT particles easily formed a conductive path in the composites. When the composites become more conductive, a leakage current occurred, causing part of the electrical energy to be transformed into other energy (mainly thermal) [96, 97]. As a result, the dielectric loss (*tan δ*) of the composite increased due to the dissipation of energy when the SWCNT loading increased and a conductive route created in the whole sample, the high leakage current originated from direct contact between the SWCNTs. The values of dielectric constant (ε') and dielectric loss tangent (*tanδ*) at the frequency of 100 Hz of the present study compared with some previously reported similar studies are shown in Table 4.8 which agrees with the fact that Gel/SWCNT nanocomposite exhibits a gigantic dielectric permittivity simultaneously with an almost negligible loss tangent value at the frequency 100 Hz.

4.2.9.4 AC conductivity (σ_{AC})

The enhancement of the AC conductivity as a function of frequency for all the nanocomposites at room temperature is presented in Fig. 4.2.13. The graphs consist of three distinct regions depending upon the frequency. First is the low-frequency region with a sharp rise in the conductivity due to electrode polarization, followed by a frequency-independent plateau region at an intermediate frequency (corresponds to maximum relaxation time) and, high-frequency dispersive region owing to the fast reversal of the field. All Fig. indicates that at low frequency there was a decrease in the conductivity value and may be due to the dominance of the electrode polarization effect [89, 90]. The nearly pleatue region in the intermediate frequency window may be attributed to the long-range conduction of the charged carriers and the maximum relaxation peak slows down the increase of AC

Fig. 4.2.13 Variation of the AC conductivity of the Gel /SWCNT nanocomposites as a function of applied frequency.

conductivity. The high-frequency dispersion region is due to the short-range ion transport (hopping) associated with AC conductivity [24, 39].

At a lower frequency range, the interfacial polarization takes place in between the electrode and sample surface as well as between the grains and other heterogeneous areas of the sample can be observed. The bulk resistance decreases with an increase in the filler content. The conduction process is controlled by interfiller tunneling. SWCNT is fairly well dispersed randomly in the gelatin matrix composite. Moreover, the SWCNT may connect with each other in part, and form a partly continuous random cluster. Therefore, charges transfer easily from one domain to another results increase in conductivity. Among all nanocomposites, sample D shows high conductivity of 8×10^{-4} S/m at 10 kHz when compared to others. Whereas the pure Gel sample (A) exhibits low conductivity of about 4.6×10^{-4} S/m at the same frequency. The low AC conductivity at a lower frequency may be due to different types of polarization (i.e., interfacial, dipolar, atomic, ionic, electronic contribution) in the material [89, 90, 97].

At higher frequencies, the doping of SWCNT results in a decrease in both permittivity because of the contribution of the presence of dielectric relaxation characteristics in the nanocomposites. SWCNT helps in the formation of the dipole in nanocomposites i.e., dipole polarization phenomena. The overall results enhance the conductivity of the nanocomposites. Another cause for increasing the frequency-dependent conductivity may be caused by the hopping of the charge carriers in the localized states and also due to the excitation of the charge carriers to the states in the conduction band [97].

4.2.9.5 Cole-Cole plot
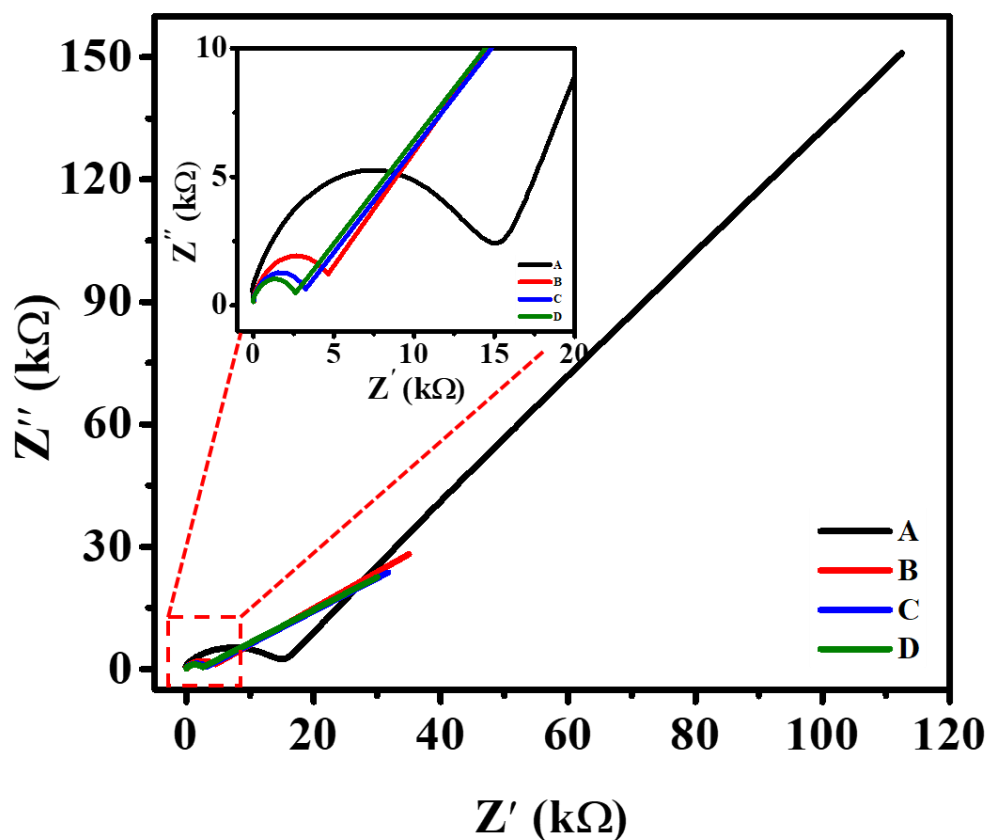
Fig. 4.2.14 Cole-Cole plots of the Gel/SWCNT nanocomposites at room temperature for different amount of filler incorporation (the high frequency region is shown in the inset).

The Cole-Cole plot is constructed by plotting the imaginary impedance, Z'' as a function of real impedance, Z', and is presented in Fig. 4.2.14. The modulus of the complex impedance of the composites is given by [98]: $|Z| = Z'+iZ''$. The plot clearly shows that there is a semicircular arc at the higher frequency region followed by an inclined straight line at the lower frequency region which is due to a non-Debye type relaxation in the nanocomposites [99]. In general, the values of resistance (R) and capacitance (C) of a perfect crystal can be analyzed by an equivalent circuit of one parallel resistance-capacitance (RC) element. This RC element gives rise to one semicircular arc on the complex plane, which intercepts the x-axis. For a bulk crystal containing interfacial layers, the equivalent circuit may be considered as several parallel RC elements connected in serial. It is observed that, as

the filler content increases, the intercept of the semicircular arcs on the real axis approaches the origin of the complex plane, indicating a decrease in the sample's resistivity properties.

The simulated impedance spectra best fitted with the equivalent circuit shown in Fig. 4.2.15. The equivalent circuit for the nanocomposites consists of two parallel circuits in series, each of them contains a resistance, R, and a Constant Phase Element (CPE) Q, which is a capacitive element. For getting the best fitting results, CPE is defined as: $Z_{CPE} = Z_0 \frac{1}{(j\omega)^n}$. Here Z_{CPE} is the impedance of the constant phase angle component, Z_0 is a constant, ω is the angular frequency, j is the imaginary unit, and n is the exponential factor. When $n = 1$, -1, or 0. CPE is equivalent to an ideal capacitor, an inductance, or a pure resistance, respectively [39, 100, 101]. Table 4.9 gives the corresponding parameters of equivalent circuits for the Gel/SWCNT nanocomposite.

Table 4.9 Different parameters of the equivalent circuit components of the fitting Cole-Cole curves of the Gel/SWCNT nanocomposites.

Sample	Grain resistance, R_1 (kΩ)	Grain capacitance, Q_1 (pF)	n_1	Grain boundary resistance, R_2 (kΩ)	Grain boundary capacitance, Q_2 (nF)	n_2
A	14.83	5.929	0.91	16950	66.88	0.78
B	4.68	9.198	0.88	53.29	96.34	0.84
C	3.31	8.982	0.83	39.87	164.61	0.85
D	2.54	9.352	0.79	24.10	275.88	0.88
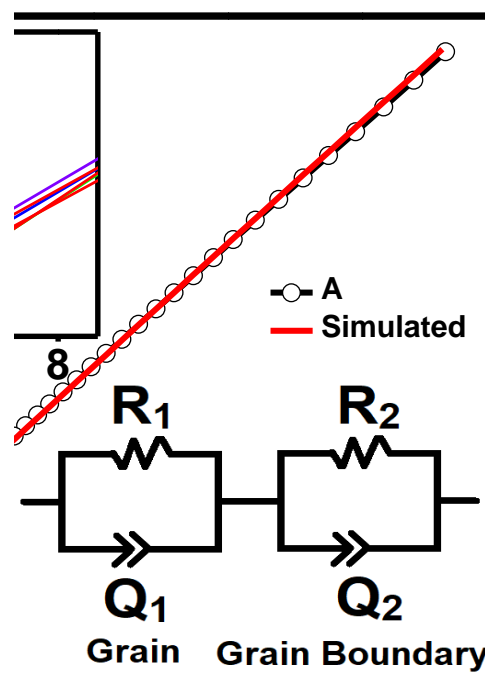
Fig. 4.2.15 The complex impedance spectrum of the pure gelatin with the fitting curve. The insets show the complex impedance spectra for the Gel/SWCNT composites and the equivalent circuit for the best-fitted curves.

The first parallel circuit of the equivalent circuit of the nanocomposites refers to the grain i.e., the conductive regions created between the incorporated SWCNTs in the Gel matrix. The grain resistance R_1 decreases and the value of the capacitive element of the grain Q_1 increases with an increasing amount of SWCNT. Sample D shows the resistance decreases down to 2.54 kΩ from the initial value that of sample A 14.83 kΩ. The second parallel part of the circuit contains the grain boundary resistance R_2 and the grain boundary capacitive element Q_2. They refer to the region separating two grains. The grain boundary resistance displays a dramatic decrease of about three orders of magnitude as the SWCNT contents are added. Grain boundary elements also show changes of a similar trend which confirm less reactive and more capacitive behavior.

4.2.10 Electrochemical properties

4.2.10.1 Cyclic voltammetry

Cyclic voltammetry was conducted to investigate the electrochemical properties of the prepared materials. Fig. 4.2.15(a-d) shows the CV curves of the four samples-A, B, C, and D respectively at different scan rates: 5 mV/s, 10 mV/s, 20 mV/s, 50 mV/s, 80 mV/s and 100 mV/s in the voltage range from -0.2 V to 0.7 V. Observed CV curves found to be near rectangular and approximately symmetric in shape. Fig. 4.2.17(a) gives a comparative illustration of all the nanocomposite materials at a 100mV/s voltage sweep rate. The corresponding values of the specific capacitance (C_s) at different scan rates for all the samples were measured and listed in Fig. 4.2.17(b). From Fig. it was found that the material holds the larger value of C_s in a lower scan rate. At 5 mV/s the C_s value calculated was 180 mF/g, 193 mF/g, 197 mF/g, and 219 mF/g of active material for Gel, Gel/0.125 vol% SWCNT, Gel/0.25 vol% SWCNT, and Gel/0.5 vol% SWCNT nanocomposites respectively. This is due to the ions of the electrolyte have enough time for getting diffused into the SWCNT intermolecular regions at low scan rates [102]. Thus, ions can utilize more surface area of SWCNTs rather than they can in higher scan rates [103]. At higher scan rates the charging and discharging happens too rapidly to diffuse the ions properly thus, the C_s value decreases. At 100 mV/s C_s of the sample, D was calculated 129.42 mF/g where the rate capability is about 40% of the initial value at 5 mV/s. Although the shape of the CV curve is nearly rectangular, a slight bump of redox peak is observed at around 2.5 V. This peak and the cumulative quasi-rectangular shape of the CV curves with the incorporation of the higher amount of SWCNT in the Gel matrix confirms the existence of pseudo-capacitance [104]. Pseudo-capacitance could be raised from the interaction of SWCNT with the open
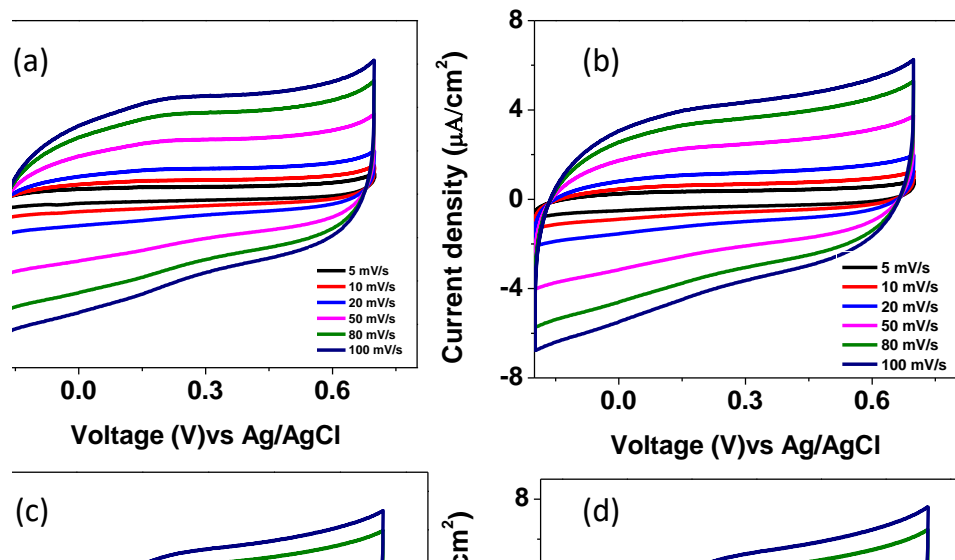
Fig. 4.2.16 Cyclic voltammetry of (a) Gel, (b) Gel/0.125 vol% SWCNT, (c) Gel/0.25 vol% SWCNT, (d) Gel/0.5 vol% SWCNT at different voltage scan rates.

bonds of the gelatin skeleton in the ionic electrolyte [33, 45]. The collective effect of forming a capacitive layer and pseudo-capacitance is the reason for the increase of the C_s value with the incorporation of SWCNT [105].

4.2.10.2 Galvanostatic charging-discharging

To have more substantial information about the electrochemical properties of the Gel/SWCNT materials, Galvanostatic charging and discharging (GCD) was performed. The GCD operated at -0.2 V to 0.7 V voltage window at different current densities (0.3 $\mu A/cm^2$, 0.5 $\mu A/cm^2$, 0.8 $\mu A/cm^2$, 1 $\mu A/cm^2$ and 2 $\mu A/cm^2$). Fig. 4.2.17(c) gives a comparative illustration of GCD of all the nanocomposite materials at 0.3 $\mu A/cm^2$ current density and all
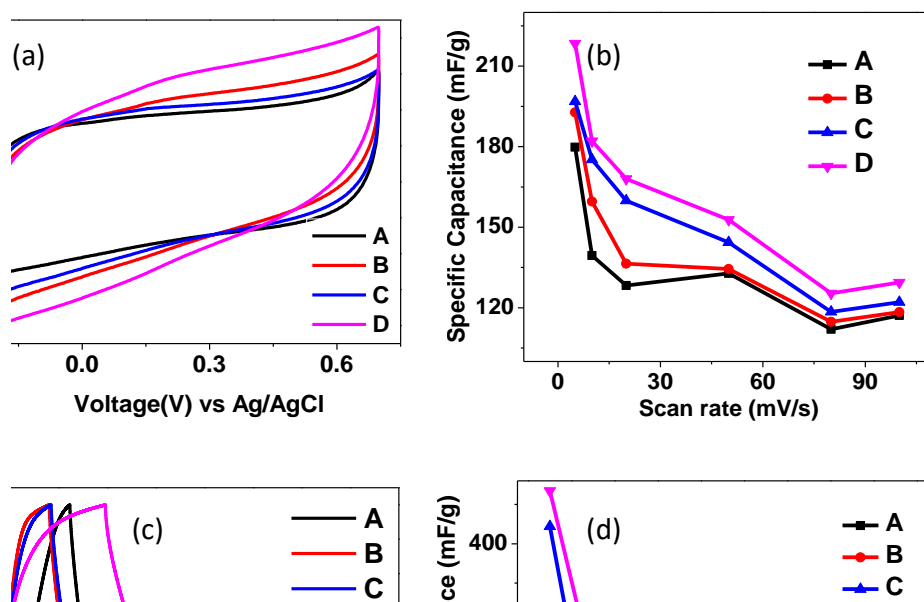
Fig. 4.2.17 Cyclic voltammetry of all the nanocomposite at 100 mV/s voltage sweep rate (a), associated specific capacitance values of all the samples at different voltage scan rates (b). Galvanostatic charging-discharging of all the samples at a current density of 0.3 $\mu A/cm^2$ (c), calculated specific capacitance of all the samples at different current densities (d).

the corresponding specific capacitance, C_s values shown in Fig. 4.2.17(d) exhibits an increase of C_s with SWCNT increment in the Gel matrix. Here also observed the specific capacitance is higher at lower current densities. C_s of about 124 mF/g, 291 mF/g, 422 mF/g, and 467 mF/g were found for samples A, B, C, and D respectively at 0.3 μA/cm^2 current density. The reason is that at lower current density lesser amount ions come close to a certain portion of the surface area of the SWCNT wall and can diffuse themselves properly [33, 106]. Whereas at the higher surface area more ions traffic at the same certain portion of SWCNT wall and cannot diffuse themselves enough into the SWCNT surface [106-108]. As a result, the value of C_s lowers down. Also, the charging-discharging rate accelerates at the higher current densities results in a lower value of C_s. At a higher current density of 2 μA/cm^2, the value of C_s was calculated 60 mF/g, 73 mF/g, 88 mF/g, and 128 mF/g for the sample A, B, C, and D respectively. The specific capacitance of the highest SWCNT contained sample increases about 4 times that of the pure Gel sample as the SWCNTs form a conductive channel throughout the electrode material and increase the ion transportation [72, 104]. The distorted triangular shape of the GCD curve also confirms the pseudocapacitance of the nanocomposites discussed in the CV part [108].

4.2.10.3 Electrochemical impedance spectroscopy

Nyquist plots were equipped to analyze the electrochemical impedance of the nanocomposite samples. To evaluate the contribution of different electrical parts in the Nyquist plot a simulation was run and the best-fitted curves along with the equivalent circuit are shown in Fig. 4.2.18. Corresponding values of the components of the equivalent circuit are recorded in Table 4.10. Different portions of the Nyquist plot carry different information about the sample's electrochemical status according to the applied frequency. In the high-frequency region, the point where the Nyquist plot intercepts the real axis represents the value of combined series resistance, R_s. This value is the combination of the actual resistance of the electrode material, the resistance of the electrolyte, and the contact resistance of the electrode and current collector [109]. R_s value tends to decrease with the incorporation of SWCNTs in the polymer matrix from 7.45 Ω for Gel sample to 7.41 Ω for Gel/0.5 vol% SWCNT nanocomposite. SWCNTs might have created an easy route for

current collectors to decrease the R_s value [110, 111]. The semi-circle in the high-frequency region is indicative of the electrode conductivity and the charge transfer resistance of the electrode material [110-112]. The radius of the semi-circle represents the value of charge
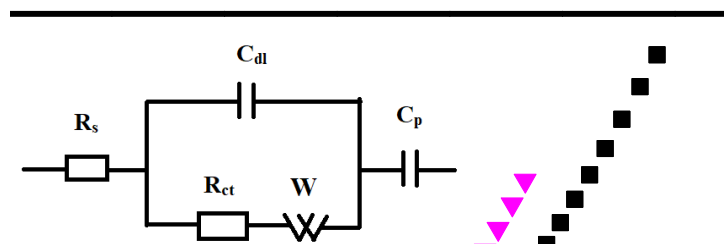
Fig. 4.2.18 The simulated Nyquist plots of the Gel/SWCNT nanocomposites. The inset shows the equivalent circuit used for simulation.

transfer resistance, R_{ct} [104, 105]. The value of R_{ct} obtained from the simulation is 106.6 Ω, 88.98 Ω, 81.33 Ω, 74.80 Ω for samples A, B, C, D respectively. The extraordinary electric conductivity of SWCNTs helps to decrease the charge transfer resistance of the electrode [111]. The semicircular shape arises for a parallel relation of C_{dl} with R_{ct}. C_{dl} is the capacitance of the double layer formed near the electrode-electrolyte interaction area [109]. The fitted values obtained for C_{dl} are increased from 3.76 nF for the Gel to 6.46 nF for Gel/0.5 vol% SWCNT nanocomposite. The internal spaces where SWCNTs are located might have created a charge capacitive region and thus C_{dl} value increased [110]. In the intermediate frequency region, the nearly 45° slope of the curves is described as the Warburg

Table 4.10 Corresponding values of the different components of the equivalent circuit used in simulation of the Gel/SWCNT nanocomposites.

Sample	Series Resistance, R_s (Ω)	Double layer Capacitance, C_{dl} (nF)	Charge tranfer Resistance, R_{ct} (Ω)	Pseudo Capacitance, C_P (μF)
A	7.45	3.76	106.60	9.40
B	7.44	4.85	88.98	12.77
C	7.43	5.35	81.33	21.07
D	7.41	6.46	74.80	30.90

resistance region, which represents the ion diffusion/transport on the electrolyte and electrode contact surface [112]. In the low-frequency region, the capacitive behavior dominates as the bulk capacitance of the nanocomposite material, which is mainly pseudo capacitance, C_p took place [104, 105]. The C_p value of the Gel/0.5 vol% SWCNT electrode (30.9 µF) increased more than three times the value obtained for the Gel electrode (9.4 µF). Overall, as electrode material, the prepared nanocomposites display well capacitive behavior.

4.2.10.4 Cyclic stability

Fig. 4.2.19(a) displays capacitance retention of the Gel/0.5 vol% SWCNT nanocomposite and the sample retains 98% of its maximum capacitance after completing 2000 charging/discharging cycles at 2 µA/cm^2 current density. Fig. 4.2.19(b) reveals the almost unchanged shape of the 1st and 2000th charging/ discharging cycle. Then again, the Fig. 4.2.19(c) image shows the EIS performed before and after 2000 GCD cycles. The series resistance of them remains nearly similar. The minor alteration of the resistance happens as
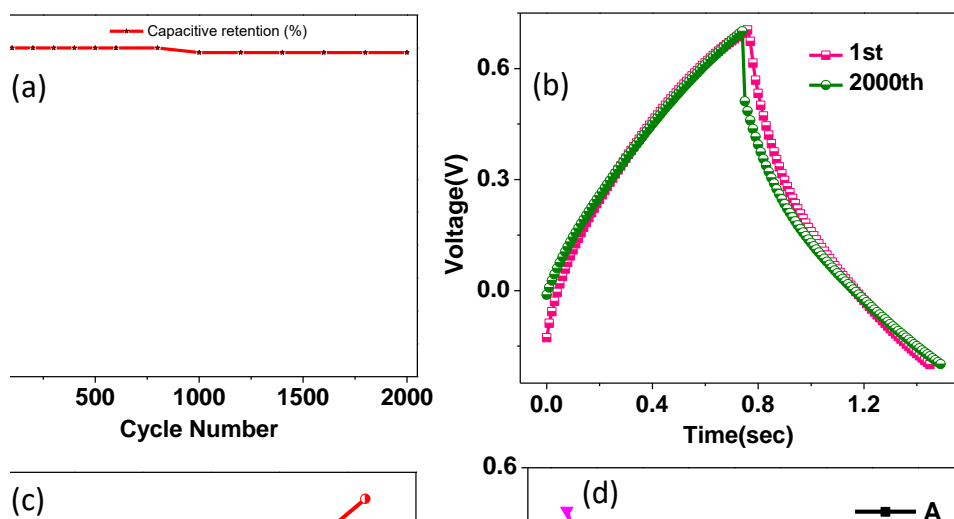
Fig. 4.2.19 The capacitive retention for 2000 GCD cycles (a), the 1st and the 2000th GCD cycles (b), the Nyquist plots before and after of 2000 GCD cycles (c) for Gel/0.5 vol% SWCNT nanocomposite. Ragone plot for the nanocomposites (d).

some faradaic reaction or corrosion occurs on the electrolyte-electrode material surface [106, 107]. The slope of the Warburg resistance gets more inclined as the diffusion of ions from the faradaic reaction increases on the contact surface [109]. This impressive cyclic stability with long cycle life enhances their compatibility as an electrode material of supercapacitor uses. Fig. 4.2.19(d) shows the Ragone plot of the nanocomposites or the energy density vs. power density graph. This analysis provisions their use as supercapacitors [122].

4.2.11 Biodegradability analysis
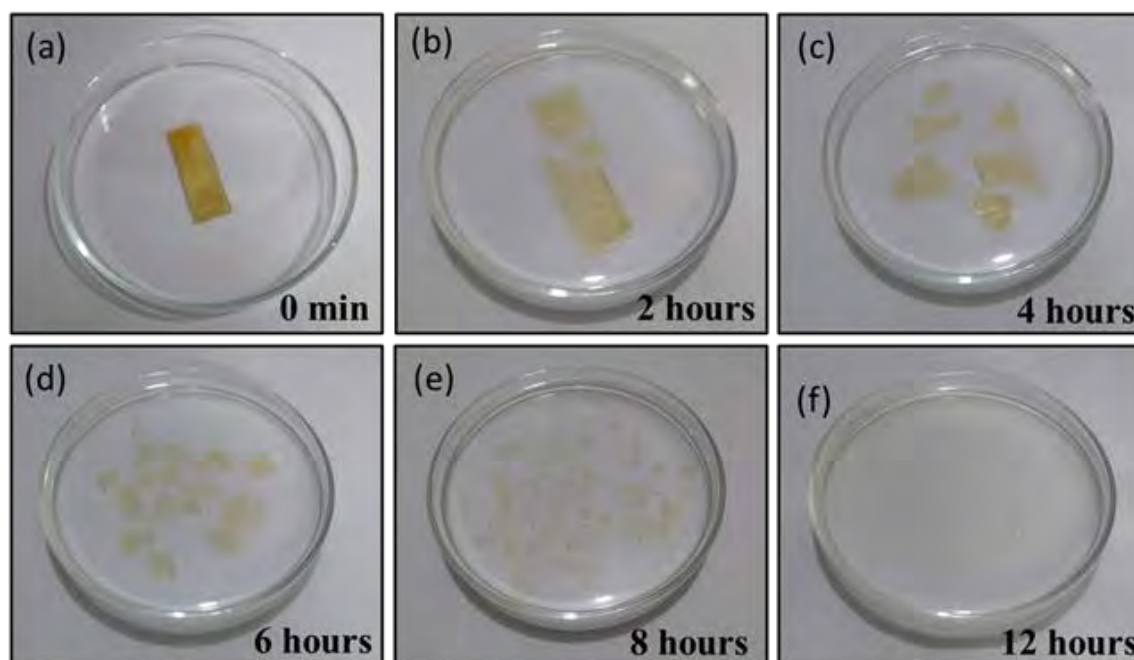
Fig. 4.2.20 Biodegradability analysis of the Gel/SWCNT samples in DI water.

Fig. 4.2.20 (a) to (f) shows the degradation of the Gel/SWCNT nanocomposite film with respect to time in DI water at room temperature. It took only 12 hours to fully and safely disappear the film from the system for a $30 \times 10 \times 1$ mm^3 film. Biopolymers like gelatin are substituted or incorporated with some hydrophilic groups such as amino acid group, alcoholic group, etc. into their backbone that can dissolve, disperse, or swell in water [56, 113]. The swelling of the gelatin sample is understandable by comparing Fig. 4.2.20(a) and Fig. 4.2.20(b). At that point, the swelled film breaks into pieces only by a little stirring, Fig. 4.2.20(c). Similarly, by applying a little stirring every 2 hours pictures were taken. Finally, the film fully dissolves into the water without remaining any tress after 12 hours from the beginning.

CHAPTER 5
CONCLUSIONS

5.1 Conclusions

Gel/MWCNT and Gel/SWCNT nanocomposites with different CNT concentrations were successfully prepared by a facile solution casting method. FTIR, FESEM, Raman spectroscopy, and WCA measurements were performed to study the structural and morphological properties of the nanocomposite. The electrochemical performance of the as-prepared nanocomposites was investigated using cyclic voltammetry and Galvanostatic charging-discharging. The specific capacitance of the nanocomposite was found to be as high as 12.7 F/g at a current density of 0.3 $\mu A/cm^2$ for the Gel/CNT nanocomposites. EIS analysis was performed by Nyquist plots and the contributions of the different electrical components were evaluated using an equivalent ac circuit. Incorporation of CNT was found to decrease the charge-transfer resistance (from 127 Ω to 75 Ω), and improve the double-layer capacitance (from 4 nF to 9 nF) and pseudocapacitance from (9.4 μF to 30.9 μF) that improve the electrochemical performance of the nanocomposite. The Gel/CNT nanocomposite showed super cyclic stability with capacitance retention of 95% of the initial capacitance after completing 5000 charging/discharging cycles at a current density of 0.3 $\mu A/cm^2$. These electrochemical properties of the nanocomposites suggest their potential use as electrode material in energy storage devices. The dielectric constant of the Gel/MWCNT nanocomposite was found to be ~10^4 together with a loss tangent of 1.13 at 100 Hz. The dielectric permittivity data were fitted by the modified Cole-Cole model to evaluate the dielectric strength and the relaxation time of the nanocomposite. The relaxation time of the nanocomposite decrease with the incorporation of CNT nanofiller. The minimum relaxation time obtained for the nanocomposite was 0.93 μsec. A quantitative analysis from the fitting of the Cole-Cole plot revealed that the incorporation of CNT into the nanocomposite reduces the grain boundary resistance by few orders of magnitude and increases the capacitive element by several times. The mechanism behind the improved dielectric performance of the Gel/CNT nanocomposites was elucidated by a suitable model. Moreover, the

biodegradability test proved the Gel/ 0.05 wt% MWCNT nanocomposite degraded after 30 hours, and the Gel/ 0.5 vol% SWCNT nanocomposite degraded after 12 hours of emerging them into the water. This fully biocompatible nature of the nanocomposites can be helpful to fabricate a fully nature-friendly electrode material for energy storage purposes. These nanocomposite materials with high dielectric constant and low dielectric loss may have possible applications in highly efficient capacitive devices.

5.2. Suggestions for Future Work

The following characterization can be performed to better understand the properties of Gel/MWCNT and Gel/SWCNT nanocomposite:

- ➤ X-ray diffraction analysis can be performed to elucidate more information on the structure of the nanocomposites.

- ➤ Atomic force microscopy can be used for the further investigation of the structure and morphology.

- ➤ The biodegradability of the Gel/CNT nanocomposites can be studied in soil.

References

[1]   Patil, R. A., and Ramakrishna, S., "A comprehensive analysis of e-waste legislation worldwide", *Environ. Sci. Pollut. Res.*, vol. 27, no. 13, pp. 14412–14431, 2020.

[2]   Chatterjee, A., and Abraham, J., "Efficient management of e-wastes", *Int. J. Environ. Sci. Technol.,* vol. 14, no. 1, pp. 211–222, 2017.

[3]   Luhar, S., and Luhar, I., "Potential application of E-wastes in construction industry: A review", *Constr. Build. Mater.*, vol. 203, pp. 222–240, 2019.

[4]   Kiddee, P., Naidu, R., and Wong, M. H., "Electronic waste management approaches: An overview", *Waste Manage.*, vol. 33, no. 5, pp. 1237–1250, 2013.

[5]   Gu, F., Ma, B., Guo, J., Summers, P. A., and Hall, P., "Internet of things and Big Data as potential solutions to the problems in waste electrical and electronic equipment management: An exploratory study", *Waste Manage.*, vol. 68, pp. 434–448, 2017.

[6]   Liu, Q., Cao, J., Li, K. Q., Miao, X. H., Li, G., Fan, F. Y., and Zhao, Y. C., "Chromosomal aberrations and DNA damage in human populations exposed to the processing of electronics waste", *Environ. Sci. Pollut. Res.*, vol. 16, no. 3, pp. 329–338, 2009.

[7]   Bakhiyi, B., Gravel, S., Ceballos, D., Flynn, M. A., and Zayed, J., "Has the question of e-waste opened a Pandora's box? An overview of unpredictable issues and challenges", *Environ. Int.*, vol. 110, pp. 173–192, 2018.

[8]   Zhao, G., Wang, Z., Wang, H., Zhao, H., Fu, Y., and Yang, J., "Effect of doping nanoparticles on the output force performance of chitosan-based nanocomposite gel actuator", *Polym.-Plast. Tech. Mat.*, vol. 58, no. 9, pp. 967–977, 2019.

[9]   Bagheri, H., Afkhami, A., Khoshsafar, H., Hajian, A., and Shahriyari, A., "Protein capped Cu nanoclusters-SWCNT nanocomposite as a novel candidate of high performance platform for organophosphates enzymeless biosensor", *Biosens. Bioelectron.,* vol. 89, pp. 829–836, 2017.

[10]   Yan, Y., Sencadas, V., Jin, T., Huang, X., Lie, W., Wei, D., and Jiang, Z., "Effect of multi-walled carbon nanotubes on the cross-linking density of the poly(glycerol sebacate) elastomeric nanocomposites", *J. Colloid Interface Sci.*, vol. 521, pp. 24–32, 2018.

[11]   Fu, K. K., Wang, Z., Dai, J., Carter, M., and Hu, L., "Transient Electronics: Materials and Devices", *Chem. Mater.*, vol. 28, no. 11, pp. 3527–3539, 2016.

[12]   Hwang, S. W., Song, J. K., Huang, X., Cheng, H., Kang, S. K., Kim, B. H., Kim, J. H., Yu, S., Huang, Y., and Rogers, J. A., "High-performance biodegradable/transient electronics on biodegradable polymers", *Adv. Mater.*, vol. 26, no. 23, pp. 3905–3911, 2014.

[13]   Lee, G., Kang, S. K., Won, S. M., Gutruf, P., Jeong, Y. R., Koo, J., Lee, S. S., Rogers, J. A., and Ha, J. S., "Fully Biodegradable Microsupercapacitor for Power Storage in Transient Electronics," *Adv. Energy Mater.*, vol. 7, no. 18, pp. 1–12, 2017.

[14]   Quero, F., Padilla, C., Campos, V., Luengo, J., Caballero, L., Melo, F., Li, Q., Eichhorn, S. J., and Enrione, J., "Stress transfer and matrix-cohesive fracture mechanism in microfibrillated cellulose-gelatin nanocomposite films," *Carbohydr. Polym.*, vol. 195, pp. 89–98, 2018.

[15]   Sanjay, M. R., Madhu, P., Jawaid, M., Senthamaraikannan, P., Senthil, S. and Pradeep, S., "Characterization and properties of natural fiber polymer composites: A comprehensive review", *J. Clean. Prod.*, vol. 172, pp.566-581, 2018.

[16]   Chandran, S., Baschnagel, J., Cangialosi, D., Fukao, K., Glynos, E., Janssen, L. M. C., Müller, M., Muthukumar, M., Steiner, U., Xu, J., Napolitano, S., and Reiter, G., "Processing Pathways Decide Polymer Properties at the Molecular Level", *Macromolecules*, vol. 52, no. 19, pp. 7146–7156, 2019.

[17]   Gentekos, D. T., Sifri, R. J., and Fors, B. P., "Controlling polymer properties through the shape of the molecular-weight distribution", *Nat. Rev. Mater.*, vol. 4, no. 12, pp. 761–774, 2019.

[18]   Suderman, N., Isa, M. I. N., and Sarbon, N. M., "The effect of plasticizers on the functional properties of biodegradable gelatin-based film: A review", *Food Biosci.*, vol. 24, pp. 111–119, 2018.

[19]   Popescu, M. C., "Structure and sorption properties of CNC reinforced PVA films," *Int. J. Biol. Macromol.*, vol. 101, pp. 783–790, 2017.

[20]   Chen, H., Ling, M., Hencz, L., Ling, H. Y., Li, G., Lin, Z., Liu, G., and Zhang, S., "Exploring Chemical, Mechanical, and Electrical Functionalities of Binders for Advanced Energy-Storage Devices", *Chem. Rev.*, vol. 118, no. 18, pp. 8936–8982, 2018.

[21]   Jiang, X., Zhao, X., Peng, G., Liu, W., Liu, K., and Zhan, Z., "Investigation on crystalline structure and dielectric relaxation behaviors of hot pressed poly(vinylidene fluoride) film", *Curr. Appl. Phys.*, vol. 17, no. 1, pp. 15–23, 2017.

[22]   Yuan, J. K.,Yao, S. H., Dang, Z. M., Sylvestre, A., Genestoux, M., and Bai, J., "Giant dielectric permittivity nanocomposites: Realizing true potential of pristine carbon

nanotubes in polyvinylidene fluoride matrix through an enhanced interfacial interaction", *J. Phys. Chem. C*, vol. 115, no. 13, pp. 5515–5521, 2011.

[23] Rubio, R., Santander, J., Fonseca, L., Sabate, N., Gracia, I., Cane, C., Udina, S., and Marco, S., "Non-selective NDIR array for gas detection", *Sens. Actuator B-Chem.*, vol. 127, no. 1, pp. 69-73, 2007.

[24] Mollik, S. I., Alam, R. B., and Islam, M. R., "Significantly improved dielectric properties of bio-compatible starch/reduced graphene oxide nanocomposites", *Synth. Met.*, vol. 271, p. 116624, 2021.

[25] Xu, X., Zhou, J., Jestin, J., Colombo, V., and Lubineau, G., "Preparation of water-soluble graphene nanoplatelets and highly conductive films", *Carbon*, vol. 124, pp. 133–141, 2017.

[26] Haniffa, M. A. C. M., Ching, Y. C., Abdullah, L. C., Poh, S. C., and Chuah, C. H., "Review of bionanocomposite coating films and their applications", *Polymers*, vol. 8, no. 7, p. 246, 2016.

[27] Müller, K., Bugnicourt, E., Latorre, M., Jorda, M., Sanz, Y. E., Lagaron, J. M., Miesbauer, O., Bianchin, A., Hankin, S., Bölz, U., Pérez, G., Jesdinszki, M., Lindner, M., Scheuerer, Z., Castelló, S., and Schmid, M., "Review on the processing and properties of polymer nanocomposites and nanocoatings and their applications in the packaging, automotive and solar energy fields", *Nanomaterials*, vol. 7, no. 4. p. 74, 2017.

[28] Stokes, P., Islam, M. R., and Khondaker, S. I., "Low temperature electron transport spectroscopy of mechanically templated carbon nanotube single electron transistors", *J. Appl. Phys.*, vol. 114, no. 8, pp. 1–7, 2013.

[29] Sarker, B. K.,Islam, M. R., Alzubi, F., and Khondaker, S. I., "Fabrication of aligned carbon nanotube array electrodes for organic electronic devices", *Mater. Express*, vol. 1, no. 1, pp. 80–85, 2011.

[30] Islam, M. R., Joung, D., and Khondaker, S. I., "Towards parallel fabrication of single electron transistors using carbon nanotubes", *Nanoscale*, vol. 7, no. 21, pp. 9786–9792, 2015.

[31] Islam, M. R., Kormondy, K. J., Silbar, E., and Khondaker, S. I., "A general approach for high yield fabrication of CMOS-compatible all-semiconducting carbon nanotube field effect transistors", *Nanotechnology*, vol. 23, no. 12, p. 125201, 2012.

[32] Islam, M. R., and Khondaker, S. I., "Recent progress in parallel fabrication of individual single walled carbon nanotube devices using dielectrophoresis", *Mater. Express*, vol. 4, no. 4, pp. 263–278, 2014.

[33]   Tiwari, P., Jaiswal, J., and Chandra, R., "Hierarchal growth of MoS$_2$@CNT heterostructure for all solid state symmetric supercapacitor: Insights into the surface science and storage mechanism", *Electrochim. Acta*, vol. 324, p. 134767, 2019.

[34]   Wang, H., Yang, Y., and Guo, L., "Nature-Inspired Electrochemical Energy-Storage Materials and Devices", *Adv. Energy Mater.*, vol. 7, no. 5, p.1601709, 2017.

[35]   Kharlamova, M. V., "Advances in tailoring the electronic properties of single-walled carbon nanotubes", *Prog.Mater. Sci.*, vol. 77, pp. 125–211, 2016.

[36]   Fan, B., Liu, Y., He, D., and Bai, J., "Achieving polydimethylsiloxane/carbon nanotube (PDMS/CNT) composites with extremely low dielectric loss and adjustable dielectric constant by sandwich structure", *Appl. Phys. Lett.*, vol. 112, no. 5, p.052902, 2018.

[37]   Liao, X., Ye, W., Chen, L., Jiang, S., Wang, G., Zhang, L., and Hou, H., "Flexible hdC-G reinforced polyimide composites with high dielectric permittivity", *Compos. Part A Appl. Sci. Manuf.*, vol. 101, pp. 50–58, 2017.

[38]   Xiao, Y. J.,Wang, W. Y., Lin, T., Chen, X. J., Zhang, Y. T., Yang, J. H., Wang, Y., and Zhou, Z. W., "Largely Enhanced Thermal Conductivity and High Dielectric Constant of Poly(vinylidene fluoride)/Boron Nitride Composites Achieved by Adding a Few Carbon Nanotubes", *J. Phys. Chem. C*, vol. 120, no. 12, pp. 6344–6355, 2016.

[39]   Wang, B., Liang, G., Jiao, Y., Gu, A., Liu, L., Yuan, L., and Zhang, W., "Two-layer materials of polyethylene and a carbon nanotube/cyanate ester composite with high dielectric constant and extremely low dielectric loss", *Carbon*, vol. 54, pp. 224–233, 2013.

[40]   Huang, C., Qian, X., and Yang, R., "Thermal conductivity of polymers and polymer nanocomposites", *Mater. Sci. Eng. R Rep.,* vol. 132, pp. 1–22, 2018.

[41]   Rouhi, J., Mahmud, S., Naderi, N., Raymond, O. C. H. and Mahmood, M. R., "Physical properties of fish gelatin-based bio-nanocomposite films incorporated with ZnO nanorods", *Nanoscale Res. Lett.*, vol. 8, no. 1, pp. 1–6, 2013.

[42]   Rahman, M. M., "Preparation of Carbon Nanotube Reinforced Gelatin-Chitosan-Hydroxyapatite Biocomposite for Bone Tissue Engineering", *J. Biosci. Bioeng.*, vol. 1, no. 3, pp. 66–72, 2018.

[43]   Ren, K., Wang, Y., Sun, T., Yue, W., and Zhang, H., "Electrospun PCL/gelatin composite nanofiber structures for effective guided bone regeneration membranes", *Mater. Sci. Eng. C*, vol. 78, pp. 324–332, 2017.

[44] Rajkumar, C., Thirumalraj, B., Chen, S. M., and Chen, H. A., "A simple preparation of graphite/gelatin composite for electrochemical detection of dopamine", *J. Colloid Interface Sci.*, vol. 487, pp. 149–155, 2017.

[45] Landi, G., Sorrentino, A., Iannace, S., and Neitzert, H. C., "Differences between graphene and graphene oxide in gelatin based systems for transient biodegradable energy storage applications", *Nanotechnology*, vol. 28, no. 5, p.054005, 2017.

[46] Darder, M., Aranda, P., and Ruiz-Hitzky, E., "Bionanocomposites: a new concept of ecological, bioinspired, and functional hybrid materials", *Adv. Mater.*, vol. 19, no. 10, pp.1309-1319, 2007.

[47] Zhou, K., Liu, J., Zeng, W., Hu, Y., and Gui, Z., "In situ synthesis, morphology, and fundamental properties of polymer/MoS_2 nanocomposites", *Compos. Sci. Technol.,* vol. 107, pp. 120–128, 2015.

[48] Du, H., Yuan, C., Huang, K., Wang, W., Zhang, K., and Geng, B., "A novel gelatin-guided mesoporous bowknot-like Co_3O_4 anode material for high-performance lithium-ion batteries", *J. Mater. Chem. A*, vol. 5, no. 11, pp. 5342–5350, 2017.

[49] Islam, M. R., and Mollik, S. I., "Enhanced electrochemical performance of flexible and eco-friendly starch/graphene oxide nanocomposite", *Heliyon*, vol. 6, no. 10, p.e05292, 2020.

[50] Li, Y., Li, R., Fu, X., Wang, Y., and Zhong, W. H., "A bio-surfactant for defect control: Multifunctional gelatin coated MWCNTs for conductive epoxy nanocomposites", *Compos. Sci. Technol.*, vol. 159, pp. 216–224, 2018.

[51] Sui, C., Pan, Z., Headrick, R. J., Yang, Y., Wang, C., Yuan, J., He, X., Pasquali, M., and Lou, J., "Aligned-SWCNT film laminated nanocomposites: Role of the film on mechanical and electrical properties", *Carbon*, vol. 139, pp. 680–687, 2018.

[52] Wang, L., Yang, H., Pan, G., Miao, L., Chen, S., and Song, Y., "Polyaniline-Carbon Nanotubes@Zeolite Imidazolate Framework-67-Carbon Cloth Hierarchical Nanostructures for Supercapacitor Electrode", *Electrochim. Acta*, vol. 240, pp. 16–23, 2017.

[53] Torkaman, R., Darvishi, S., Jokar, M., Kharaziha, M., and Karbasi, M., "Electrochemical and in vitro bioactivity of nanocomposite gelatin-forsterite coatings on AISI 316 L stainless steel", *Prog. Org. Coat.*, vol. 103, pp. 40–47, 2017.

[54] Yan, X., Yang, J., Chen, F., Zhu, L., Tang, Z., Qin, G., Chen, Q., and Chen, G., "Mechanical properties of gelatin/polyacrylamide/graphene oxide nanocomposite double-network hydrogels", *Compos. Sci. Technol.*, vol. 163, pp. 81–88, 2018.

[55] Zhang, X., Jiao, Y., Sun, L., Wang, L., Wu, A., Yan, H., Meng, M., Tian, C., Jiang, B., and Fu, H., "GO-induced assembly of gelatin toward stacked layer-like porous carbon for advanced supercapacitors", *Nanoscale*, vol. 8, no. 4, pp. 2418–2427, 2016.

[56] Landi, G., Sorrentino, A., Fedi, F., Neitzert, H. C., and Iannace, S., "Cycle stability and dielectric properties of a new biodegradable energy storage material", *Nano Energy*, vol. 17, pp. 348–355, 2015.

[57] Zheng, K., Xiao, S., Li, W., Wang, W., Chen, H., Yang, F., and Qin, C., "International Journal of Biological Macromolecules antimicrobial, antioxidant and structural properties", *Int. J. Biol. Macromol.,* vol. 135, pp. 344–352, 2019.

[58] Sadeghfar, F., Ghaedi, M., Asfaram, A., Jannesar, R., Javadian, H., and Pezeshkpour, V., "Polyvinyl alcohol/Fe$_3$O$_4$@carbon nanotubes nanocomposite: Electrochemical-assisted synthesis, physicochemical characterization, optical properties, cytotoxicity effects and ultrasound-assisted treatment of aqueous based organic compound", *J. Ind. Eng. Chem.*, vol. 65, pp. 349–362, 2018.

[59] Gao, B., Zhang, R., He, M., Sun, L., Wang, C., Liu, L., Zhao, L., Cui, H., and Cao, A., "Effect of a multiscale reinforcement by carbon fiber surface treatment with graphene oxide/carbon nanotubes on the mechanical properties of reinforced carbon/carbon composites", *Compos. Part A Appl. Sci. Manuf.,* vol. 90, pp. 433–440, 2016.

[60] Mousa, M. H., Dong, Y., and Davies, I. J., "Recent advances in bionanocomposites: Preparation, properties, and applications", *Int. J. Polym. Mater.*, vol. 65, no. 5, pp. 225–254, 2016.

[61] Coppola, D., Oliviero, M., Vitale, G. A., Lauritano, C., D'Ambra, I., Iannace, S., and de Pascale, D., "Marine collagen from alternative and sustainable sources: Extraction, processing and applications" *Mar. Drugs.*, vol. 18, no. 4, p.214, 2020.

[62] Das, M.P., Suguna, P.R., Prasad, K.A.R.P.U.R.A.M., Vijaylakshmi, J.V., and Renuka, M., "Extraction and Characterization of Gelatin: a Functional Biopolymer", *Int. J. Pharm. Pharm. Sci,* vol. 9, no. 9, p. 239, 2017.

[63] Gupta, N., Gupta, S. M., and Sharma, S. K., "Carbon nanotubes: synthesis, properties and engineering applications", *Carbon Lett.*, vol. 29, no. 5, pp. 419–447, 2019.

[64] Hu, L., Hecht, D. S., and Gruner, G., "Carbon nanotube thin films: fabrication, properties, and applications", *Chem. Rev.*, vol. 110, no. 10, pp. 5790–5844, 2010.

[65] Zhou, Y., Xu, H., Lachman, N., Ghaffari, M., Wu, S., Liu, Y., Ugur, A., Gleason, K. K., Wardle, B. L., and Zhang, Q. M., "Advanced asymmetric supercapacitor based

on conducting polymer and aligned carbon nanotubes with controlled nanomorphology", *Nano Energy*, vol. 9, pp. 176–185, 2014.

[66]   Shin, S. R., Jung, S. M., Zalabany, M., Kim, K., Zorlutuna, P., Kim, S. B., Nikkhah, M., Khabiry, M., Azize, M., Kong, J., Wan, K. T., Palacios, T., Dokmeci, M. R., Bae, H., Tang, X., and Khademhosseini, A., "Carbon-nanotube-embedded hydrogel sheets for engineering cardiac constructs and bioactuators", *ACS Nano*, vol. 7, no. 3, pp. 2369–2380, 2013.

[67]   Islam, M. R., Pias, S. M. N. S., Alam, R. B., and Khondaker, S. I., "Enhanced electrochemical performance of solution-processed single-wall carbon nanotube reinforced polyvinyl alcohol nanocomposite synthesized via solution-cast method", *Nano Express*, vol. 1, no. 3, p. 030013, 2020.

[68]   van der Pauw, L. J., "A method of measuring the resistivity and Hall coefficient on lamellae of arbitrary shape", *Philips Techn. Rev.*, vol. 20, pp. 220-224, 1958.

[69]   Yao, S., Yuan, J., al Mehedi, H., Gheeraert, E., and Sylvestre, A., "Carbon nanotube forest based electrostatic capacitor with excellent dielectric performances", *Carbon*, vol. 116, pp. 648–654, 2017.

[70]   Shao, Y., El-Kady, M. F., Sun, J., Li, Y., Zhang, Q., Zhu, M., Wang, H., Dunn, B., and Kaner, R. B., "Design and Mechanisms of Asymmetric Supercapacitors", *Chem. Rev.*, vol. 118, no. 18, pp. 9233–9280, 2018.

[71]   Liu, L., Weng, W., Zhang, J., Cheng, X., Liu, N., Yang, J., and Ding, X., "Flexible supercapacitor with a record high areal specific capacitance based on a tuned porous fabric", *J. Mater. Chem. A*, vol. 4, no. 33, pp. 12981–12986, 2016.

[72]   Sha, R., and Badhulika, S., "Few layered MoS2 grown on pencil graphite: A unique single-step approach to fabricate economical, binder-free electrode for supercapacitor applications", *Nanotechnology*, vol. 30, no. 3, p.035402, 2019.

[73]   Liu, F., Chiou, B. S., Avena-Bustillos, R. J., Zhang, Y., Li, Y., McHugh, T. H., and Zhong, F., "Study of combined effects of glycerol and transglutaminase on properties of gelatin films", *Food Hydrocoll.*, vol. 65, pp. 1–9, 2017.

[74]   Hoque, M. S., Benjakul, S., and Prodpran, T., "Properties of film from cuttlefish (Sepia pharaonis) skin gelatin incorporated with cinnamon, clove and star anise extracts", *Food Hydrocoll.*, vol. 25, no. 5, pp. 1085–1097, 2011.

[75]   Chao, S. C., Wang, M. J., Pai, N. S. and Yen, S. K., "Preparation and characterization of gelatin–hydroxyapatite composite microspheres for hard tissue repair" *Mater. Sci. Eng. C*, vol. 57, pp.113-122, 2015.

[76] Salem, K. S., Lubna, M. M., Rahman, A. M., Nurnabi, M., Islam, R., and Khan, M. A., "The effect of multiwall carbon nanotube additions on the thermo-mechanical, electrical, and morphological properties of gelatin-polyvinyl alcohol blend nanocomposite", *J. Compos. Mater.*, vol. 49, no. 11, pp. 1379–1391, 2015.

[77] Papageorgiou, D. G., Li, Z., Liu, M., Kinloch, I. A., and Young, R. J., "Mechanisms of mechanical reinforcement by graphene and carbon nanotubes in polymer nanocomposites", *Nanoscale*, vol. 12, no. 4, pp. 2228–2267, 2020.

[78] Spizzirri, U. G., Hampel, S., Cirillo, G., Nicoletta, F. P., Hassan, A., Vittorio, O., Picci, N., and Iemma, F., "Spherical gelatin/CNTs hybrid microgels as electro-responsive drug delivery systems", *Int. J. Pharm.*, vol. 448, no. 1, pp. 115–122, 2013.

[79] Poduval1, R. K., Noimark, S., Colchester, R. J., Macdonald, T. J., Parkin, I. P., Desjardins, A. E., and Papakonstantinou, I., "Optical fiber ultrasound transmitter with electrospun carbon nanotube-polymer composite", *Appl. Phys. Lett.*, vol. 110, no. 22, p.223701, 2017.

[80] Said, Z., "Thermophysical and optical properties of SWCNTs nanofluids", *Int. Commun. Heat Mass Transf.*, vol. 78, pp. 207–213, 2016.

[81] Devi, P. I., and Ramachandran, K., "Dielectric studies on hybridised PVDF-ZnO nanocomposites", *J. Exp. Nanosci.*, vol. 6, no. 3, pp. 281–293, 2011.

[82] Basith, M. A., Yesmin, N., and Hossain, R., "Low temperature synthesis of $BiFeO_3$ nanoparticles with enhanced magnetization and promising photocatalytic performance in dye degradation and hydrogen evolution", *RSC Adv.*, vol. 8, no. 52, pp. 29613–29627, 2018.

[83] Islam M. R., and Azam, M. G., "Enhanced photocatalytic activity of Mg-doped ZnO thin films prepared by sol–gel method", *Surf. Eng.*, pp.1-9, 2020.

[84] Hoseini, A. H. A., Arjmand, M., Sundararaj, U., and Trifkovic, M., "Significance of interfacial interaction and agglomerates on electrical properties of polymer-carbon nanotube nanocomposites", *Mater. Des.*, vol. 125, pp. 126–134, 2017.

[85] Ahmad, K., and Pan, W., "Dramatic effect of multiwalled carbon nanotubes on the electrical properties of alumina based ceramic nanocomposites", *Compos. Sci. Technol.*, vol. 69, no. 7–8, pp. 1016–1021, 2009.

[86] Prodromakis, T., and Papavassiliou, C., "Engineering the Maxwell-Wagner polarization effect", *Appl. Surf. Sci.*, vol. 255, no. 15, pp. 6989–6994, 2009.

[87] Akhtar, M. N., Khan, M. A., Raza, M. R., Ahmad, M., Murtaza, G., Raza, R., Shaukat, S. F., Asif, M. H., Saleem, M., and Nazir, M. S., "Structural, morphological,

dielectric and magnetic characterizations of NiO.6CuO.2ZnO.2Fe$_2$O$_4$ (NCZF/MWCNTs/PVDF) nanocomposites for multilayer chip inductor (MLCI) applications", *Ceram. Int.*, vol. 40, no. 10, pp. 15821–15829, 2014.

[88]   Kim, S. W., Kim, T., Kim, Y. S., Choi, H. S., Lim, H. J., Yang, S. J., and Park, C. R., "Surface modifications for the effective dispersion of carbon nanotubes in solvents and polymers", *Carbon*, vol. 50, no. 1, pp. 3–33, 2012.

[89]   Fumagalli, L., Esfandiar, A., Fabregas, R., Hu, S., Ares, P., Janardanan, A., Yang, Q., Radha, B., Taniguchi, T., Watanabe, K., Gomila, G., Novoselov, K. S., and Geim, A. K., "Anomalously low dielectric constant of confined water", *Science*, vol. 360, no.6395, pp.1339-1342, 2018.

[90]   Dong, W., Chen, D., Hu, W., Frankcombe, T. J., Chen, H., Zhou, C., Fu, Z., Wei, X., Xu, Z., Liu, Z., Li, Y., and Liu, Y., "Colossal permittivity behavior and its origin in rutile (Mg$_{1/3}$Ta$_{2/3}$)$_x$Ti$_{1-x}$O$_2$", *Sci. Rep.*, 2017, vol. 7, no. 1, pp. 1–8, 2017.

[91]   Glamazda, A. Y., Plokhotnichenko, A. M., Leontiev, V. S., and Karachevtsev, V. A., "DNA-wrapped carbon nanotubes aligned in stretched gelatin films: Polarized resonance Raman and absorption spectroscopy study", *Physica E Low Dimens. Syst. Nanostruct.,* vol. 93, pp. 92–96, 2017.

[92]   Choudhary, S., and Sengwa, R. J., "Effects of different inorganic nanoparticles on the structural, dielectric and ion transportation properties of polymers blend based nanocomposite solid polymer electrolytes", *Electrochim. Acta*, vol. 247, pp. 924–941, 2017.

[93]   Atawa, B., Correia, N. T., Couvrat, N., Affouard, F., Coquerel, G., Dargent, E., and Saiter, A., "Molecular mobility of amorphous N-acetyl-α-methylbenzylamine and Debye relaxation evidenced by dielectric relaxation spectroscopy and molecular dynamics simulations", *Phys. Chem. Chem. Phys.*, vol. 21, no. 2, pp. 702–717, 2019.

[94]   Havriliak S., and Negami, S., "A complex plane analysis of α-dispersions in some polymer systems", *J. Polym. Sci. Part C: Polym. Symp.*, vol. 14, no. 1, pp. 99–117, 2007.

[95]   Cole, K. S., and Cole, R. H., "Dispersion and absorption in dielectrics I. Alternating current characteristics", *J. Chem. Phys.*, vol. 9, no. 4, pp. 341–351, 1941.

[96]   Zhang, X., Liang, G., Chang, J., Gu, A., Yuan, L., and Zhang, W., "The origin of the electric and dielectric behavior of expanded graphite-carbon nanotube/cyanate ester composites with very high dielectric constant and low dielectric loss", *Carbon*, vol. 50, no. 14, pp. 4995–5007, 2012.

[97] Roy, A. S., Gupta, S., Sindhu, S., Parveen, A., and Ramamurthy, P. C., "Dielectric properties of novel PVA/ZnO hybrid nanocomposite films", *Compos. B. Eng.*, vol. 47, pp. 314–319, 2013.

[98] Intatha, U., Eitssayeam, S., Wang, J., and Tunkasiri, T., "Impedance study of giant dielectric permittivity in BaFe0.5Nb0.5O3 perovskite ceramic", *Curr. Appl. Phys.*, vol. 10, no. 1, pp. 21–25, 2010.

[99] Grosse, C., "A program for the fitting of Debye, Cole-Cole, Cole-Davidson, and Havriliak-Negami dispersions to dielectric data", *J. Colloid Interface Sci.*, vol. 419, pp. 102–106, 2014.

[100] Hirschorn, B., Orazem, M. E., Tribollet, B., Vivier, V., Frateur, I., and Musiani, M., "Determination of effective capacitance and film thickness from constant-phase-element parameters", *Electrochim. Acta*, vol. 55, no. 21, pp. 6218–6227, 2010.

[101] Córdoba-Torres, P., Mesquita, T. J., Devos, O., Tribollet, B., Roche, V., and Nogueira, R. P., "On the intrinsic coupling between constant-phase element parameters α and Q in electrochemical impedance spectroscopy", *Electrochim. Acta*, vol. 72, pp. 172–178, 2012.

[102] Ates, M., Serin, M. A., and Calisskan, S., "Electrochemical supercapacitors of PANI/MWCNT, PEDOT/MWCNT and P(ANI-co-EDOT)/MWCNT nanocomposites", *Polym. Bull.*, vol. 76, no. 6, pp. 3207–3231, 2019.

[103] Liu, X. M., Huang, Z. D., Oh, S. W., Zhang, B., Ma, P. C., Yuen, M. M.F., and Kim, J. K., "Carbon nanotube (CNT)-based composites as electrode material for rechargeable Li-ion batteries: A review", *Compos. Sci. Technol.*, vol. 72, no. 2, pp. 121–144, 2012.

[104] Sayah, A., Habelhames, F., Bahloul, A., Nessark, B., Bonnassieux, Y., Tendelier, D., Jouad, M. E., "Electrochemical synthesis of polyaniline-exfoliated graphene composite films and their capacitance properties", *J. Electroanal. Chem.,* vol. 818, no. April, pp. 26–34, 2018.

[105] Wang, S., Zhu, J., Shao, Y., Li, W., Wu, Y., Zhang, L., and Hao, X., "Three-Dimensional MoS$_2$@CNT/RGO Network Composites for High-Performance Flexible Supercapacitors", *Chem. Eur. J.*, vol. 23, no. 14, pp. 3438–3446, 2017.

[106] Abdah, M. A. A. M., Zubair, N. A., Azman, N. H. N., and Sulaiman, Y., "Fabrication of PEDOT coated PVA-GO nanofiber for supercapacitor", *Mater. Chem. Phys.*, vol. 192, pp. 161–169, 2017.

[107] Wang, Z., Li, H., Tang, Z., Liu, Z., Ruan, Z., Ma, L., Yang, Q., Wang, D., and Zhi, C., "Hydrogel Electrolytes for Flexible Aqueous Energy Storage Devices", *Adv. Funct. Mater.*, Vol. 28, no. 48, pp. 1–30, 2018.

[108] Ma, X., Fang, W., Ying, W., Chen, D., Li, Z., Deng, Z., Gao, C., and Peng, X., "A robust asymmetric porous SWCNT/Gelatin thin membrane with salt-resistant for efficient solar vapor generation", *Appl. Mater. Today*, vol. 18, p.100459, 2020.

[109] Mohapatra, D., Parida, S., Singh, B. K., and Sutar, D. S., "Importance of microstructure and interface in designing metal oxide nanocomposites for supercapacitor electrodes", *J. Electroanal. Chem.*, vol. 803, pp. 30–39, 2017.

[110] Zhang, J. J., Gu, M. M., Zheng, T. T., and Zhu, J. J., "Synthesis of gelatin-stabilized gold nanoparticles and assembly of carboxylic single-walled carbon nanotubes/Au composites for cytosensing and drug uptake", *Anal. Chem.*, vol. 81, no. 16, pp. 6641–6648, 2009.

[111] Nguyen, T. Q., and Breitkopf, C., "Determination of Diffusion Coefficients Using Impedance Spectroscopy Data", *J. Electrochem. Soc.*, vol. 165, no. 14, pp. E826–E831, 2018.

[112] Xu, X. Y., Liu, J. H., Ouyang, X., Cui, L., Hong, J., Meng, X., Qin, S., Liu, C., Tang, J., and Chen, D. Z., "In-situ temperature regulation of flexible supercapacitors by designing intelligent electrode with microencapsulated phase change materials", *Electrochim. Acta*, vol. 334, p.135551, 2020.

[113] Sifuentes-Nieves, I., Rendón-Villalobos, R., Jiménez-Aparicio, A., Camacho-Díaz, B. H., Gutiérrez López, G. F., and Solorza-Feria, J., "Physical, physicochemical, mechanical, and structural characterization of films based on gelatin/glycerol and carbon nanotubes", *Int. J. Polym. Sci.*, vol. 2015, 2015.

[114] Hoseini, A. H. A., Arjmand, M., Sundararaj, U., and Trifkovic, M., "Significance of interfacial interaction and agglomerates on electrical properties of polymer-carbon nanotube nanocomposites", *Mater. Des.*, vol. 125, pp. 126–134, 2017.

[115] Park, S. H., Hwang, J., Park, G. S., Ha, J. H., Zhang, M., Kim, D., Yun, D. J., Lee, S., and Lee, S. H., "Modeling the electrical resistivity of polymer composites with segregated structures", *Nat. Commun.*, vol. 10, no. 1, pp. 1–11, 2019.

[116] An, J., Gou, Y., Yang, C., Hu F., and Wang, C., "Synthesis of a biocompatible gelatin functionalized graphene nanosheets and its application for drug delivery", *Mater. Sci. Eng. C*, vol. 33, no. 5, pp. 2827–2837, 2013.

[117] Pavese, M., Musso, S., Bianco, S., Giorcelli, M., and Pugno, N., "An analysis of carbon nanotube structure wettability before and after oxidation treatment", *J. Phys. Condens. Matter*, vol. 20, no. 47, p.474206, 2008.

[118] Das, A. K., Mukherjee, A., Baba, K., Hatada, R., Bhowmik, R., and Meikap, A. K., "Current-Voltage Hysteresis Behavior of PVA-Assisted Functionalized Single-

Walled Carbon Nanotube Free-Standing Film", *J. Phys. Chem. C*, vol. 122, no. 51, pp. 29094–29105, 2018.

[119] Kong, Y., and Hay, J. N., "The measurement of the crystallinity of polymers by DSC", *Polymer*, vol. 43, no. 14, pp. 3873–3878, 2002.

[120] Kong, Y., and Hay, J. N., "The enthalpy of fusion and degree of crystallinity of polymers as measured by DSC", *Eur. Polym. J.*, vol. 39, no. 8, pp. 1721–1727, 2003.

[121] Ren, K., Wang, Y., Sun, T., Yue, W., and Zhang, H., "Electrospun PCL/gelatin composite nanofiber structures for effective guided bone regeneration membranes", *Mater. Sci. Eng. C,* vol. 78, pp. 324–332, 2017.

[122] Alam, R. B., Ahmad, M. H., and Islam, M. R., "Bio-inspired gelatin/single-walled carbon nanotube nanocomposite for transient electrochemical energy storage: An approach towards eco-friendly and sustainable energy system", *Heliyon*, vol.7, no. 7, p. e07468, 2021.

Appendices

Published Papers:

[1] Islam, M. R., Pias, S. M. N. S., Alam, R. B., and Khondaker, S. I., "Enhanced electrochemical performance of solution-processed single-wall carbon nanotube reinforced polyvinyl alcohol nanocomposite synthesized via solution-cast method", *Nano Express*, vol. 1, no. 3, p. 030013, 2020.

[2] Mollik, S. I., Alam, R. B., and Islam, M. R., "Significantly improved dielectric properties of bio-compatible starch/reduced graphene oxide nanocomposites", *Synth. Met.,* vol. 271, p. 116624, 2021.

[3] Alam, R. B., Ahmad, M. H., and Islam, M. R., "Bio-inspired gelatin/single-walled carbon nanotube nanocomposite for transient electrochemical energy storage: An approach towards eco-friendly and sustainable energy system", *Heliyon*, vol.7, no. 7, p. e07468, 2021.

Submitted Papers:

[1] "Significantly Improved Dielectric Performance of Bio-derived Polymer/Single walled Carbon Nanotube Nanocomposite" under review in Results in Physics.

[2] "Submission Confirmation Improved thermal, mechanical and electrochemical performance of bio-degradable starch/reduced graphene oxide nanocomposites" under review in Advanced Composites and Hybrid Materials.

Papers Under Preparation:

[1] "Significantly Improved Dielectric Performance of Bio-derived Polymer/Multi walled Carbon Nanotube Nanocomposite"

[2] "Gelatin/MWCNT Biocompatible Electrode Materials for Transient Electrochemical Energy Storage: An Approach towards Ecofriendly and Sustainable Energy System"

Conference Presentations:

[1] Oral Presentation on "Tailoring the Dielectric Properties of Bio-derived Polymer by Incorporating Ultralow Amount of Single walled Carbon Nanotube" in the International Conference on Physics-2020, organized by Bangladesh Physical Society.

[2] Poster Presentation on "Gelatin/Multi Walled Carbon Nanotube Bio-friendly Composites for Transient Electronics Energy Storage Application" in the International Conference on Science and Technology for Celebrating the Birth Centenary of Bangabandhu (ICSTB-2021) organized by Bangladesh Council of Scientific and Industrial Research (BCSIR).